DEVELOPMENT OF α/β-SIALON NANO CERAMIC FOR WEAR RESISTANCE APPLICATIONS

BY

Moath Mohammad Al Malki

A Thesis Presented to the
DEANSHIP OF GRADUATE STUDIES

KING FAHD UNIVERSITY OF PETROLEUM & MINERALS

DHAHRAN, SAUDI ARABIA

In Partial Fulfillment of the
Requirements for the Degree of

MASTER OF SCIENCE

In

Material Science and Engineering

December 2015

KING FAHD UNIVERSITY OF PETROLEUM & MINERALS

DHAHRAN, SAUDI ARABIA

DEANSHIP OF GRADUATE STUDIES

This thesis, written by **Moath Mohammad Al Malki** under the direction of his thesis advisor and approved by his thesis committee, has been presented to and accepted by the Dean of Graduate Studies, in partial fulfillment of the requirements for the degree of MASTER OF SCIENCE in **Material Science and Engineering**

Thesis Committee

Thesis Advisor
Prof. Tahar Laoui

Member
Dr. Abbas Hakeem

Member
Prof. Zafarullah Khan

Department Chairman

Dr. Zuhair Mattoug Gasem

Dean of Graduate Studies

Prof. Salam A. Zummo

21/4/16

Date

This Thesis is Dedicated to My Parents For Their Endless Love, Support And Encouragement

..

..

for my Father *Mohammad*

and for my Mother *Fatima*

..

..

the most beloved parents

ACKNOWLEDGMENT

First and foremost , thanks to God Almighty for completion of master thesis. Only due to his blessings, I could finish my thesis. Then, I would like to express my sincere thanks to my wonderful parents, for whom I refer my success in life. I would like also to thank my hard working brothers and sisters, who offered me endless motivation and an environment full of positiveness.

I would like to express my deep gratitude to my thesis advisor Prof. Tahar Laoui for the boundless help, patience and guidance throughout my master research. I would like, also, to thank my co-advisor Dr. Abbas Hakeem for his generous help and support especially in the experimental part of the study. Further, I would like to thank Prof. Zafarullah Khan for the useful comments, remarks and engagement through the course of my master thesis.

I would like to thank the chairman of the mechanical engineering department, Dr. Zuhair Gasem, for the continuous boosting and advices he offered. Also, I would like to express my deep thanks to Dr. Zain Yamani, the director of the center of excellence in nanotechnology(CENT), for offering my access to their laboratories and equipment, and for fostering me during the research course.

I would like to thank Mr. Mohammad Lateef Hashmi; the great lab engineer of materials science laboratory in the department, for helping me passionately and sincerely in performing my experimental work. Special thanks go to Mr. Idris Bakare, the lab engineer of Nanopowders laboratory in CENT, for easing my research activities and for the valuable discussions and the “always-available” smiling comments. I should not forget

Mr. Sadaqat Ali, who turned with me on the automatic diamond grinding and polishing machine for the first time and pushed up my skills in handling scientific equipment.

I would like, also, to thank deeply my sincere research-mate Mr. Raja Muhammad Awais Khan for the wonderful time we spent together performing experiments and discussing results. I was fortuitous by his passion , talent and more importantly patience. Great thanks go to my colleagues and friends in the mechanical engineering department and CENT for the magnificent, and sometimes brutal, scientific discussions and argumentations.

I feel grateful to Prof. Stuart Hampshire for reviewing and interspersing his proficiency and experience in our papers. His humbleness and cooperation was more than just a lesson for me. KACST is acknowledged for supporting financially our research through the national program for science and technology.

TABLE OF CONTENT

LIST OF FIGURES

LIST OF TABLES

ABSTRACT (ENGLISH)

Si_3N_4 ceramics are known for their outstanding performance in challenging environments. However, due to the covalent binding present between Si and N, fully-dense Si_3N_4 ceramics are difficult to achieve via solid state sintering. Thus, SiAlON ceramics have been introduced into the field, in which part of Si and N are replaced by Al and O, respectively.

The use of nano-size starting powder materials in the present work proved its positive impact in accelerating the reaction kinetics, yielding lower sintering temperature and shorter holding (dwell) time. Spark plasma sintering technique was utilized for consolidation to benefit from its novelty in limiting phase transformation and undesirable grain growth, along with being an economical processing route when compared to conventional sintering techniques. Furthermore, calcium (Ca) additive was shown to enhance the densification and wetting through the production of a liquid phase, with the least crystal distortion in α- SiAlON unit cell, which was reflected in a higher stability of the latter phase.

Aluminum (Al) metal precursor was also explored in the context of improving sinterability at lower temperature, by partial substitution of aluminum nitride (AlN), up to 30% mol. It was observed that by such replacement, Ca- α- SiAlON could be sintered at lower peak temperature (1450^{o}C) with either retained or enhanced mechanical properties. Additionally, Al metal precursor was shown to be a novel tool in preserving α-SiAlON at high sintering temperature (1600^{o}C) by hindering alpha to beta phase transformation. Si metal precursor was examined as well in a similar context, however, it did not show the

same behavior due to the limited chemical reactivity and its relative high melting point when compared to Al metal.

Barium (Ba) additive was also investigated in this study to establish a basis for comparison with Ca additive. The formation of S-SiAlON was shown to be typical with Ba additive. Moreover, an increase in the amount of β-phase occurred when β-Si_3N_4 was introduced into the starting mixtures in place of amorphous Si_3N_4. The mechanical properties of the sintered Ba-SiAlON were far below than those of Ca- α- SiAlON due to the ionic radius of Ba, which lowered the stability of α- SiAlON, and the presence of low- hardness phases, such as SiO_2 and S-SiAlON.

In an attempt to improve the fracture toughness of sintered Ca- α- SiAlON ceramics, post-sintering heat treatment of selected samples was carried out at 1500^{o}C for 12 hours in Ar environment. The fracture toughness was measured using crack indentation technique. An enhancement in the fracture toughness was observed after heat treatment, due to several contributing phenomena, such as crack deflection and crack bridging mechanisms as well as alpha to beta phase transformation. As a result of the devitrification process after heat treatment, Ca amount and N:O ratio increased in the grain boundary, as revealed by energy dispersive spectroscopy analysis, leading to harder grain boundary and, consequently, intergranular crack propagation.

ABSTRACT (ARABIC)

تعتبر المواد المركبة من نيتريد السيلكون من أفضل المواد الملائمة للبيئات الصعبة ، ولكن نظرا لصعوبة تصنيعها في صورة كاملة الكثافة بوسائل التلبيد الإعتيادية بسبب الرابطة التساهمية بين السيلكون والنيتروجين، قام الباحثون بابتكار بديل أسموه " السايلون"، والذي تم فيه استبدال جزء من السليكون بالألمنيوم وجزء من النيتروجين بالأوكسجين.

أثبت استخدام المواد الأولية في حجم النانو جدواه في جعل عملية التلبيد أكثر كفاءة من خلال تقليل وقت العملية وتخفيض درجة حرارة التلبيد. تم اعتماد تقنية التلبيد بالبلازما والشرارة الكهربائية في هذه الدراسة للاستفادة من قدرة هذه التقنية في تحجيم تحول الأطوار والنمو غير المرغوب للحبيبات ، بالإضافة للجدوى الإقتصادية عند مقارنته بتقنيات التلبيد التقليدية. أثبتت هذه الدراسة كذلك أن استخدام إضافات الكالسيوم تساهم في عمليتي التكثيف و التبليل من خلال إنتاج الطور السائل ، إلى جانب تسبيبها الحد الأدنى من التخلخل الكرستالي في خلايا طور الألفا-سايلون والذي ينعكس على استقرار أكبر لهذا الطور.

استكشف في هذه الرسالة أيضا دور معدن الألمنيوم -كمادة أولية من ضمن المتفاعلات- من أجل تحسين عملية التكثيف في درجات تلبيد حرارية منخفضة . أثبت البحث الدور الإيجابي لمعدن الألمنيوم في إمكانية تلبيد المادة في درجة حرارة منخفضة سبيا ($1450^{o}C$) مع المحافظة على الخواص الميكانيكية أو تحسينها. بالإضافة إلى ذلك ، فقد أظهر البحث دورا فريدا للألمنيوم في المحافظة على طور الألفا-سايلون في حال لبدت المادة في درجة حرارة عالية نسبيا ($1600^{o}C$) عن طريق منع تحول الأطوار من الألفا إلى البيتا. إلى جانب معدن الألمنيوم ، تم اختبار معدن السيلكون -كمادة أولية من

ضمن المتفاعلات- في ذات السياق إلا أنه لم يكن له ذلك الأثر الإيجابي بسبب محدودية نشاطه الكيميائي وارتفاع درجة انصهاره مقارنة بمعدن الألمنيوم.

من أجل بناء أساس للمقارنة مع إضافة الكالسيوم ، اختبر هذا البحث إضافة الباريوم والتي نتج عنها تكون طور الأس-سايلون كناتج أساسي. إلى جانب ذلك ، وجد أن كمية طور البيتا-سايلون تزيد عند البدء بطور البيتا من نيتريد السيليكون عوضا عن الطور اللابلوري من نيتريد السيليكون. بالمقارنة مع الخواص الميكانيكية لسيراميك السايلون المحضر بإضافة الكالسيوم، فسيراميك السايلون المحضر بإضافة الباريوم أظهر تدهورا نسبيا في الخواص الميكانيكية بسبب كبر نصف القطر الأيوني للباريوم والذي يضعف من استقرار طور الألفا-سايلون. شكل تكون بعض الأطوار ذات الصلابة المنخفضة – كأكسيد السيليكون و طور الأس-سايلون – سببا آخرا لضعف الخواص الميكانيكية لسيراميك السايلون المحضر بإضافة الباريوم.

في محاولة لتحسين خاصية المتانة لسيراميك السايلون المحضر بإضافة الكالسيوم، تم تطبيق المعالجة الحرارية على درجة حرارة $1500^{o}C$ ولمدة 12 ساعة في محيط غاز الآرجون بعد انتهاء عملية التلبيد. استخدمت تقنية قياس طول الصدع الناتج عن تغلغل رأس الألماس المستخدم في اختبار الصلابة لقياس متانة المواد الملبدة من السايلون. أظهرت النتائج تطورا ملحوظا في قيم المتانة، والتي يمكن إرجاعها إلى عدة عوامل كظاهرة تغيير مسار الصدع وظاهرة رأب الصدع بالإضافة إلى تحول أطوار السايلون من الألفا إلى البيتا. كنتيجة لعملية تبلور حدود الحبيبات ، ازدادت نسبة النيتروجين إلى الأكسجين في أطوار الحدود وكمية معدن الكالسيوم – كما أثبت عن طريق مشتت

الطاقة السبكتروميتري – والتي بدورها زادت من صلابة حدود الحبيبات و دفعت الصدع للتغلغل عن طريقها.

CHAPTER 1

INTRODUCTION

The industry of hard materials is expanding vastly to accommodate the increasing demand in the field of the wear resistance materials, such as drilling and cutting tools materials. Si_3N_4 has been recognized as one of the top candidates in the field of hard ceramics, exhibiting high hardness, chemical inertness and distinguishable wear and oxidation resistance. The common issue of fracture toughness in ceramic materials does not exclude Si_3N_4. Nevertheless, researchers have attempted to overcome the difficulty of synthesizing/ densifying Si_3N_4 with the minimal energy input . Reaction bonded (RB) and hot pressed (HP) Si_3N_4 ceramics exemplify different attempts to synthesize Si_3N_4, targeting reasonable densification and appropriate mechanical properties. However, results were not encouraging and alternative routes need to be discovered.

K.Jack and Y. Oyama, independently, proposed the incorporation of Al_2O_3 in the powder mixture with Si_3N_4 to improve densification and sinterability. The product of such modification has been known to be "SiAlON", in which Al and O replace partially Si and N in Si_3N_4 respectively. SiAlON is composed, generally, of two major phases; alpha and beta, in which α-SiAlON shows higher hardness than β-SiAlON, which in turn exhibits better fracture toughness. Thus, an intuitive balance between α-SiAlON and β-SiAlON phases amount and distribution would satisfy the goal of sintering Si_3N_4 –based ceramics with optimal mechanical properties.

It has been established that α-SiAlON can be sintered with no additional cations. However, and due to the nature of its unit cell, added cations enhance the phase stability and the sinterability of SiAlON ceramic. Lanthanides have been considered as typical additives for the last decades due to the remarkable level of refractoriness that elevated the mechanical response of the sintered SiAlON ceramics. Nonetheless, and due to crystal defects originating from these additives, the focus has been shifted to other additives, such as alkaline elements, namely magnesium, barium and calcium. Calcium is the most suitable additive, after being proved to stabilize the α-SiAlON structure and, further, to expand its area in the phase diagram.

One of the well-established ways to lower the sintering temperature and to ameliorate the sinterability and densification of ceramic materials is the use of nano starting precursors. Nano powder materials are associated with shorter diffusion path and enhanced diffusion velocity, along with un-comparatively larger surface area. This puts forward a milestone in developing any future Si_3N_4/ SiAlON ceramics.

The invention of spark plasma sintering(SPS) in Japan has contributed to the advancing of powder metallurgy techniques . SPS has shown its novelty over other traditional sintering techniques, like hot pressing and hot isostatic pressing, such that the required mechanical and physical properties can be obtained with the least energy input, represented by relatively low sintering time and temperature.

1.1 THESIS AIM

The aim of the present work is to develop a nano ceramic-based material composed mainly of a mixture of α-SiAlON and β- SiAlON to tailor the hardness and fracture toughness properties for high wear resistance applications. This aim calls for deep understanding of SiAlON system and its related subjects, and leads to the following objectives :

- To synthesize dense α/β-SiAlON ceramic, incorporating Ca and Ba metal cations
- To prepare α/β-SiAlON ceramic mixture at relatively low sintering temperature and shorter holding time by utilizing nano-size starting powder precursors.
- To investigate the role of Al and Si metal precursors on the densification, sinterability and the mechanical properties.
- To study the effect of varying the structure of Si_3N_4 starting powder precursor (crystalline Vs. amorphous) on the mechanical properties of the sintered sample.
- To utilize Spark Plasma Sintering, as a synthesis technique, to prepare SiAlON ceramics in relatively short time and low sintering temperature.
- To characterize the resultant microstructures, phase assemblages and physical and mechanical properties of the sintered samples.

CHAPTER 2

LITERATURE REVIEW

The hard materials industry is growing vastly to meet the increasing demand in the real-time applications. Among a long list of competitors, ceramic materials have shown their capability in withstanding extraordinary conditions, namely their superior mechanical, chemical and thermal performance.

The typical requirements for any engineering ceramics are mostly confined to two aspects; mechanical strength and the decomposing/melting temperature. Mechanical strength is satisfied by the presence of strong inter-atomic bonding, such as covalent and ionic bonding. However, people are concerned more about the strength to weight ratio. Thus, elastic modulus / the specific gravity ratio (specific elastic modulus) is a good measure to assign the above mentioned concern. The requirement of high decomposing/melting temperature, is usually achieved by a covalently-bonded structure

Table.1 lists several engineering materials with their respective properties [1]. AlN is readily hydrolysed, which ,in turn, limits its use in certain applications [1]. Further, Al_2O_3 shows poor thermal shock resistance [1]. Although carbon has the highest strength to weight ratio and decomposition temperature, it is easily prone to oxidation [1]. The usage of BeO may involve toxicity hazards. This leaves us with SiC and Si_3N_4 ceramics as optimum choices for harsh environments.

TABLE 1 Specific elastic modulus and melting temperature of common engineering materials

	Specific elastic modulus (10^6 Ib.in^{-2})	**Decomposing/melting temperature ^{o}C**
AlN	15	2450
Al_2O_3	13	2050
BeO	18	2530
C Whiskers	61	3500
SiC	25	2600
Si_3N_4	17	1900
Steel, glass , wood	4	-

2.1 SILICON NITRIDE

Si_3N_4 is known for its superior properties, namely wear resistance , oxidation resistance, thermal stability, thermal shock resistance and hot hardness . Surprisingly, the utilization of Si_3N_4 goes back to more than 100 years. In 1896, a German patent was secured on production of Si_3N_4 by carbothermal reaction of SiO_2 [1]. After 1955, people started to consider it as a refractory material, serving as a perfect binder in SiC matrix, a thermocouple sheath material that performed four times better that Al_2O_3 in withstanding thermal cycles and as a mold for non-ferrous materials. Later in 1960, internal combustion engines started utilization of Si_3N_4 materials taking advantage of its perfect thermal stability, i.e. by the help of its low thermal expansion. 1961 was a breakthrough in a sense, researchers were able to sinter Si_3N_4 using hot pressing technique (HP), before which reaction bonding (RB) was the common route to consolidate Si_3N_4 powder [2]. Further, United States started a huge Si_3N_4 development program in 1970 for five years, with special collaboration with Ford Motors and Westinghouse Electric companies, aimed at examining the capability of Si_3N_4 in functioning well in mobile and stationary gas-turbine engine parts [3].

Generally, Si_3N_4 is formed in two ways; reaction-bonded and hot pressed. When Si metal undergoes nitridation reaction at high temperature , say 1400^oC, then the product is said to be reaction-bonded Si_3N_4 . The advantage of such a technique is the freedom in forming complex shapes and geometries, however, a porosity of 25% cannot be prevented. The typical alternative is to utilize hot pressing with some selected additive, like MgO, to remove porosity. Nevertheless, the presence of second phases, that has a different thermal expansion coefficient, may cause crack initiation/ propagation in the mismatch area.

Additionally, the product is rarely homogenous whether an additive is used or not [1]**.** **Figure .1** displays the acting areas for both forms of Si_3N_4.

Si_3N_4 is present naturally in two modifications; namely α and β, both of which exhibit hexagonal crystal structure. However, c-axis of α-Si_3N_4 is proven to be larger than the corresponding axis in β-Si_3N_4. A unit cell of β-Si_3N_4 consists of S_6N_8 in a way that each silicon is centered in a tetrahedron and each nitrogen is situated in a trigonal cell with approximate coordination by three silicon atoms. The structure can be thought to be eight Si-N rings, being joined into sheets, which are linked in three dimensions through Si-N bonds [4].

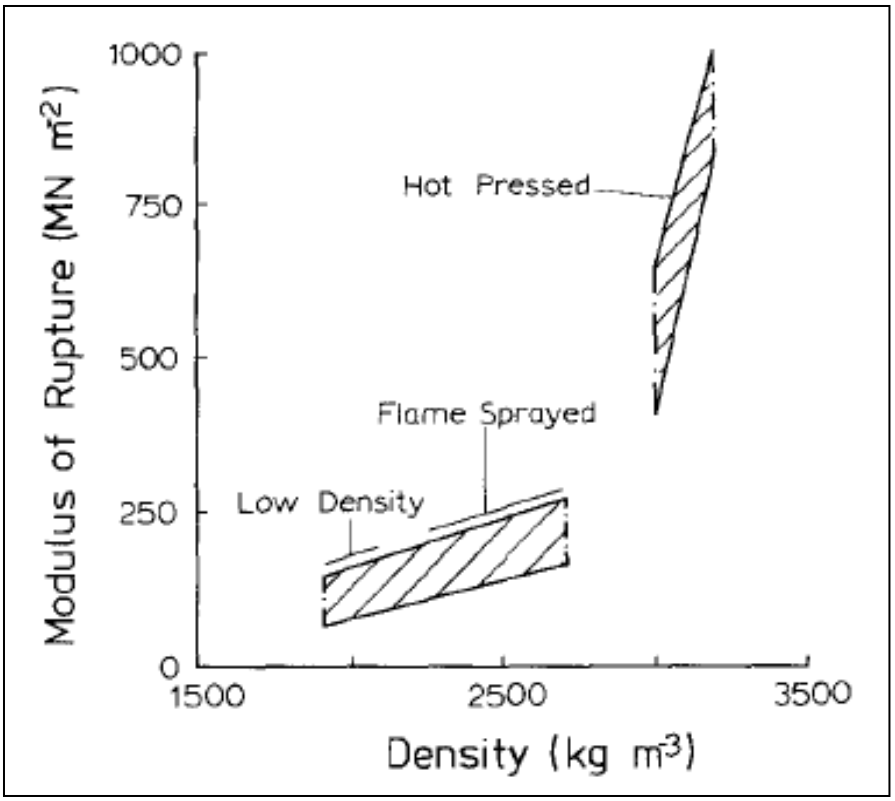

Figure 1 Mechanical properties for the two main forms of Si_3N_4 [1]

In contrary, α-Si_3N_4 follows crystallographically $Si_{12}N_{16}$ structure [4]**.** A clear distinction between the above mentioned phases of Si_3N_4 , which is reflected greatly on the doping feasibility, is the presence of large interstices in α- Si_3N_4 , linked by 140 pm channels. In contrary, β-Si_3N_4 structure offers continuous channels along the c-axis, having diameters of 300 pm [5]**.** Early XRD work has revealed some variation in α-Si_3N_4 bond lengths [6], and small divergence in unit cell parameters [7].By utilization of Archimedes's method, density of Si_3N_4 was obtained to be 3.169±0.004 g/cm^3 , which agrees well with the calculated value (3.168 g/cm^3) [4]**.**

A doubt was covering the nature of α-Si_3N_4, after claiming the inherent inclusion of oxygen in its structure. However, several evidences were presented to prove the presence of oxygen in α-Si_3N_4 , with an amount of 1.5% w.t, being allocated in normal nitrogen sites. One of these evidences was worked out by H.K. Jack [7], in which he claimed that the definite variation in the relative intensities of the XRD peaks could be understood if α-Si_3N_4 was considered to have a defect structure. Another evidence was shown by a group of researchers [8], who pointed out the same observation, where they identified the presence of 2% w.t of oxygen in α- β mixed Si_3N_4 , while this percentage was reduced as the amount of α phase was decreased . Priest [9] concluded form his research of the oxygen content in α-Si_3N_4 that there was no doubt that α-Si_3N_4 could host oxygen atoms, however, that was not compulsory to achieve stability.

The phase transformation of α to β -Si_3N_4 was studied extensively [9-11]**.** The first attempt was not encouraging, where people annealed α-Si_3N_4 at 1800^oC. Later, Brook [11] concluded that such transformation was possible only in the presence of liquid phase, such as silicides and silicates, due to the activation energy barrier.

2.2 SiAlON

Although Si_3N_4 can serve well in a variety of applications, it is difficult to achieve fully dense products by normal solid –state sintering[12]. Peoples' thought about this was like the following. AlO_4 has the same structure as SiO_4, with a difference in the overall charge, being -4 for silica and -5 for alumina. Thus, it seems feasible that Al_2O_3 replaces SiO_2, in which Si^{4+} is substituted by Al^{+3} [1]. It should be noted down that oxygen arises due to the inherent oxygen impurities in α-Si_3N_4 as discussed before.

Basically, SiAlON is considered to be a solid solution of Si_3N_4, where Si and N are replaced by Al and O, respectively. The replacement should be simultaneous to maintain the charge neutrality. SiAlON forms two major modifications; alpha and beta. α- SiAlON follows this general stoichiometry $M_x Si_{12-(m+n)} Al_{(m+n)} O_n N_{16-n}$ with $x = m/v$, M represents the added cation such as many of lanthanides and alkaline earth elements , $x \leq 2$ and v indicates the number of valences of the added cation. On the other hand, β–SiAlON obeys the general formula $Si_{6-z} Al_z O_z N_{8-z}$, where z value lies between 0 and 4.2 [1]. Both modifications possess HCP crystal structure, however, α- SiAlON follows ABCD stacking sequence ,with c glide plane that holds two interstices. In contrary, β–SiAlON follows AB stacking sequence. Another divergence lies in the c lattice parameter, being double for α-SiAlON, which is responsible for the lattice strain. This makes α-SiAlON less thermally stable than β–SiAlON.

Generally, α-SiAlON possesses higher hardness than β–SiAlON, while the latter shows better fracture toughness than the former. The reason behind this variation in the mechanical properties is explained usually through the consideration of the nitrogen

cross-linking and the phase morphology, in which α-SiAlON is produced mostly in equiaxed grains, while β–SiAlON grains tend to be more elongated . However, several researchers have reported the formation of α-SiAlON with elongated morphology, which elevates the value of the fracture toughness [13,14]

Initially, SiAlON system was represented by a ternary phase diagram, cornered by AlN, Al_2O_3 and Si_3N_4 [1]**,** see **Figure.2**. However, these diagrams were shown later to be inaccurate in predicting the homogeneity range of β–SiAlON. Later, people developed the tetrahedral representation, cornered by Al, Si, N and O, see **Figure.3(a)**. However, the diagram was constructed on atomic basis, i.e. on molar concentration . To get a simpler representation, one may find out the equivalents concentration, by which each corner quantifies 12 positive and negative charges, see **Figure.3(c)** . As we move from left to right, $4Al^{3+}$ replaces $3Si^{4+}$ and as similarly from the bottom to the top $4O^{2-}$ replaces $4N^{3-}$. Note that, although the number of atoms/moles changes with the position of the composition, equivalents remain the same. The central composition in this diagram can be represented by $Si_{1.5}Al_2O_3N_2$. However, if the system of SiAlON incorporates other additives, such as lanthanides and alkaline earth elements, then a more sophisticated representation is needed. For that, people have developed the so-called Janecke prism, as shown in **Figure.4**, that includes the oxide and nitride of the additive. When examining it carefully, one can see that the prism is made of two ternary and three quaternary phase diagrams. Thus, for simplicity, it is preferred occasionally to present these constituting diagrams separately. A very important plane of interest is shown in **Figure.4**, where alpha and beta phases are present along with other major phases, such as AlN polytypoids. A sample extraction of this plane is shown in **Figure.5.**

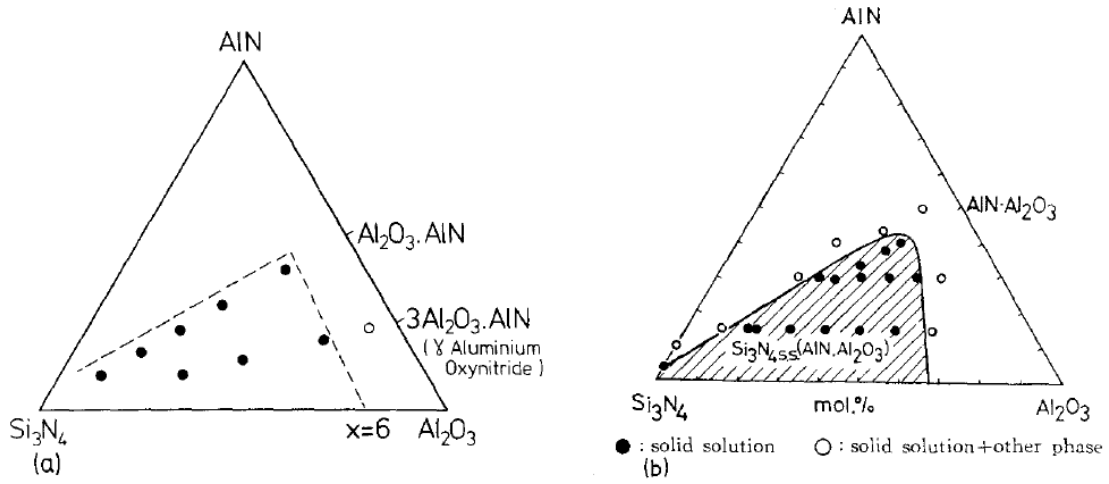

Figure 2 SiAlON Phase Diagrams above 1700°C prepared by LK Jack (a) and Oyama (b) [1]

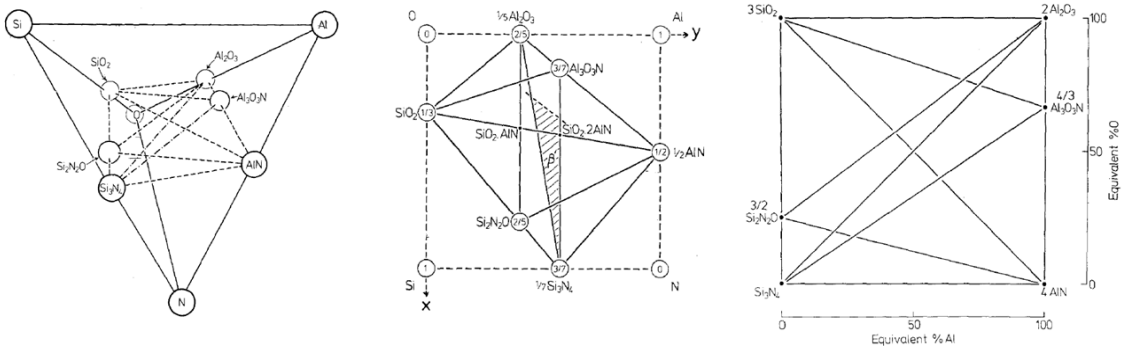

Figure 3 From left to right (a-b-c) : **(a)** Tetrahedral representation of Si-Al-O-N system. **(b)** An extracted quadrilateral plane from (a) . **(c)** The normal quaternary representation of SiAlON system with concentrations being expressed in equivalents [1]

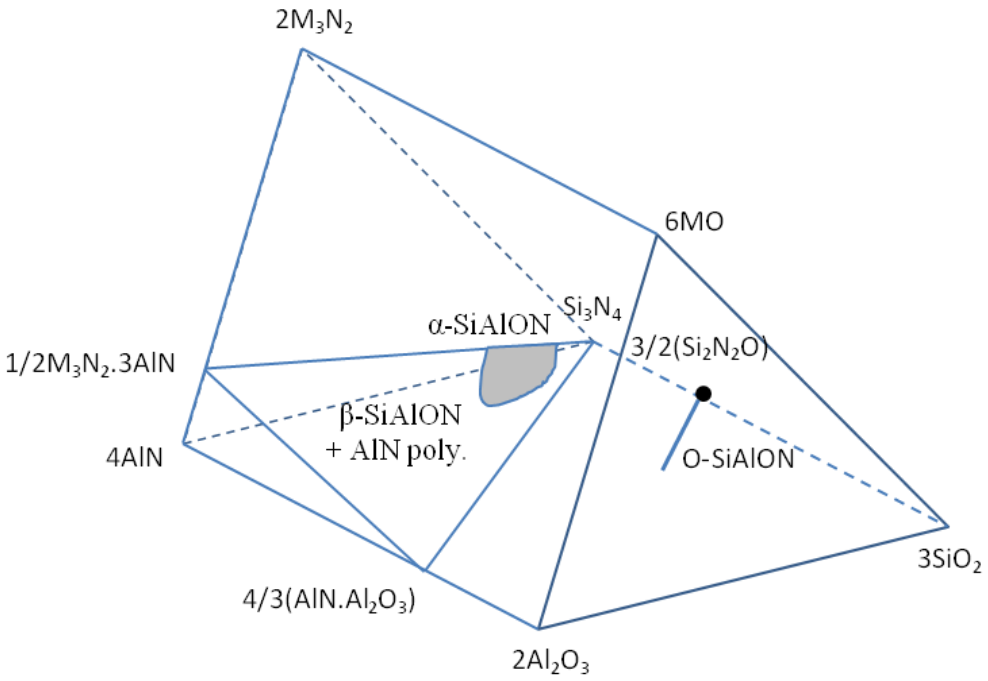

Figure 4 Janecke prism representing the SiAlON system with alkaline nitrides and oxides

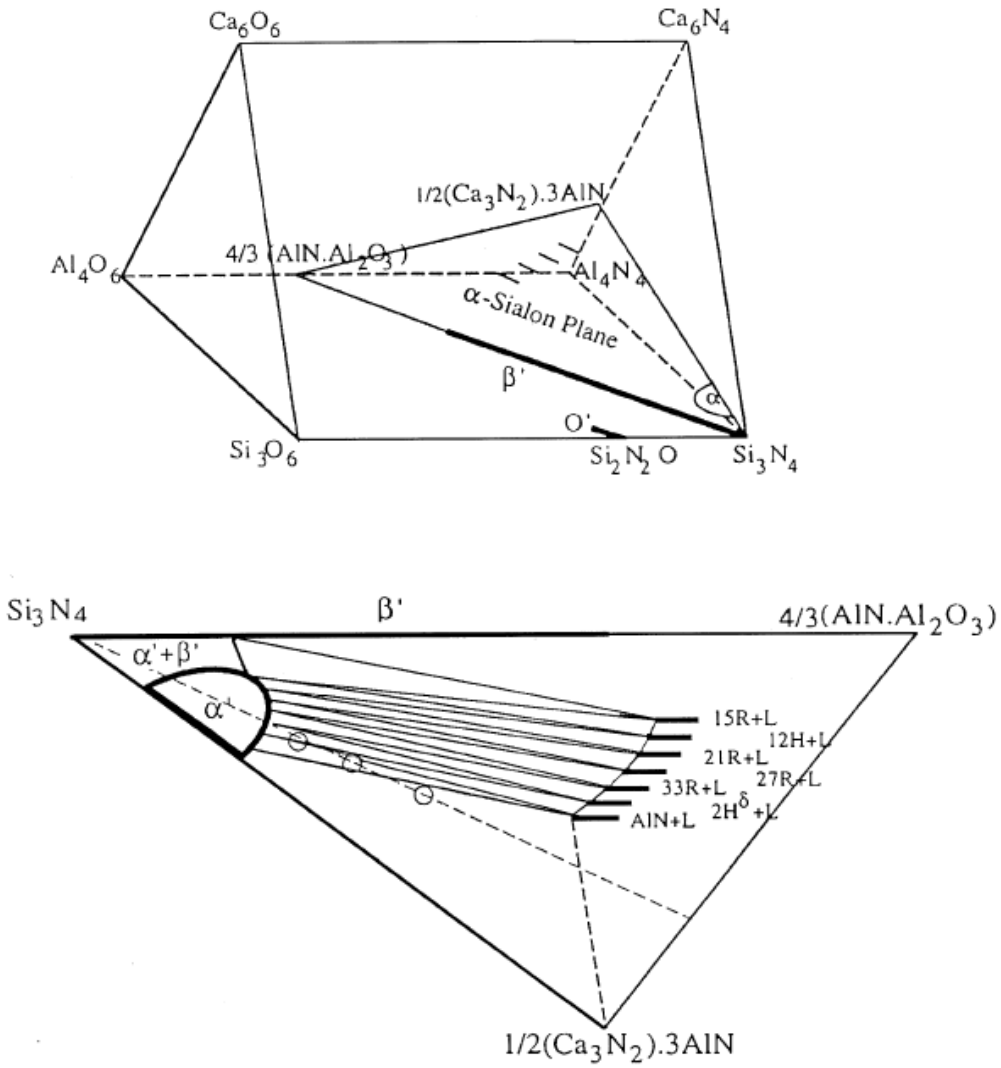

Figure 5 Janecke prism of Ca-α-SiAlON system with the extracted α-β plane [15]

In addition to the common phases α and β SiAlON, Si_3N_4 can form other phases when it reacts with Al_2O_3. O-SiAlON is one of these phases, which is similar in structure to Si_2N_2O possessing SiN_3O structural unit. X-SiAlON is another known phase, following this composition $3Al_2O_32Si_3N_4$. Initially, Drew and Lewis tried to show that X-SiAlON has a triclinic structure[16] . However, K. Jack has shown that it has a monoclinic unit cell [1].

AlN- polytypoids phases are considered to be defected structures of AlN, at which oxygen and silicon get involved in their crystal lattice [17]. They usually exist whenever the composition offers a large amount of liquid phase. Mainly, these polytypoids posses either rhombohedral or hexagonal unit cells, at which each hexagon contains two blocks, each holds n/2 layers, where n has a value of 8, 12 and 2. The technical significance of such phases lies in the enhancement of both hardness and fracture toughness of the synthesized samples. The advancement in the hardness arises due to the consumption of the liquid phase, that is responsible in many cases for the deterioration in the mechanical behavior of SiAlON materials. Additionally, since AlN-polytypoids form elongated morphology, namely lathe-like structure, they can easily enhance the fracture toughness by the crack deflection toughening mechanism [1,17]**.**

2.3 SINTERING OF CERAMICS

2.3.1 OVERVIEW ON SINTERING

German defined sintering as " *a thermal treatment for bonding particles into a coherent , predominantly solid structure via mass transport events that often occur on the atomic scale*"[18] . In simpler words, sintering can be thought to be a

manufacturing process by which powder materials are converted into solid parts by means of heat and with or without pressure. A basic classification of sintering considers whether pressure is involved or not in the sintering process. For pressure assisted sintering, a material can be processed without the incorporation of any additive. However, that is not always possible, and in certain cases, additives in form of binders are used to facilitate densification. For that, pressure-assisted sintering is further divided into solid-state and liquid-phase sintering processes.

Various theories and mechanisms have been proposed to puzzle out the sintering process [18]. The typical mechanisms include bulk diffusion, surface diffusion, vapor transport and grain boundary diffusion. In a normal sintering operation, particles start to approach each other under the influence of the external applied pressure. After forming the necks, localized softening takes place and plastic deformation mechanism starts to play. This results in the enlargement of the necks. Since most of the sintering mechanisms are diffusion –controlled, and as time elapses, pores get closed due to the bulk/volume diffusion, ending up with densified structure with randomly-oriented closed pores[18,19].

The number of techniques developed for sintering is, generally, expanding being more than 100 techniques in the current time. Nevertheless, several of them are suitable to sinter SiAlON ceramics, being classified all as pressure-assisted sintering process.

Hot Pressing (**HP)** is one of these techniques, in which the sample is kept in graphite die and gets uniaxially pressed. The heating effect is provided through the heating elements surrounding the chamber, see **Figure.6**. Boron nitride spray is utilized

usually to diminish any reaction between the sample and the graphite die. It should be noted that hot pressing becomes less effective whenever pre-compacted fine powder is used, because the graphite die, at that time, cannot bear the sintering stresses developed in the fine sample [19].

The typical alternative to HP is the so-called Hot Isostatic Pressing (**HIP)**. **Figure.7** displays the common features of this technique. Basically, a sample is inserted in the canister/crucible after being compacted by Cold Isostatic Pressing (CIP), Hydraulic Pressing or any other conventional pressing technique. The canister is, therefore, inserted in the chamber and sealed under vacuum to remove contaminants from the sintering environment. Later, an inert gas is pumped into the chamber, with a pressure reaching 30,000 Psi. The canister and the sample will shrink accordingly under the influence of the pressure and the heat, provided from the heating elements. Although the highest level of densification can be achieved uniquely by HIP, it is a time-consuming process. HIP is used also to recondition damaged samples [19] , as well as to close the remaining pores for samples sintered via other sintering technique.

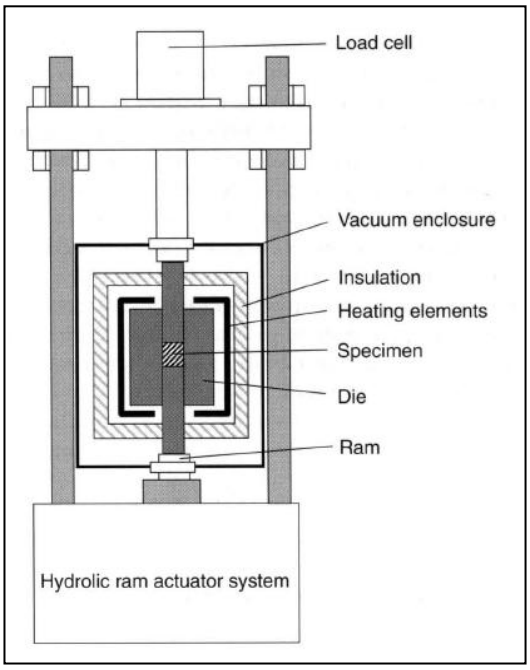

Figure 6 Schematic of HP technique [19]

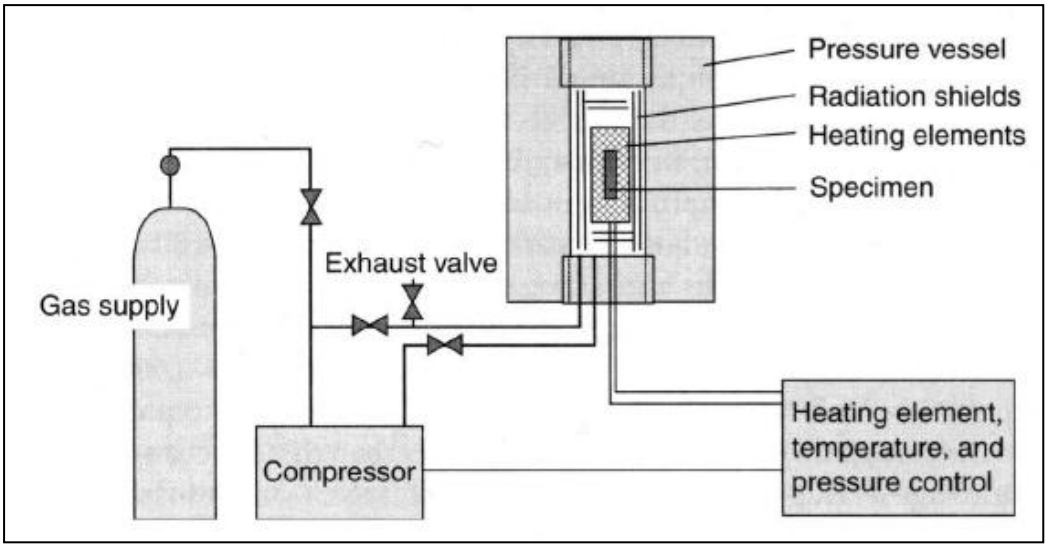

Figure 7 Schematic of the HIP technique [18]

2.3.2 SPARK PLASMA SINTERING

Spark Plasma Sintering (**SPS)** is a novel sintering technique, by which fully dense sample can be produced in very short duration of time, with the least consumption of power. The process was patented in Japan in 1960s, but it didn't spread well at that time because of the lack of technology and demanding applications. Later, in 1980s, a process called Plasma Activated Sintering (**PAS)** was developed for material research. Afterwards, people came up with the currently-known process as SPS, being an improved version of PAS [20].

Although the exact mechanism by which SPS works has not been well defined yet, one can provide the following demonstration. In conventional sintering techniques, as in HIP or HP, shrinkage is controlled by the applied external pressure and the joule heat supplied from the heating elements. However, in SPS, in the addition to the previously mentioned players, the on-off current nature is responsible of generating discharge of plasma between particles. Plasma leaves the particles at very high speed, to get attached to the neighboring particles. Within the discharge column, a field of impact pressure is generated, which removes any contaminates before plasma gets attached to the mating particle. In addition to that, a very localized high-temperature region is initiated momentarily between particles, which is responsible of particles surface melting and softening. **Figure.8** shows the major players in an SPS process.

Figure.9 displays the constituting components of an SPS machine. Basically, sample is poured in graphite die and pressed with graphite punches. Boron nitride spray is used to prevent any reaction between the die and the sample. The SPS process is controlled entirely by an automated system. An accompanied chiller is required to

control the chamber temperature. Graphite jackets are used to confine the heat to the graphite assembly

In addition to the above mentioned advantages of SPS, the high heating/cooling rates are extremely advantageous such that the formation of intermediate phases and grain growth is strictly controlled. Samples sintered by SPS secure high densification in limited processing time. The reproducibility and the reliability of SPS are deemed also as one of the advances in the sintering world , when compared to conventional sintering techniques. All of that makes SPS one of the promising sintering techniques to synthesize ceramic materials and other materials.

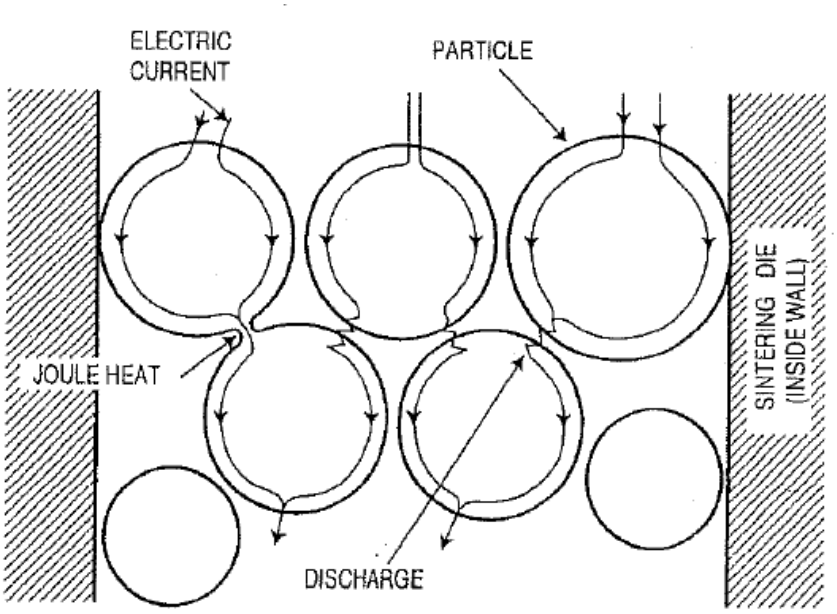

Figure 8 A schematic showing the pulsed current- induced events [20]

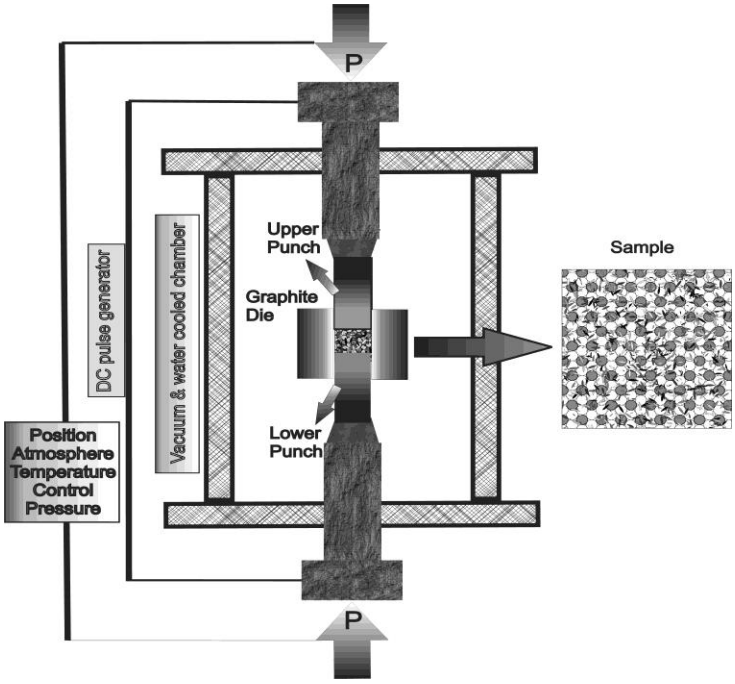

Figure 9 Schematic of SPS . **Image Courtesy of Dr. Abbas Hakeem**

2.3.2.1 APPLICATION OF SPS IN SiAlON SYSTEM

The first attempt to synthesize Si_3N_4 ceramics via SPS dates back to 1995 by Nishimura [21]. Since then, more work was performed, but not to the required extent. Up to the author's knowledge, the work done so far has not investigated widely the clear advantage of SPS, by performing an experimental comparison with the conventional techniques, such as HP and HIP, although several papers have been published on SPS to prepare SiAlON ceramics [22-27], as shown in **Figure.10**.

One exception to the above mentioned statement is found in [22] . A specific composition was sintered using HP and SPS to study the influence of the latter on the microstructural and mechanical behavior. HP was carried out at 1750 ^{o} C for 90 min using a pressure of 50 MPa. However, SPS was used at 1600 ^{o}C for 5 min holding time, under a pressure of 50 MPa. In both sintering processes, N_2 was kept as the controlling environment. Densification in both cases was complete, i.e. 100%. More importantly, α-SiAlON was secured up to 42% in the SPSed sample, while it disappeared entirely from the hot pressed sample. This is attributed to the high heating and cooling rates and the lower demanded holding time in SPS.

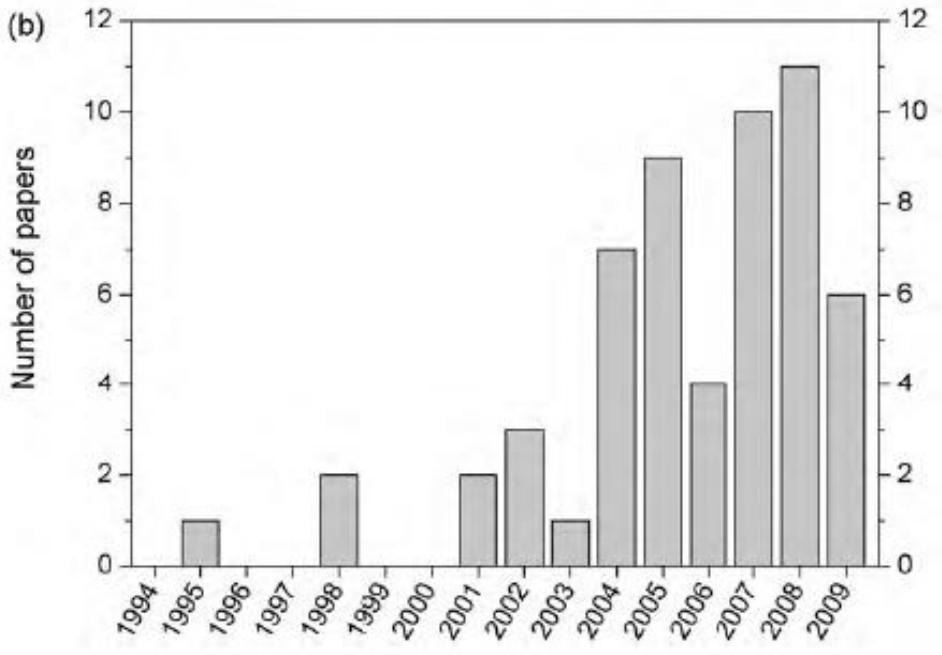

Figure 10 Histogram showing the number of publications of SPSed Si_3N_4 ceramics since 1995 [22]

2.4 EFFECT OF ADDITIVES ON THE PROPERTIES OF α-SiAlON

Initially, α-SiAlON was prepared purely without adding any sort of cations. Later, people started doping with Y to enhance the densification of α-SiAlON. Examining carefully the general formula of α-SiAlON reveals charge imbalance, which can be resolved by the incorporation of several cations, such as some of the lanthanides and alkaline earth elements.

As explained earlier, an α-SiAlON unit cell can accommodate two cations in normal conditions. The incorporation of lanthanides has been studied widely, taking advantage of their refractory properties [28]**.** It has been shown experimentally that the largest cation that can fit alone in α-SiAlON structure is Ce^{3+} [29]. Mandel has shown ,as well, that Lanthanum and Cerium can reside in the α-SiAlON lattice but along with Ca, due to their large ionic radii. He claimed that Ca plays two roles to achieve this goal; firstly it reduces the mean ionic radius of the dopants , and it enhances the stability of α-SiAlON by its lower valency [30]. **Table.2** lists several lanthanides and alkaline earth elements that are commonly doped in α-SiAlON ceramics.

TABLE 2 List of ionic radii of common lanthanides **and alkaline earth** elements **[28,30]**

Element	La	Ce	Nd	Sm	Dy	Yb	Y	Mg	Ca	Sr	Ba
Ionic Radius Å	1.06	1.03	0.99	0.97	0.9	0.858	0.89	0.72	0.99	1.26	1.35

Although Ln- α-SiAlON ceramics possess perfect mechanical properties, namely hardness and roughly flexure strength, their stability are still questionable. This can be attributed to the large radii they have, as shown in **Table.2**, which was reported to play a major role in α →β transformation [31] . In addition to the problem of the thermal instability, Cao showed the formation of crystal defects in La- α-SiAlON, which ultimately degrade the mechanical properties of the material [32] . For that, researchers started developing α-SiAlON ceramics based on alkaline earth elements.

Alkaline earth elements include Mg, Ca, Ba and Sr. The relevant ionic radii are listed in **Table.2**. Among these four additives, Ca seems to be the most attractive dopant in α-SiAlON system. Ruttan [33] listed several reasons behind this selection. Firstly, Ca can be easily manufactured from fly ash or from other resources. The residence of Ca in α-SiAlON lattice has been shown to cause the least distortion in the unit cell, which accounts for its large stability range in the phase diagram[34] . More interestingly, stable Ln- α-SiAlON can be accomplished when Ca is integrated in the composition[30,35].

Table.3 summarizes the development in SiAlON ceramics synthesis with Ca as the prime densifying additive. The scope of this table covers the studies related essentially to the mechanical properties and phase formation within SiAlON system. Studies preceded 1995 were excluded to keep the recency of data/ information.

Examining **Table.3** reveals the following aspects. SPS has been used rarely in synthesizing SiAlON ceramics, and instead, HP, HIP and Pressureless sintering (PLS) have been utilized in the field. Although PLS is less costly than its competitors, the drop in the densification, and thereafter the mechanical properties, shifted the focus to HP,

HIP and later to SPS. However, newly developed approaches applied PLS with proper design of the additives to compensate for the lose in the densification. The range of compositions covered in literature is pretty wide, starting with pure α-SiAlON and approaching the solubility limit of α-β-SiAlON and AlN-polytypoids. Nano starting powders have not been tested a lot, but rather micron and sub-micron materials have dominated the field in the last two decades. Ca additive has been used as a supporting cation for other additives of large-radii to improve their solubility and hence the stability.

TABLE 3 Literature Review of Ca-α-SiAlON

	Author	Title	Year	sample name	Starting composition	Powder Size	Synthesis Technique	Density	Hardness Hv_{10}	Fracture Toughness	Product phases	Comment
1	J. W. T. van Rutten etc.	Phase Formation of Ca-α-SiAlON by reaction sintering	1996	1	[m=1.6, n=0.8]	micron	Pressureless- 1700 ^{0}C- no holding - N_2	-	-	-	α-SiAlON , $CaSiO_3$	
2	Catherine L. Hewett etc.	Phase Relationships and Related Microstructural Observations in the Ca-Si-Al-O-N System	1998	0510	m = first two numbers/100 n = the second two numbers/100	micron	Pressuerless- 1800 ^{0}C- 2h - N_2	2.73	-	-	α-SiAlON, β-SiAlON	
				0515				2.94	-	-	α-SiAlON, β-SiAlON	
				0520				2.93	-	-	α-SiAlON, β-SiAlON , 12H	
				0530				2.83	-	-	α-SiAlON, β-SiAlON , 12H	
				1020				2.84	-	-	α-SiAlON, β-SiAlON , 12H	
				1030				2.8	-	-	α-SiAlON, β-SiAlON , 12H	
				1520				2.89	-	-	α-SiAlON, 21R	
				1535				2.74	-	-	α-SiAlON, β-SiAlON , 12H	
				2020				2.85	-	-	α-SiAlON, 21R	
				2030				2.82	-	-	α-SiAlON, 21R	
				2520				2.82	-	-	α-SiAlON, 27R	
				2530				2.8	-	-	α-SiAlON, 21R, 27R	
				3022				2.67	-	-	α-SiAlON, 33R	
				0015				2.95	-	-	β-SiAlON	
				0025				2.91	-	-	β-SiAlON , 15R	
				1616				2.88	-	-	α-SiAlON	
				1616E				3.17	-	-	α-SiAlON	
				0510E				2.81	-	-	α-SiAlON, β-SiAlON	
				0520E				2.93	-	-	α-SiAlON, β-SiAlON , 12H	
				1020E				2.93	-	-	α-SiAlON, 21R	
				1025E				2.94	-	-	α-SiAlON, 12H	
				1035E				2.9	-	-	α-SiAlON, β-SiAlON , 12H	
				1320E				2.89	-	-	α-SiAlON, 21R	
				1330E				2.9	-	-	α-SiAlON, 12H	
				1530E				2.88	-	-	α-SiAlON, 21R	
				2017E				2.91	-	-	α-SiAlON	
				2020E				2.83	-	-	α-SiAlON, 21R	
				2030E				2.93	-	-	α-SiAlON, 21R	
				2035E				2.68	-	-	α-SiAlON, 21R	
				2318E				2.71	-	-	α-SiAlON	
				3021E				2.53	-	-	α-SiAlON, 33R	
				3030E				2.8	-	-	α-SiAlON, 33R	
				3035E				2.81	-	-	α-SiAlON, 33R	
3	Wenguang Zhang etc.	Tribological behaviors of (Ca, Mg)–Sialon under lubricating of polyols	1998	1	$(Ca,Mg)_{0.6}Si_{10.2}Al_{18}O_{0.6}N_{15}$	-	HP-1750 ^{0}C-1h-	3.2	20.21	5.5	-	

	Author	Title	Year	sample name	Starting composition	Powder Size	Synthesis Technique	Density	Hardness Hv_{10}	Fracture Toughness	Product phases	Comment
4	Wang etc.	characteristics of ca-alpha sialon	1999	C30	[x=0.3]	micron	HP-1750°C-1h-20MPa-N_2	3.02	1886	4.4	α-SiAlON, β-SiAlON , α-Si_3N_4	
				C60	[x=0.6]			3.17	1975	5.1	α-SiAlON , α-Si_3N_4	
				C100	[x=1]			3.21	1815	5.6	α-SiAlON , 21R	
				C140	[x=1.4]			3.21	2767	5.5	α-SiAlON , 21R	
				C160	[x=1.6]			-	1638	5.6	α-SiAlON , 21R	
				C180	[x=1.8]			-	1550	5.8	α-SiAlON , AlN, 21R	
5	Mandal etc.	alpha to beta SialON Trnasformation in Ca containing alpha SiAlON Ceramics	1999	HM1	**intended** : 100% α	micron	HP-1800°C-1h	3.2	-	-	α-SiAlON	
				HM5	**intended** : 100% α [Ca+ Nd]			3.35	-	-	α-SiAlON, β-SiAlON , SrO-$1.3Al_2O_3$ -$0.7Si_2N_2O$	
				HM6	**intended** : 100% α [Ca+ Sr]			3.26	-	-	α-SiAlON , α-Si_3N_4	
				HM8	**intended** : 90% α , 10%β			3.21	-	-	α-SiAlON	
				HM9	**intended** : 50% α , 50%β			3.19	-	-	α-SiAlON, β-SiAlON	
				HM10	**intended** : 55% α , 35%β, 10%glass			3.13	-	-	α-SiAlON, β-SiAlON , $Ca_2Al_2SiO_7$	
6	Wang etc.	Formation behavior of multi-cation SiAlON containing Ca and Mg	1999	1	[x=0.3]	micron	HP-1750°C-1h-20MPa-N_2	3.02	1886	4.4	α-SiAlON, β-SiAlON , α-Si_3N_4	
				2	[x=0.6]			3.17	1975	5.1	α-SiAlON, α-Si_3N_4	
				3	[x=1]			3.21	1815	5.6	α-SiAlON, 21R	
				4	[x=1.4]			3.21	1767	5.5	α-SiAlON, 21R	
				5	$[(Ca+Mg)_{12-x}Si_{12-x}Al_{3x}O_xN_{16-x}][x=0.3]$			3.09	1969	4.9	α-SiAlON, β-SiAlON , α-Si_3N_4	50%Mg, 50%Ca
				6	$[(Ca+Mg)_{12-x}Si_{12-x}Al_{3x}O_xN_{16-x}][x=0.6]$			3.2	2021	5.5	α-SiAlON, α-Si_3N_4	
				7	$[(Ca+Mg)_{12-x}Si_{12-x}Al_{3x}O_xN_{16-x}][x=1]$			3.22	2051	5.6	α-SiAlON, MgAlN-polytypoid	
				8	$[(Ca+Mg)_{12-x}Si_{12-x}Al_{3x}O_xN_{16-x}][x=1.4]$			3.23	1831	5.6	α-SiAlON, MgAlN-polytypoid	
7	Mandal	New Development in α-SiAlON Cermics	1999	1	[Ca+Nd] [m=1.25, n=1.15]	micron	Pressureless-1800°C-2h	94.80%	19.76	3.96	α-SiAlON, 21R	
				2	[Ca+Ce] [m=1.25, n=1.15]			98.50%	-	-	α-SiAlON, 21R	
				3	[Ca+La] [m=1.25, n=1.15]			97%	-	-	α-SiAlON, 21R	
				4	[Ca+Sr] [m=1.25, n=1.15]			94.50%	-	-	α-SiAlON, 21R	
				5	[Ca+Nd] [m=1.2, n=2]			100%	19.3	6.31	α-SiAlON, 21R	
				6	[Ca+Ce] [m=1.2, n=2]			100%	-	-	α-SiAlON, 21R	
8	Wang etc.	Effect of dual elements (Ca,Mg) and (Ca, La) on cell dimensions of multi-cation α-SiAlON	2000	CM1	[x=0.3]	micron	HP-1750°C-1h-20MPa-N_2	-	-	-	α-SiAlON, β-SiAlON , α-Si_3N_4	$Ca_{0.15}Mg_{0.15}$
				CM2	[x=0.6]			-	-	-	α-SiAlON, α-Si_3N_4	$Ca_{0.3}Mg_{0.3}$
				CM3	[x=1]			-	-	-	α-SiAlON, MgAlN-polytypoid	$Ca_{0.5}Mg_{0.5}$
				CM4	[x=1.4]			-	-	-	α-SiAlON, MgAlN-polytypoid	$Ca_{0.7}Mg_{0.7}$
				CL1	[x=0.6]			-	18.48	5.5	α-SiAlON	$Ca_{0.42}La_{0.18}$
				CL2	[x=1]			-	16.67	4.9	α-SiAlON , gehlnite	$Ca_{0.7}La_{0.3}$
				C2	[x=0.6]			-	18.79	4.7	-	
				C3	[x=1]			-	17.94	5.3	-	

	Author	Title	Year	sample name	Starting composition	Powder Size	Synthesis Technique	Density	Hardness Hv_{10}	Fracture Toughness	Product phases	Comment
9		Control of grain morphology in Ca-α-SiAlON ceramics by changing the heating rate	2000	1	[m=1.6, n=1.6]	micron	Pressuerless-1800°C-1h	3.18	1782	4.5	α-SiAlON	Heating rate=20
				2	[m=1.6, n=1.6]			3.16	1798	5.4	α-SiAlON	Heating rate=60
10	Wood etc.	Phase relationships and microstructures of Ca and Al-rich α-sialon ceramics	2000	CA2040	[m=2, n=4]	micron	Pressureless-1800°C-2h-N_2	2.69	-	-	α-SiAlON - 12H - 21R	
				CA2050	[m=2, n=5]			2.57	-	-	α-SiAlON - 12H - 21R	
				CA3040	[m=3, n=4]			2.673	-	-	α-SiAlON - 21R -27R	
				CA3050	[m=3, n=5]			2.529	-	-	α-SiAlON - 21R -27R	
				CA4040	[m=4, n=4]			2.838	-	-	α-SiAlON - AlN	
				CA4050	[m=4, n=5]			-	-	-	α-SiAlON - AlN	
				CA5040	[m=5, n=4]			-	-	-	α-SiAlON - AlN	
				Ca5050	[m=5, n=5]			-	-	-	AlN	
11	Ya-Wen Li etc.	Effect of processing on toughness of Ca-α-sialon ceramics	2000	C60	[x=0.6]	micron	HP-1750°C-1h-N_2	-	-	4.2	α-SiAlON	
				C100	[x=1]		HP-1750°C-1h-N_2	-	-	4.9	α-SiAlON - AlN polytypoids	
				C180	[x=1.8]		Pressuerless-1800°C-2h	-	-	-	α-SiAlON - AlN polytypoids	
12	Ya-Wen Li etc.	Phase formation and microstructural evolution of Ca-α-sialon using different Si_3N_4 starting powders	2000	C180A	1.8CaO:2.2Si_3N_4 :5.4AlN	micron	Pressuerless-1800°C-2h-N_2	2.8	-	-	α-SiAlON - AlN polytypoids	Si_3N_4 size=0.4μ
				C180B				2.78	-	-	α-SiAlON - AlN polytypoids	Si_3N_4 size=0.6μ
				C180C				2.6	-	-	α-SiAlON - AlN polytypoids	Si_3N_4 size=0.5μ
13	Ya-Wen Li etc.	Effect of additives on microstructure of Ca-α-sialon	2001	C60	[x=0.6]	micron	HP-1750°C-1h-20MPa-N_2	-	18.79	4.2	α-SiAlON, α-Si_3N_4	
				C60L5				-	18.02	4.6	α-SiAlON	
				C60L10				-	16.92	4.8	α-SiAlON	
				C60M5	5 wt% MgO			-	17.19	5.1	α-SiAlON , $MgAlSiN_3$	
				C60M10	10 wt% MgO			-	15.33	5.3	α-SiAlON , $MgAlSiN_3$	
				C60R5	5 wt% La_2O_3			-	18.2	4.5	α-SiAlON , Unknown phase	
				C60R10	10 wt% La_2O_3			-	16.67	4.8	α-SiAlON , Unknown phase	
14	Y. Zhang etc	Influence of microstructure on the erosive wear behaviour of Ca-α-sialon materials	2001	CA1005[AS]	[m=1, n=0.5]	micron	HP-1800°C-4h-N_2 HT: 1300°C-12h-N_2	3.055	16.4	4.5	α-SiAlON	
				CA1005[HT]				3.033	15.5	4.6	α-SiAlON	
				CA2613[AS]	[m=2.6, n=1.3]			3.15	15	5.4	α-SiAlON - 2H	
				CA2613[HT]				3.15	14.7	5.5	α-SiAlON - 2H - gehlenite	
				CA3618[AS]	[m=3.6, n=1.8]			3.25	14.5	5.7	α-SiAlON - 2H - AlN polytypoid	
				CA3618[HT]				3.2	14.1	5.9	α-SiAlON - 2H - AlN polytypoid- gehlenite	
15	A.A. Kudyba-Jansen etc.	Ca-α/β-sialon ceramics synthesised from fly ash—preparation, characterization and properties	2001	P	[m=1.53, n=0.56]	micron		97%	12.8	6.5	β-SiAlON	
				Sc	[m=1.17, n=3.41]			97%	14.8	9	β-SiAlON	
				M1	[m=0.78, n=3.52]		Slip Casting	91%	11.1	7.1	α-SiAlON , β-SiAlON , 12H , 21R	
				M2	[m=1.59, n=2.92]			99%	20.3	8.9	α-SiAlON , β-SiAlON , 12H, $Y_3AlSi_2O_7N$, $YSiO_2N$	
				M3	[m=1.56, n=2.83]			98%	17.7	8	α-SiAlON , β-SiAlON , 12H , 21R	

	Author	Title	Year	sample name	Starting composition	Powder Size	Synthesis Technique	Density	Hardness Hv_{10}	Fracture Toughness	Product phases	Comment
16	Ya-Wen Li etc.	Formation behavior, microstructure and mechanical properties of multi-cation α-sialons containing calcium and neodymium	2001	ND100	[x=1]	micron	HP-1750°C-1h-20MPa-N_2	3.51	15.87	4.2	α-SiAlON-Melilite - AlN polytypoid	Ca:Nd = 0:1
				CN3070				3.5	16.36	4.6	α-SiAlON-Melilite - AlN polytypoid	Ca:Nd =0.3:0.7
				CN5050				3.42	16.9	5.1	α-SiAlON-Melilite - AlN polytypoid	Ca:Nd = 0.5:0.5
				CN7030				3.36	18.79	4.8	α-SiAlON-Melilite - AlN polytypoid	Ca:Nd = 0.7:0.3
				CA100				3.21	18.21	4.9	α-SiAlON - AlN polytypoid	Ca:Nd = 1:0
17	Zong-Han Xie and Mark Hoffman	Microstructural Tailoring and Characterization of a Calcium α -SiAlON Composition	2002	EQ	[m=2.6, n=1.3]	micron	1550°C/0.5 hr HPed 25 MPa 1600°C/0.5 hr HPed 25 Mpa	3.19	-	3.7	α-SiAlON	
				EE			1550°C/0.5 hr HPed 25 MPa 1700°C/0.5 hr HPed 25 Mpa	3.2	-	6.1	α-SiAlON	
				EL			1750°C/1.0 hr Pressureless 1750°C/1.0 hr HPed 25 Mpa	3.21	-	7.5	α-SiAlON	
18	Y. Zhang, Y. and B. Cheng	Microstructural design of Ca α-sialon ceramics: effects of starting compositions and processing conditions	2003	CA1005	[m=1.3, n=1.8]	micron	PLS-1800°C-4 h	3.05	16.4	4.5	α-SiAlON	
				CA1005F			PLS - 1800 °C-3 h+HP-1700°C -1h	3.158	18.6	4.3	α-SiAlON	
				CA1005C			PLS -1800 °C-8 h+HP- 1700°C-1 h	3.141	19.1	4.7	α-SiAlON	
				CA2613			PLS-1800°C-4 h	3.16	15	5.4	α-SiAlON- 33R	
				CA2613F			HP-1550°C-0.5 h+HP-1600 °C-0.5 h	3.189	16.2	5	α-SiAlON- AlN poltypoid	
				CA2613C			PLS-1800°C-3 h+HP-1700°C-1 h	3.208	18.3	5.6	α-SiAlON- 33R	
				CA3618			PLS-1800°C-4 h	3.205	14.5	5.7	α-SiAlON- AlN poltypoid	
19	Guanghua Liu and etc.	Fabrication of (Ca + Yb)- and (Ca + Sr)-stabilized α-SiAlON by combustion synthesis	2006	YS	$Yb_{0.5}Si_{9.5}Al_{2.5}O_{1.0}N_{15}$	micron	combustion synthesis - 1 min-1800°C -N_2	-	-	-	α-SiAlON - β-SiAlON - Si - AlN polytypoid - Yb_2SiO_2	
				CYS1	$Yb_{0.4}Ca_{0.15}Si_{9.5}Al_{2.5}O_{1.0}N_{15}$			-	-	-	α-SiAlON	
				CYS2	$Yb_{0.3}Ca_{0.3}Si_{9.5}Al_{2.5}O_{1.0}N_{15}$			-	-	-	α-SiAlON	
				SS	$Sr_{0.8}Si_{8.8}Al_{3.2}O_{1.6}N_{14.4}$			-	-	-	α-SiAlON - β-SiAlON - Si - AlN polytypoid	
				CSS	$Sr_{0.4}Ca_{0.4}Si_{8.8}Al_{3.2}O_{1.6}N_{14.4}$			-	-	-	α-SiAlON - β-SiAlON - Si - AlN polytypoid	

	Author	Title	Year	sample name	Starting composition	Powder Size	Synthesis Technique	Density	Hardness Hv_{10}	Fracture Toughness	Product phases	Comment
20	Guanghua Liu and etc.	Preparation of Ca a-SiAlON powders with rod-like crystals by combustion synthesis	2006	CS1610	[m=1.6, n=1]	micron	combustion synthesis - 1800°C -N2	-	-	-	α-SiAlON	
				CS1616	[m=1.6, n=1.6]			-	-	-	α-SiAlON - Si - AlN polytypoid	
				CS1616-2	[m=1.6, n=1.6]			-	-	-	α-SiAlON - Si - AlN polytypoid	CaO was used instead of $CaCO_3$
				CS2416	[m=2.4, n=1.6]			-	-	-	α-SiAlON - Si	
21	K. L. Smirnov	Spark Plasma Sintering of SiAlON Ceramics	2009	1	$Ca_{0.5}Si_{11.5}Al_{1.5}O_{0.5}N_{15.5}$	Sub-micron	SPS-1650°C-50MPa-4min (avg.) -VAC	3.04	12.8	-	α-SiAlON, β-SiAlON , α-Si_3N_4	
				2			SPS-1700°C-50MPa-4min (avg.) -VAC	3.11	19.1	-	α-SiAlON, β-SiAlON , α-Si_3N_4	
				3				3.07	18.7	-	α-SiAlON, β-SiAlON , α-Si_3N_4	+ 8% α-SiAlON powder
				4			SPS-1750°C-50MPa-4min (avg.) -VAC	3.13	19	-	α-SiAlON, β-SiAlON	
				5			SPS-1800°C-50MPa-4min (avg.) -VAC	3.13	19.1	-	α-SiAlON, β-SiAlON	
22	Yanbing Cai	Synthesis and Characterization of Nitrogen-rich Calcium a-Sialon Ceramics **[Thesis Dissertation]**	2009		[x=0.4]	Nano & micron	HP - 1800°C -4 h-35MPa	-	22	5.4	α-SiAlON - β-Si_3N_4 - $CaSiAlN_3$ -AlN polytypoid	other results can be seen in the Thesis
23	Mikinori Hotta and etc	Preparation of Ca-α SiAlON hollow spheres by carbothermal reduction–nitridation of $CaO–Al_2O_3–SiO_2$ glass	2011	1	[x=0.3]	micron	Nitridation in Normal Furnace - 2 h- 1450°C -N2	-	-	-	α-SiAlON - β-SiAlON-AlN	
				2	[x=0.8]			-	-	-	α-SiAlON - β-SiAlON-AlN	
				3	[x=1]			-	-	-	α-SiAlON - β-SiAlON-AlN	
				4	[x=1.4]			-	-	-	α-SiAlON - AlN	
24	Hong-shun Hao and etc.	Synthesis and performance of Ca-α/β-SiAlON composites from tailings	2014	1	See paper	micron	PLS-1520°C-6h	-	Hv_5=11.2	4.8	α-SiAlON - β-SiAlON	

2.5 FORMATION OF ELONGATED α-SiAlON GRAINS

Typically, α-SiAlON forms in equiaxed grains, which are associated with high hardness values. However, this takes place usually at the expense of fracture toughness. A novel way to capture both properties lies in the formation of elongated α-SiAlON grains, i.e. having high aspect ratio. It has been reported that the elongation increases as the x value increases in the general formula of α-SiAlON ($M_xSi_{12-(m+n)}Al_{(m+n)}O_nN_{16-n}$) [36]. This is understood in terms of the amount of the glassy phase, which follows the same trend with x. However, the viscosity of the liquid phase should be considered as well, since viscous liquid phase may retard the process of elongation, if the amount of liquid present is small [36].

The basic mechanism by which α-SiAlON elongation takes place is of interest. Wen [34] Stated that the growth of α-SiAlON grains in width is more controlled by diffusion than the length. Consequently, if the liquid phase is highly viscous, then diffusion will slow down and isotropic growth is hindered. This results in the formation of elongated morphology of α-SiAlON. This seems to be a bit contradictory with [36], however, the conclusion of Wen in [36] was incorrect, since he combined the effect of the amount of the glassy phase and its viscosity, while the playing factor was the insufficient amount of the glassy phase, which can prevent the anisotropic growth whether the viscosity effect is present or not.

A different route to develop elongated α-SiAlON grains was proposed by Zhang [37] , in which high heating rate (60^{o}C/min) resulted in α-SiAlON with high aspect ratio. However, the lower heating rate (20^{o}C/min) developed larger amount of α-SiAlON, which

can be explained in term of the glassy phase. In case of low heating rate, the liquid phase was consumed entirely during the heating stage to form α-SiAlON. In contrary, and in the case of high heating rate, there was sufficient amount of liquid phase at the sintering temperature, which induced the anisotropic growth.

2.6 GLASSY PHASE CRYSTALLIZATION THROUGH POST-HEAT TREATMENT

The involvement of densifying additives in the structure of α-SiAlON has been shown to participate in the formation of the grain boundary phase, which ultimately derives the mechanical response of the ceramic. At low temperatures, the amount of the grain boundary phase, which is amorphous in nature, has the prominent role in altering the mechanical properties. Sun *et al.* [38] has shown the direct relation between the increase in (Y:Al) ratio and the fracture toughness of β-Si_3N_4 due to the extensive debonding between the grains. Another example of the impact of the grain boundary phase on the ceramic properties is the effect of increasing nitrogen on Young's modulus, microhardness and glass transition temperature, if (M:Si:Al) ratio is kept constant [39,40]. However, as the operation temperature rises up, approaching the softening temperature of the glassy phase, the form and the composition of the grain boundary phase becomes influential in the game. Lange *et al.* showed that for Si_3N_4 ceramics, slight stress is needed at the softening temperature of the glassy phase to initiate subcritical cracks and sliding creep at the grain boundary, which ultimately results in a complete failure [41]. Similar

conclusion has been presented by Iskoe *et al.* with regard to the effect of impurities present in the glassy phase in slackening the creep and strength of Si_3N_4 ceramics[42].

This issue urges to establish a way for synthesizing Si_3N_4 ceramic with no intergranular glassy phase, however this seems to be unattainable since the starting materials are covered by oxide layers [7-9]. Nevertheless, several approaches were experimented in the last two decades to either lessen the amount of the glassy phase or to convert it to more crystalline/refractory form. Jasper and Lewis tried replacing MgO by Y_2O_3, which possess higher solidus temperature, to raise the softening temperature of the resultant glassy phase [43]. 150^oC increase in the softening temperature of the glassy phase was noticed after the aforementioned replacement, but this is still away from the requirement of normal operation conditions of Si_3N_4 ceramics.

Another approach which has been investigated a lot is the combination of selected densifying additives, such as Y_2O_3 along with La_2O_3 or Nd_2O_3, and the use of powerful sintering process such as HIP. Through this coupling, Naoto Hirosaki *et al.* succeeded in getting an operation temperature of 1350^oC with retained mechanical strength at high temperatures[44]. However, this increase is still far less than the decomposing temperature of Si_3N_4 (1873^oC), that is recognized as a measure of the performance quality of these ceramics.

The more recent and efficient approach is the post-heat treatment, that was purposed to convert, fully or partially, the grain boundary glassy phase into a crystalline phase with higher level of refractoriness. It has been established that complete crystallization of the grain boundary sounds impossible [45-47]. However, a certain degree of crystallization is

required to optimize the mismatch between the grain boundary phase and other phases. The crystallization of the intergranular phase results usually in negative volume change, which, in turn, produces residual tensile stress at multi-grain junctions. This ultimately enhances the fracture toughness through the intergranular crack propagation mechanism [48]. Besides, the chemistry of the resultant crystalline phase in the grain boundary is of major concern. The availability of refractory phase in the grain boundary is directly related to the incorporated cation chemical nature and the N:O ratio. This places a challenge in designing the chemical composition and choosing the right parameters of the preceding treatment.

Mandel *et al.* examined the effect of vacuum heat-treatment of sintered Si_3N_4 with MgO additive. The intension was to tear out the volatile metal oxide, which is accompanied with relative shrinkage, and thus to minimize its influence on the mechanical properties at high temperatures [49,50]. The good thing about this treatment is its applicability on SiAlON ceramics, with the exception of its limited capability of removing entirely the intergranular glassy phase, since Al-rich phases present in SiAlON materials require higher decomposition temperatures. Another design of the post-heat treatment performed by Mandel *et al.* differed from the preceding treatment in a way that hydrogen was replacing the vacuum as an agent for removing metal oxides. In fact, hydrogen helped to form Si_2N_2O, which shows comparable refractoriness to Si_3N_4, for which the operation temperature can be elevated to 1450^{o}C [51].

The formation of pores during devitrification below the eutectic point and the limited control on the resultant phase have pushed researchers to find out an alternative design of the post heat treatment. To crystallize specific nitrogen-rich phases, heat treatment should

be carried out above the eutectic point of the system. One example of these phases is nitrogen melilite with the corresponding formula $M_2Si_{3-x}Al_xO_{3+x}N_{4-x}$, in which M stands for either Y or Ln [52,53]. A side from this, Ramesh *et al* proposed another design for the post-heat treatment to optimize the nucleation of the grain boundary crystals and, subsequently, their growth, in which he adopted two-stage glass- ceramic heat treatment process [54].

CHAPTER 3

MATERIALS AND EXPERIMENTAL PROCEDURE

3.1 RAW MATERIALS

Table.4 displays the starting materials in powder form with their corresponding specifications. Nano powders were utilized in most of the work carried out for this project. Micron-sized powders were used limitedly for specific precursors, such as Al and Si metals.

TABLE 4 Chemical Starting Materials

UN	Chemical Formula	Company	Size	
			mesh	other
1	Amp-Si_3N_4	Chempur		20 nm
2	α-Si_3N_4	SN-10 Japan		150 nm
3	β-Si_3N_4	Sigma Aldrich	325	
4	SiO_2	Sigma Aldrich		10-20 nm
5	Al_2O_3	Chempur		150 nm
6	CaO	Sigma Aldrich		< 160 nm
7	BaO	Sigma Aldrich		< 100 nm
8	AlN	Sigma Aldrich		150 nm
9	Al	Loba Chemie(India)	325	
10	Si	Loba Chemie(India)	200	

3.2 CHEMICAL COMPOSITION

The whole work is based on the general formula of α-SiAlON, that is $M_x Si_{12-(m+n)} Al_{(m+n)} O_n N_{16-n}$, in which M stands for Ca, Mg and Ba. This does not mean the resultant sintered ceramic would encompass only α-SiAlON, since phase transformation takes place on part of alpha to convert it to β-SiAlON and other AlN-polytypoids. Phase diagrams acted as good aids to roughly estimate the expected phases after sintering. However, the absence of phase diagrams that include the effect of nano precursors and rapid consolidation processes made our estimations somehow difficult. Due to the variation in the chemical compositions throughout this study, the corresponding composition is mentioned at the beginning of each section in the results chapter.

To establish a specific composition for α-SiAlON, we selected m and n values and substituted them in the general formulas from $M_x Si_{12-(m+n)} Al_{(m+n)} O_n N_{16-n}$, based on which the chemical reactants were chosen. The chemical equation was then established and balanced in mole ratios. Utilizing molar weights of the adopted reactants, the required weight of each reactant was calculated based on the total mass of the product.

3.3 MIXING THE POWDER MIXTURES

After weighing the respected precursors in powder form, mixing was carried out using ultrasonic probe sonicator *(Model VC 750, Sonics, Connecticut,USA)* in ethanol medium

for 20 minutes, unless stated otherwise. To keep the mixing process clean, ethanol was used as a mixing medium.

3.4 SINTERING TECHNIQUES

Powder mixtures were dried in a standard drying oven for 12 hours to remove ethanol. 5 grams samples were weighed and poured into 20 mm diameter graphite dies. Spark plasma sintering (*Type HP D-50, FCT Systeme, Rauenstein, Germany*) was performed at different temperatures for 30 min, unless stated otherwise. The sintering environment was either vacuum or nitrogen, depending on the reaction requirements. The uniaxial pressing was fixed to 16 KN, which corresponds to a pressure of about 50 MPa. Heating rate of 100°C/min was adopted to avoid formation of intermediate phases. To freeze the formed structure, samples were then rapidly cooled down to room temperature. Other details are mentioned in the corresponding sections.

3.5 CHARACTERIZATION TECHNIQUES

3.5.1 SAMPLE PREPARATION

Samples were cleaned carefully from graphite to measure their densities. Afterwards, samples were mounted (*Evolution, IPA 40 Remet, Bologna, Italy*) in transparent polymeric powder to help handling the sample for subsequent processing. Diamond grinding wheels were utilized in automatic grinder (*Automet 300 Buehler grinding machine*), following the standard sequence; 74, 40, 20 and 10µm particle size. Later, polishing wheel was used with a series of diamond polishing suspensions, starting by 9 µm and ending up with 0.25 µm, passing through 6, 3 and 1µm diamond

suspensions. To reveal the microstructure, several etchants were adopted, including concentrated and diluted HF and molten NaOH at 400^{o}C. For SEM examination, samples were gold-coated, either by the sputter coater *(Model Q150T, Quorum Technologies, UK)* or by the metal evaporation coating machine.

3.5.2 ARCHIMEDES METHOD FOR DENSITY MEASUREMENT

Density measurement plays an essential role in qualifying the sintered samples. A typical way to evaluate the density is to use the rule of mixture to evaluate the theoretical density, and thereafter the densification, through the consideration of the individual densities of the resultant phases and their weight ratios after sintering. However, individual phases densities are not often available, and hence calculating the theoretical densities was not feasible. To overcome this issue, we evaluated the density of the sintered samples using Archimedes' principle and compared it to density values of similar compositions in literature and to the density of Si_3N_4, being the prime precursor. **Equation (1)** represents the general formula to calculate the density for the sintered samples.

$$\rho = \frac{A}{A-B}(\rho_0 - \rho_L) + \rho_L$$

Equation (1)

$$\rho_L = 0.0012\ g/cm^3$$
$$\rho_0 = 1\ g/cm^3$$

A and B represent the weight of sample in air and liquid, respectively. ρ_o is the liquid density which is water in our case, while ρ_L stands for air density. Units of weights should be kept in grams and density in g/cm^3.

3.5.3 PHASE ANALYSIS

X-ray diffraction technique was used extensively in this study to identify the phases in the sintered samples. A *Rigaku MiniFlex X-ray diffractometer* (Japan) was utilized, with a wavelength of the copper target $K_{\alpha 1}$ =0.15416 nm. The accelerating voltage and the tube current were 30 kV and 10 mA, respectively. A sampling width of 0.02 degree and scanning speed of 2 degree/mins were adopted throughout the study in an attempt to reduce the noise and produce qualified patterns. To fit the patterns to the formed phases, PDXL program was used with very large and up-to-date database.

3.5.4 MICROSTRUCTURAL ANALYSIS

Filed-emission scanning electron microscope (*FESEM, Lyra 3, Tescan, Czech Republic*) was used to study the resultant microstructures of the sintered samples. The electron gun voltage was varied between 20-30 KeV to get the best possible contrast. Both secondary and backscattered imaging modes were utilized in this study. An accompanied energy dispersive spectrometer (*EDS, Oxford Inc., UK*) was of great help in linking the XRD phases with their corresponding morphologies.

3.5.5 MECHANICAL PROPERTIES

Sintered samples were tested for their hardness and fracture toughness. A load of 98 N force was used in this study, as commonly utilized in literature [15,34,35]. A universal hardness tester (*Zwick-Roell, ZHU250, Germany*) with diamond pyramid indenter was used to get the depression diagonals of the polished samples. Vickers hardness can be calculated in GPa using the following formula

$$HV_{10} = \frac{1.854}{d^2} \ (9.81\times10^{-3}) \qquad \textbf{Equation (2)}$$

in which d represents the average of the two diagonal lengths in mm.

Fracture toughness testing shows wide variation in the field of hard materials. Single-Edge Notched Beam (SENB) and Single-edge V-Edge Notched Beam (SEVNB) are two leading techniques to evaluate fracture toughness, however none of these has been commercially standardized. The requirement of having samples free of residual stresses prior to testing places a major constraint in applying SENB and SEVNB [55]. Another limitation in these techniques concerning our samples is the difficulty of initiating a precrack with the specified size. Further, the field of SiAlON has adopted the Indentation Method (IM) [56,57]. Hence, we decided to use IM to offer an easy comparison with the values obtained from literature. Several formulations have been introduced in the field of hard ceramics to evaluate fracture toughness using typical hardness indentation. Evan's equation [58] is one of the adopted relations in the SiAlON field, which is given as follows :

$$K_{IC} = 0.48\left(\frac{MCL}{d/2}\right)^{-1.5}\left(\frac{HV_{10}\sqrt{d/2}}{3}\right)$$ **Equation (3)**

MCL stands for the maximum crack length initiated from the indentation and d is the average depression diagonal.

CHAPTER 4

RESULTS AND DISCUSSION

4.1 PHASE EVOLUTION OF Ca-α-SiAlON

4.1.1 INTRODUCTION

This part of the work intends to investigate the phase formation as a function of the sintering temperature and to determine the associated microstructural development. **Table.5** displays the examined composition, which was chosen to be $CaSi_6Al_6O_4N_{12}$, having more oxygen than many of the reported compositions in the literature. Powder mixture was mixed via Ultra-probe sonicator for 1 hour to eliminate any effect of aggregation/agglomeration of powder precursors. Differential scanning calorimeter (DSC) was used to point out the temperatures at which exothermic reaction took place. DSC was carried out at a heating rate of 50^{o}C/min in Ar environment Subsequently, SPS was carried out at 1000, 1100, 1200, 1300 and 1400 ^{o}C, in a pressure of 50 MPa. The holding time was fixed to 1 hour to obtain the stable phases in sufficiently grown grains. SPS heating rate was 100^{o}C/min to avoid intermediate phase formation.

TABLE 5 Chemical powder reactants in w.t %

Sample Name	CaO	Al_2O_3	α -Si_3N_4	AlN
3-α	9.31	16.92	46.56	27.21

4.1.2 DIFFERENTIAL SCANNING CALORIMETRY

Figure.11 shows the DSC curve of the investigated sample, in which several exothermic peaks are indicated by red arrows. Typically, samples mixed in wet environments comprise moisture and vapor, depending on the mixing solution. In our standard procedure, ethanol was used as a stable mixing medium. Thus, and even after drying for 12 hours in furnace, little trace of ethanol is expected to be present in the dried sample. Peaks at approximately 150 and 300 ^{o}C can be attributed to the release of ethanol and water vapor contained in the sample.

When $CaCO_3$ is used as the source of Ca, the usual practice adopted in the field is to calcinate the sample at a temperature between 800-900 ^{o}C to convert $CaCO_3$ to CaO before the start of solution-reprecipitation process. In our case, we used CaO directly to avoid extra holding stages in the sintering process. However, and during mixing, CO_2 can react easily with CaO to form $CaCO_3$ which has been confirmed by the work of our colleagues in the lab in which the weight of the mixed sample increased when compared to the un-mixed powder mixture. Hence, the endothermic peak appearing at 800^{o}C is understood as the decomposition of $CaCO_3$ into CaO.

The peaks of interest are expected to show up in the temperature range 1000-1500^{o}C. However, and except a minor peak at 1350^{o}C and a major one at 1500^{o}C, no exothermic peaks to indicate the reprecipitation and phase transformation processes. To resolve this issue, the first and second derivatives were evaluated , as displayed in **Figure.12**, to magnify any change in the heat flux. Only two notable peaks show up at 1400^{o}C from the first derivative curve; one of them arises certainly

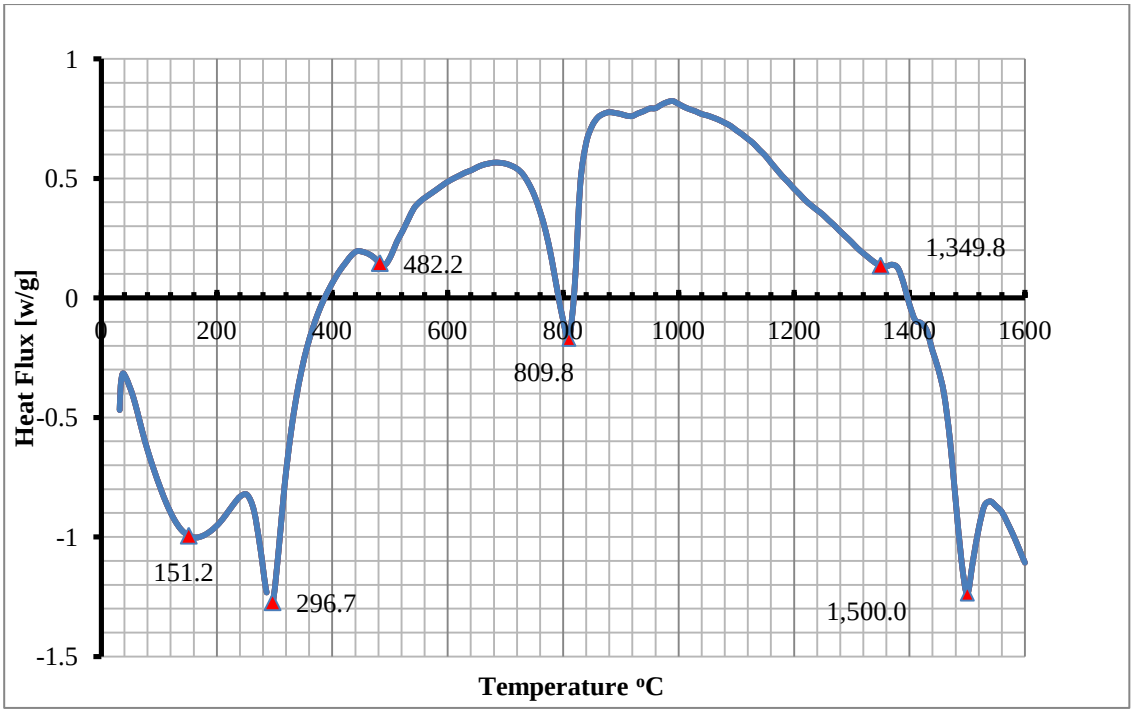

Figure 11 Differential scanning calorimetry, ran form ambient temperature to 1600°C in Ar environment.

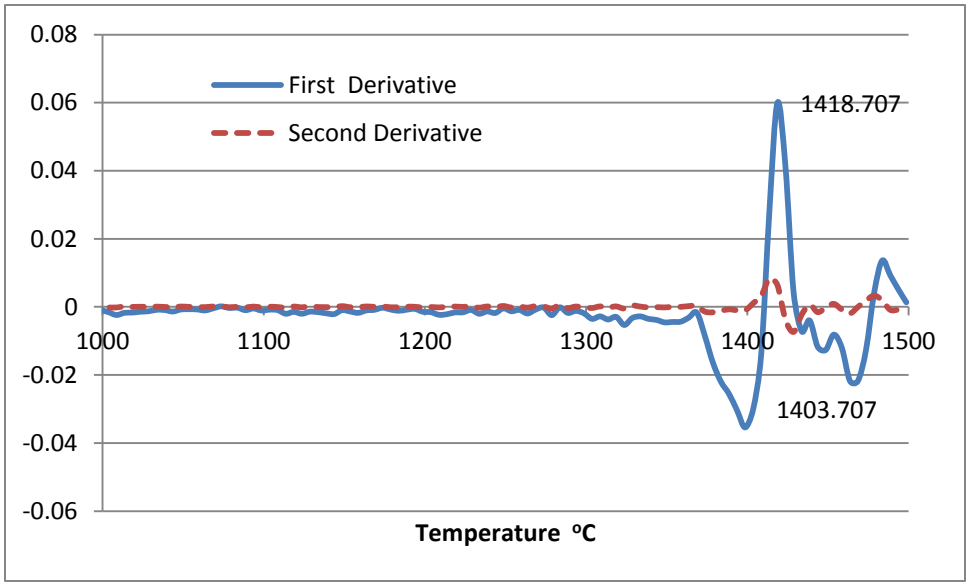

Figure 12 The first and second derivative of heat flux obtained from DSC data as a function of the temperature.

from alpha to beta transformation.

4.1.3 PHASE FORMATION AS A FUNCTION OF TEMPERATURE

Figure.13 and **Figure.14** show the phase evolution of the investigated samples sintered at 1000, 1100, 1200, 1300 and 1400^{o}C. Gehlenite ($Ca_2Al_2SiO_7$), which is a member in the family of melilite ceramics, appeared at a temperature below 1000^{o}C and continued to show up until it dissolved completely at 1300^{o}C, forming Ca-α-SiAlON. It should be noted that the relatively higher holding time in SPS (1 h) aided the dissolution of Gehlenite to SiAlON ceramics, which otherwise would require higher temperatures, as revealed by the previous research [15,59]. AlN was appearing until 1300^{o}C, at which α/β-SiAlON and AlN-defected structures, namely 15R, started to form. The start of disappearance of α-Si_3N_4 is associated with the formation of α-SiAlON at 1300^{o}C and due to the prolonged holding time, part of α-SiAlON transformed into β-SiAlON. It has been reported that Si_3N_4 powder is covered inherently by SiO_2 layers, which decompose at high temperatures, forming SiO_2 particles [7,9,60]. Zhao *et al.* has shown that the alpha to beta transformation is not a simple process of structure change, but rather different products may show up, such as AlN-polytypoids [61]. Our observations confirm the same phenomena, in which α-SiAlON partially decomposed and formed β-SiAlON and 15R at 1300^{o}C. At 1400^{o}C, only β-SiAlON survived due to its unique stability at high temperature.

The relative displacement curve during sintering for 1400^{o}C sample is shown in **Figure.15**. It can be seen very clearly that there is no much change in the displacement until 700^{o}C, which implies the absence of any reaction taking place

during this temperature range. Little change in the displacement is observed between 700^{o}C and 1000^{o}C, which can be attributed to the decomposition of $CaCO_3$ into CaO and the subsequent formation of Gehlenite ($Ca_2Al_2SiO_7$). The major increase in the relative displacement is seen between 1000^{o}C and 1300^{o}C, in which solution-reprecipitation process took place and Gehlenite and α-Si_3N_4 transformed into α-SiAlON. It should be noted that there is no much change in the displacement during the holding time, although several structural and phase transformation occur during this stage.

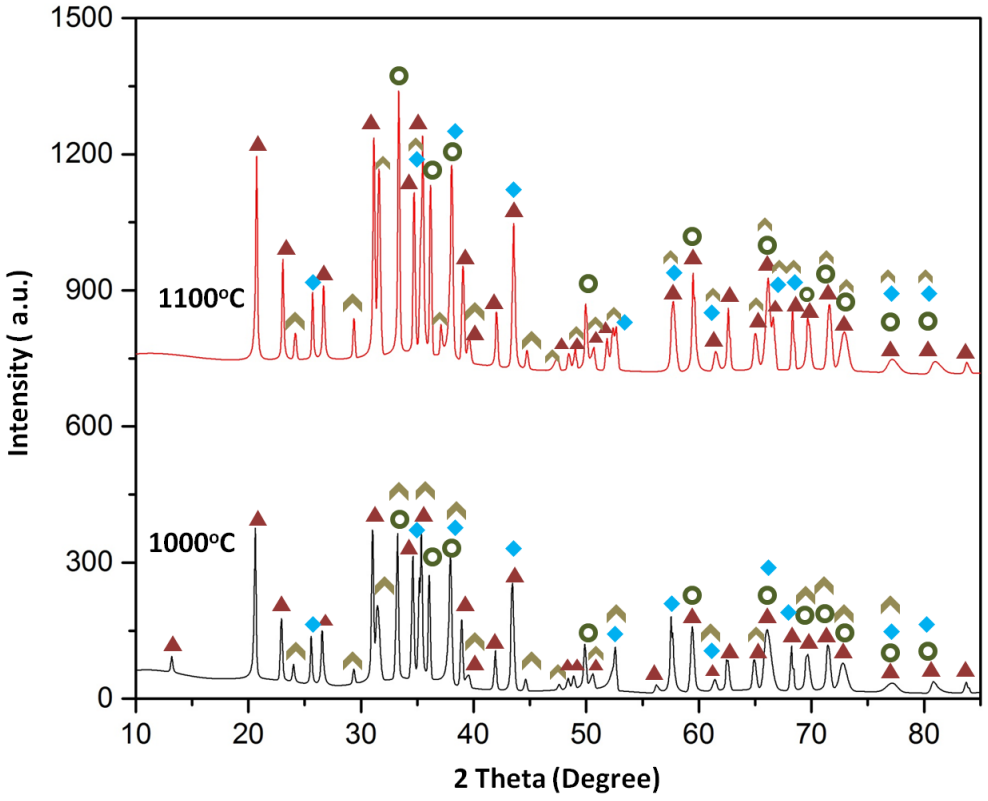

Figure 13 Phase evolution of the sintered samples at 1000 and 1100 ^{o}C.

Peak Label Key : α-Si_3N_4 (▲), AlN (○), Al_2O_3 (◆),Gehlenite ($Ca_2Al_2SiO_7$) (^).

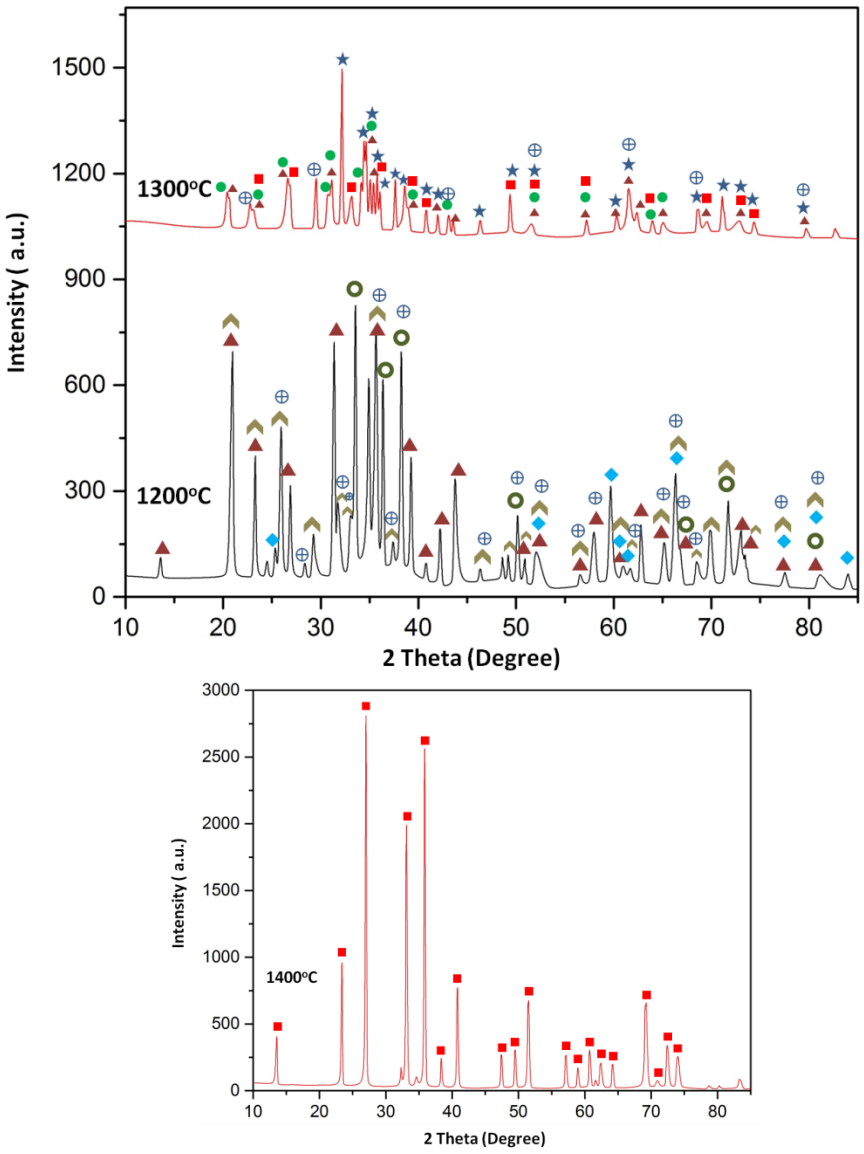

Figure 14 Phase evolution of the sintered samples at 1200,1300 and 1400 ^{o}C.

Peak Label Key : α-Si_3N_4 (▲), AlN (◎), Al_2O_3 (◆),Gehlenite ($Ca_2Al_2SiO_7$) (◢), α-SiAlON ($Ca_{0.68}Si_{9.96}Al_{2.04}O_{0.68}N_{15.32}$) (●), β-SiAlON ($Si_4Al_2O_2N_6$) (■), 15R ($SiAl_4O_2N_4$) (★), SiO_2 (⊕)

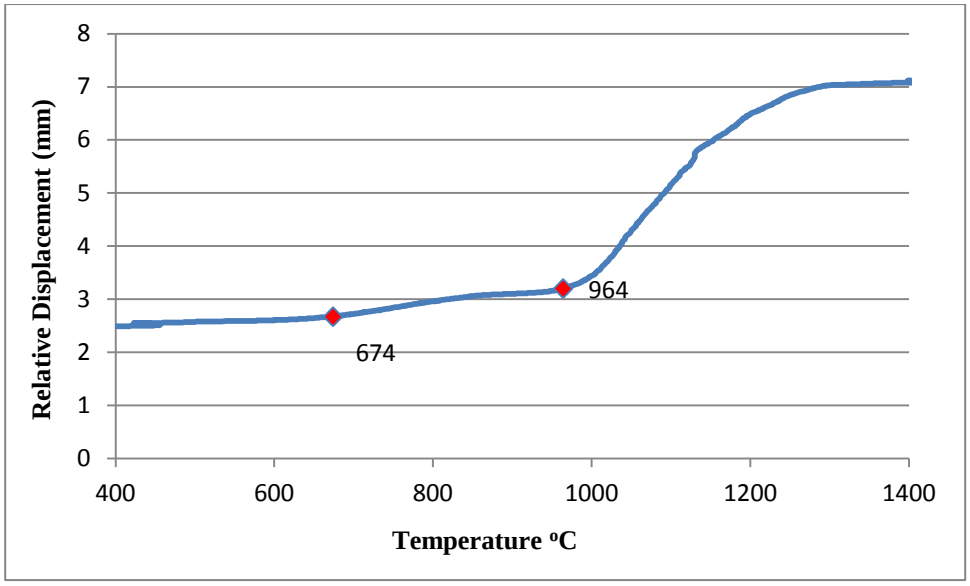

Figure 15 The relative displacement as a function of the sintering temperature for the sample sintered at 1400^{o}C

4.1.4 MICROSTRUCTURAL DEVELOPMENT

Figure.15 displays the SEM micrographs of the samples sintered at 1200, 1300 and 1400^{o}C. At 1200^{o}C, as confirmed by XRD analysis, the powder precursors did not dissolve completely, however, the formation of liquid had started, as in micrograph (b), for subsequent reactions. Micrographs (c) (d) and (e) confirm clearly the presence of α-SiAlON and β-SiAlON phases, as indicated by XRD results. Due to the relative longer holding time as for SPS conditions, β-SiAlON underwent evident growth, as in micrograph (f).

4.1.5 CONCLUDING REMARKS

- ✓ Phase evolution in SPS is much faster than in conventional sintering techniques
- ✓ The use of nano starting materials promotes faster kinetics for reactions taking place during sintering
- ✓ α-SiAlON does not transform directly and uniquely to β-SiAlON, but rather various AlN-polytypoids form as secondary products.
- ✓ Gehlenite phase is thought to be a transient stage in the formation of α-SiAlON
- ✓ β-SiAlON is the most stable phase in the SiAlON system, which is seen in the disappearance of α-SiAlON and AlN-polytypoids at 1400^{o}C at the expense of β-SiAlON

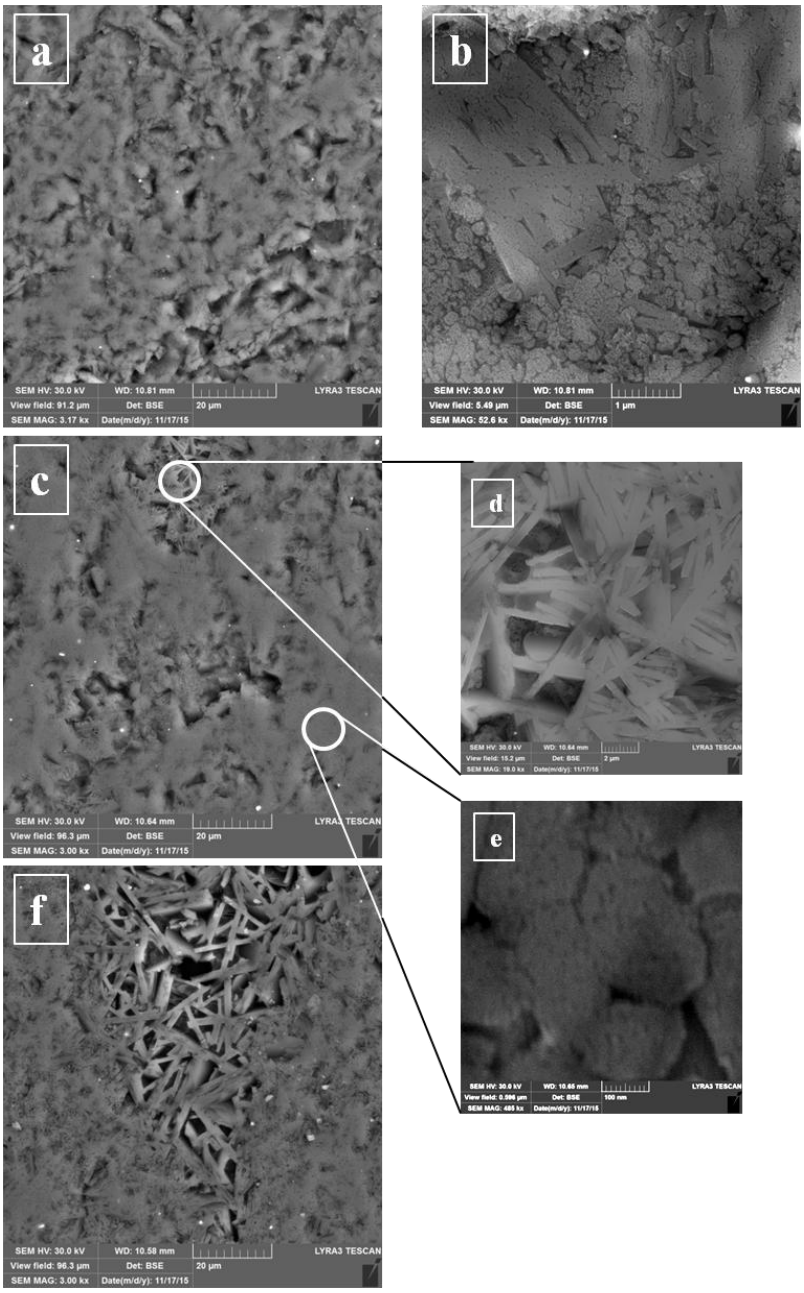

Figure 16 SEM micrographs of the investigated samples sintered at (a) (b) **1200^{o}C**, (c) (d) (e) **1300^{o}C** and (f) **1400^{o}C**

4.2 EFFECT OF Al METAL PRECURSOR ON Ca-α-SiAlON

4.2.1 INTRODUCTION

The present work intends to investigate the effect of Al metal precursor on the densification and mechanical properties of Ca-α-SiAlON ceramics using SPS. The idea of metal precursors has been introduced before by Hakeem *et al.* [62], but in the context of synthesizing high N content oxynitride glasses. It is expected that the use of such a metal precursor will increase the amount and mobility of the liquid phase and, thus, the ceramic densification. Crystalline and amorphous Si_3N_4 starting powders were used to study the impact of the structure on the mechanical properties and densification.

Table.6 lists the investigated composition with the respective proportions of the used precursors. To isolate other effects, the chemical composition was fixed to be: $CaSi_6Al_6O_4N_{12}$ which corresponds to m = 2 and n = 4 in the general formula of α-SiAlON. For each type of silicon nitride, the α-SiAlON composition was made up using only AlN or replacement of 10, 20, and 30 mol% of AlN by Al metal.

To clarify the metal precursor substitution, an example of 10 mol.% replacement is illustrated in the equation below . The chemical reaction for a sample without Al replacement can be written as follows:

$$CaO + Al_2O_3 + 2Si_3N_4 + 4AlN \longrightarrow CaSi_6Al_6O_4N_{12} \qquad \textbf{Equation (4)}$$

Now, if 10 mol.% of AlN is substituted by Al metal, the reaction can be represented in the following way:

$$CaO + Al_2O_3 + 2Si_3N_4 + 3.6AlN + 0.4Al + 0.4N \longrightarrow CaSi_6Al_6O_4N_{12}$$ **Equation (5)**

Samples were sintered by SPS process to achieve the highest possible densification in the shortest time and to prevent the formation of secondary phases due to the high heating rate. Sintering was performed firstly for all samples at 1600°C for 30 minutes in the presence of nitrogen, under a uniaxial pressing load of 50 MPa. After performing the mechanical testing, samples with α-Si_3N_4 were also sintered at 1450°C, to evaluate the role of Al in enhancing sinterability at lower temperatures at which more α-SiAlON would be expected to be retained. A heating rate of 100°C/min. was adopted in an attempt to avoid formation of intermediate phases. Samples were then rapidly cooled down to ambient temperature

TABLE 6 Starting powder chemical precursors in w.t%

Sample Name	CaO	Al_2O_3	α-Si_3N_4	Amp-Si_3N_4	AlN	Al	N*
3-α	9.31	16.92	46.56	-	27.21	-	-
3-α(0.1Al)	9.31	16.92	46.56	-	24.49	1.79	0.93
3-α(0.2Al)	9.31	16.92	46.56	-	21.77	3.58	1.86
3-α(0.3Al)	9.31	16.92	46.56	-	19.05	5.37	2.79
3-Amp	9.31	16.92	-	46.56	27.21	-	-
3-Amp(0.1Al)	9.31	16.92	-	46.56	24.49	1.79	0.93
3-Amp(0.2Al)	9.31	16.92	-	46.56	21.77	3.58	1.86
3-Amp(0.3Al)	9.31	16.92	-	46.56	19.05	5.37	2.79

*assuming stoichiometric reaction: $Al + N \rightarrow AlN$

4.2.2 SINTERING AND DENSIFICATION

Table 7 shows the densities of the SiAlON nano-ceramic samples sintered at 1600°C and 1450°C. All densities were ~3.10 $g.cm^{-3}$ or above, suggesting that most samples reached nearly theoretical density. Although evaluating theoretical densities is somewhat difficult, due to the fact that the density values for individual phases obtained from XRD are not known exactly, it can be concluded that samples are close to fully dense when compared to values obtained in the literature for similar compositions. It is notable that samples sintered at 1450°C still have the same densities as or better than those sintered at 1600°C. This would suggest that by using SPS with its inherent rapid heating rate, densification can be achieved very easily even at lower peak temperatures. The partial substitution of AlN with Al in the samples containing α-Si_3N_4 sintered at 1600°C shows a very slight increase in density whereas samples containing amorphous Si_3N_4 shows no increase with Al substitution. The fact that density values do not change much through the incorporation of metallic Al may indicates that the amount of liquid phase formed remains the same and, thus, there is no difference in overall densification

TABLE 7 Density values in g/cm^3 of samples sintered at 1600°C and 1450°C.

	3-α	**3-α(0.1Al)**	**3-α(0.2Al)**	**3-α(0.3Al)**	**3-Amp**	**3-Amp(0.1Al)**	**3-Amp(0.2Al)**	**3-Amp(0.3Al)**
1600°C	3.11	3.15	3.10	3.15	3.11	3.09	3.10	3.09
1450°C	3.17	3.16	3.16	3.15	-	-	-	-

4.2.3 PHASE ASSEMBLAGE

XRD patterns of samples **3-α, 3-α(0.1Al) , 3-α(0.2Al)** and **3-α(0.3Al)** sintered at 1600°C are shown in **Figure.17**. β-SiAlON z = 3.2 ($Si_{2.8}Al_{3.2}O_{3.2}N_{4.8}$) is the major phase in sample **3-α** along with some 15R polytypoid ($SiAl_4O_2N_4$). However, as Al metal is substituted for AlN into the starting mixture, the major phase becomes Ca-α-SiAlON, with a small amount of β-SiAlON and 12H polytypoid ($SiAl_5O_2N_5$). As more Al metal is added into the mixture, some of the 12H phase is replaced by 21R ($SiAl_6O_2N_6$) with the nitrogen to oxygen ratio of the polytypoid phase increasing. A small amount of Si is also present in the samples containing higher amount of Al i.e. **3-α(0.3Al)**.

Figure.18 presents the XRD patterns of samples 3-**Amp, 3-Amp(0.1Al), 3-Amp(0.2Al)** and **3-Amp(0.3Al)** formed from nano-sized amorphous silicon nitride and sintered at 1600°C**.** β-SiAlON z = 1.2 ($Si_{4.8}Al_{1.2}O_{1.2}N_{6.8}$) is the major phase in sample **3-Amp(0Al)** along with 12H polytypoid. When a small amount of Al is substituted for AlN in sample **3-Amp(0.1Al)** a small amount of α-SiAlON is formed, which does not appear in the samples containing higher levels of Al. The z value of β-SiAlON increases as Al is substituted for AlN to z = 3.2 in sample **3-Amp(0.2Al)** and z = 3.4 in sample **3-Amp(0.3Al)** and 15R is also observed in these samples. Contrary to what is observed in samples formed from alpha silicon nitride, N:O ratio decreases in AlN-polytypoids as more Al is incorporated

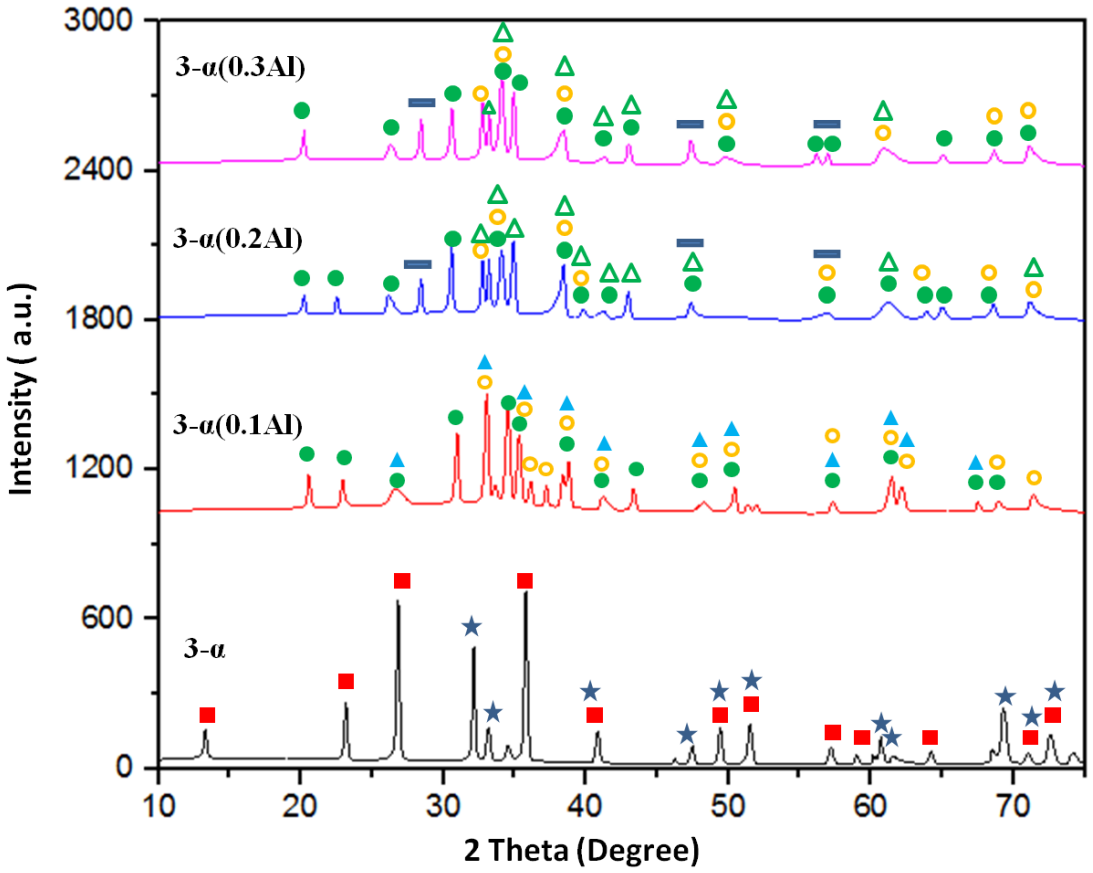

Figure 17 XRD patterns of samples **3-α , 3-α(0.1Al) , 3-α(0.2Al)** and **3-α(0.3Al)** samples, sintered at 1600°C. **Sample 3-α**: β–SiAlON z=3 (■),15R ($SiAl_4O_2N_4$) **(★). Sample 3-α(0.1Al):** α–SiAlON ($Ca_{0.7}Si_{10}Al_2O_{0.7}N_{15.3}$) (●), 12H ($SiAl_5O_2N_5$) (○), β–SiAlON z =2.9 ($Si_{3.1}Al_{2.9}O_{2.9}N_{5.1}$). **Sample 3-α(0.2Al) :** α–SiAlON ($Ca_{0.7}Si_{10}Al_2O_{0.7}N_{15.3}$) (●), 21R($SiAl_6O_2N_6$) (Δ), 12H ($SiAl_5O_2N_5$) (○), Si (▬). **Sample 3-α(0.3Al):** α–SiAlON ($Ca_{0.8}Si_{9.2}Al_{2.8}O_{1.2}N_{14.8}$) (●), 21R($SiAl_6O_2N_6$) (Δ), 12H ($SiAl_5O_2N_5$) (○), Si (▬).

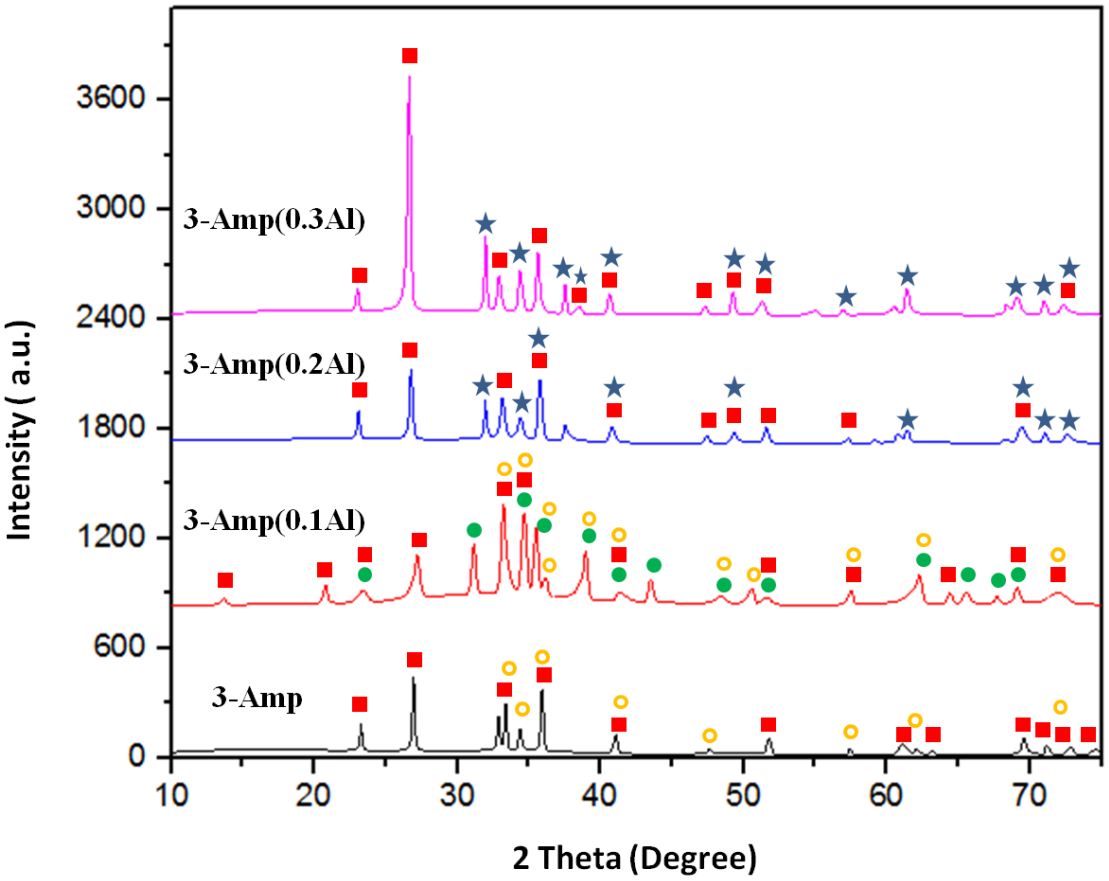

Figure 18 XRD patterns of **3-Amp , 3-Amp(0.1Al) , 3-Amp(0.2Al) and 3-Amp(0.3Al)** samples, sintered at 1600°C. **Sample 3-Amp:** β–SiAlON z = 1.2 ($Si_{4.8}Al_{1.2}O_{1.2}N_{6.8}$) (■), 12H ($SiAl_5O_2N_5$) (○). **Sample 3-Amp(0.1Al):** β-SiAlON z=2 ($Si_4Al_2O_2N_6$) (■), 12H ($SiAl_5O_2N_5$) (○), α–SiAlON ($Ca_{0.7}Si_{10}Al_2O_{0.7}N_{15.3}$) (●) . **Sample 3-Amp(0.2Al):** β–SiAlON z = 3.2 ($Si_{2.8}Al_{3.2}O_{3.2}N_{4.8}$) (■),15R ($SiAl_4O_2N_4$) (★). **Sample 3-Amp(0.3Al):** β–SiAlON z = 3.4 ($Si_{2.6}Al_{3.4}O_{3.4}N_{4.6}$) (■), 15R $SiAl_4O_2N_4$ (★).

Figure.19 displays the XRD patterns of samples containing α–Si_3N_4 sintered at 1450^{o}C. α–SiAlON is the major phase in **3-α**, along with 21R polytypoid and 12R in the samples containing Al metal. Also, SiO_2 is observed in sample **3-α(0.3Al)** as a minor phase. [7-9]. β–SiAlON is not observed in these samples sintered at 1450°C.

Comparing XRD patterns of alpha samples sintered at 1450°C and 1600°C would highlight the following points. β–SiAlON disappears completely in 1450°C samples, since alpha to beta transformation does not take place usually at this temperature. Furthermore, the decomposition of Si_3N_4 is temperature-dependent , thus, limited amount of SiO_2 is observed at 1450°C (sample **3-α(0.3Al**) **),** whereas it appears promintly in samples **3-α(0.2Al)** and **3-α(0.3Al)** sintered at 1600°C.

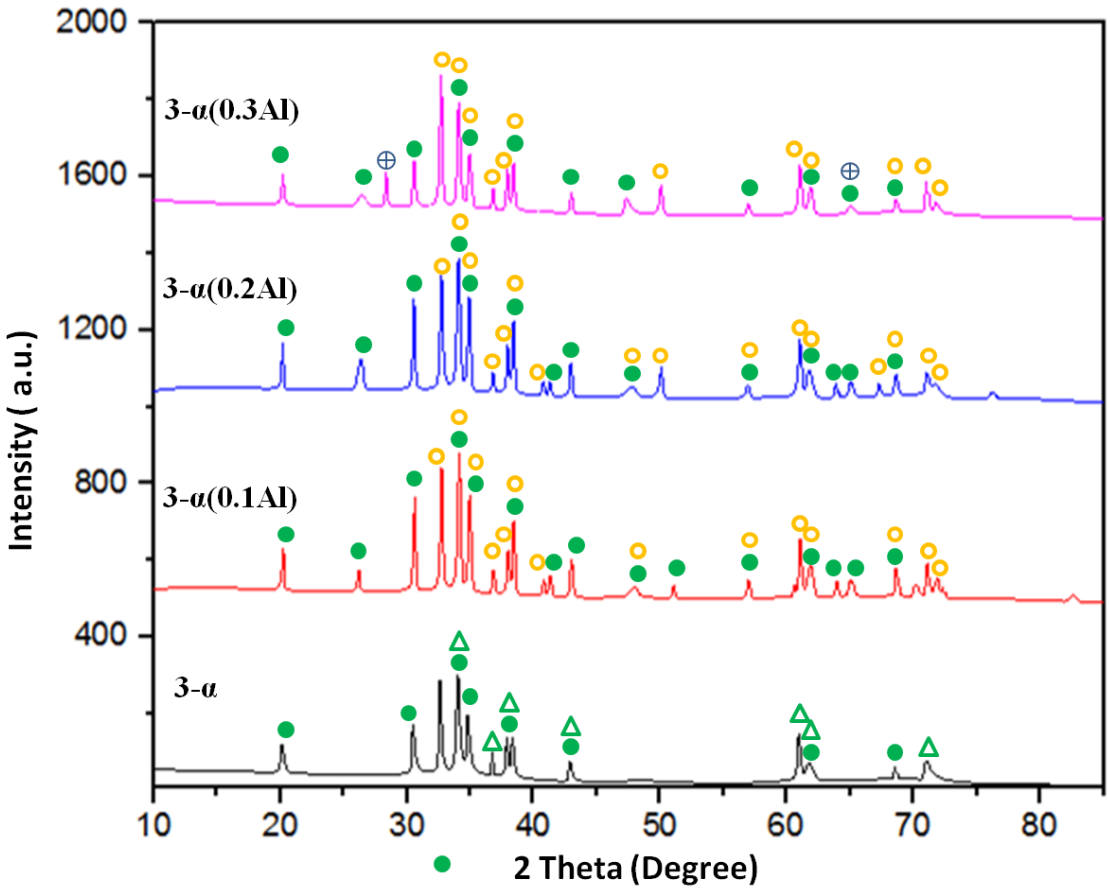

Figure 19 XRD patterns of **3-α , 3-α(0.1Al) , 3-α(0.2Al)** and **3-α(0.3Al)** samples, sintered at 1450°C. **Sample 3-α**: α–SiAlON ($Ca_{0.68}Si_{9.96}Al_{2.04}O_{0.68}N_{15.32}$) (●),21R ($SiAl_6O_2N_6$) (Δ). **Sample 3-α(0.1Al):** α–SiAlON ($Ca_{0.68}Si_{9.96}Al_{2.04}O_{0.68}N_{15.32}$) (●), 12H ($SiAl_5O_2N_5$) (○). **Sample 3-α(0.2Al) :** α–SiAlON($Ca_{0.68}Si_{9.96}Al_{2.04}O_{0.68}N_{15.32}$) (●), 12H ($SiAl_5O_2N_5$) (○). **Sample 3-α(0.3Al):** α–SiAlON($Ca_{0.8}Si_{9.2}Al_{2.8}O_{1.2}N_{14.8}$) (●), 12H ($SiAl_5O_2N_5$) (○), SiO_2 (⊕).

4.2.4 MICROSTRUCTURAL DEVELOPMENT

FESEM micrographs of samples **3-α(0Al), 3-α(0.1Al), 3-α(0.2Al)** and **3-α(0.3Al)** sintered at 1600°C are shown in **Figure.20** . Sample **3-α** is composed of two types of morphology: rod-like and equiaxed structures. XRD analysis has demonstrated that this sample consists of β-SiAlON with z = 3.2 and 15R polytypoid. It is known that β-SiAlON exhibits elongated morphology, which can be clearly observed in the FESEM image of Figure.20a. β-SiAlON hexagonal grains showing their basal planes can be seen in Figure.20b. When Al metal is substituted for AlN, α-SiAlON ($Ca_{0.7}Si_{10}Al_2O_{0.7}N_{15.3}$) is formed in samples **3-α(0.1Al), 3-α(0.2Al)** and **3-α(0.3Al)**, whereas β-SiAlON is only present in sample **3-α(0.1Al)** (according to XRD and FESEM analyses). Several AlN polytypoid phases are observed in these samples. Figures.20c and d reveal that the aspect ratio of $SiAl_5O_2N_5$ (12H) phase is lower than that of the $SiAl_6O_2N_6$ (21R) phase. Comparing Figure.20a, which corresponds to sample **3-α(0Al),** with the remaining micrographs of lower magnification, it can be seen that the level of secondary polytypoid phase(s) dispersion is enhanced as Al metal replacement is increased. The formation of elongated α-SiAlON grains occurs in sample **3-α(0.3Al)** sintered at 1600°C, as shown in Figure.20f. However, other samples does not shoow this tendency.

Kurama *et. al.* [63] reported that elongated α-SiAlON grains can be formed easily if α-SiAlON formation is hindered at low temperatures by using high heating rate sintering schemes as in the case of SPS. They also showed the necessity of having enough liquid phase, which occurs at high m and n values, to aid the elongation process that is thought to be diffusion-controlled [34]. However, Shen and Nygren

[64] noted that the grains grew so fast during the SPS process, such that diffusion controlled grain growth mechanisms proposed for traditional liquid-sintering did not fit with their observations, and grain-coarsening seemed to be controlled more by interface reactions.

FESEM micrographs of the samples produced from amorphous silicon nitride are shown in **Figure.21**. β-SiAlON is the major phase in all the samples with the maximum amount observed in sample **3-Amp(0.3Al)**. Various AlN polytypoid phases, mainly 15R ($SiAl_4O_2N_4$), are present also. α-SiAlON forms only in sample **3-Amp(0.1Al)**, as shown in Figures.21b and c.. As Al replaces AlN, more β-SiAlON is formed at the expense of other phases with the amount of 15R reduced in sample **3-Amp(0.3Al)** (Figure.21e) when compared with sample **3-Amp(0.2Al)** (Figure.21d), which is also confirmed by XRD results shown in **Figure 2.**

FESEM micrographs of samples containing α-Si_3N_4 sintered at 1450°C are shown in **Figure.22**. It is obvious that as the amount of Al increases, the formation of α-SiAlON is restrained and 12H polytypoid is formed instead. A similar trend is identified from the XRD data (Figure.19).

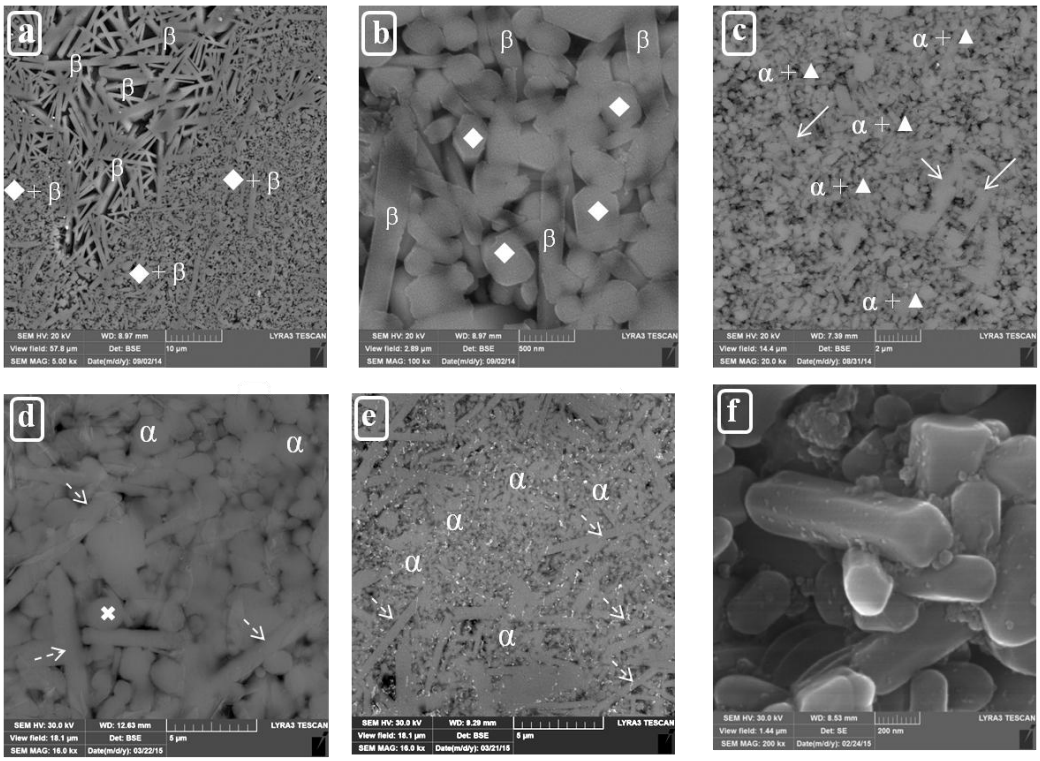

Figure 20 FESEM micrographs of samples containing α-Si_3N_4 sintered at 1600°C. (a), (b) **3-α,** (c) **3-α (0.1Al)**, (d) **3-α (0.2Al)**, (e) **3-α (0.3Al)**, (f) a fracture surface of **3-α (0.3Al)**. **Label key**: β-SiAlON (β), α-SiAlON (α), $Si_{3.1}Al_{2.9}O_{2.9}N_{5.1}$ (▲), 12H (→), 21R (---►), 15R(♦), Si (x).

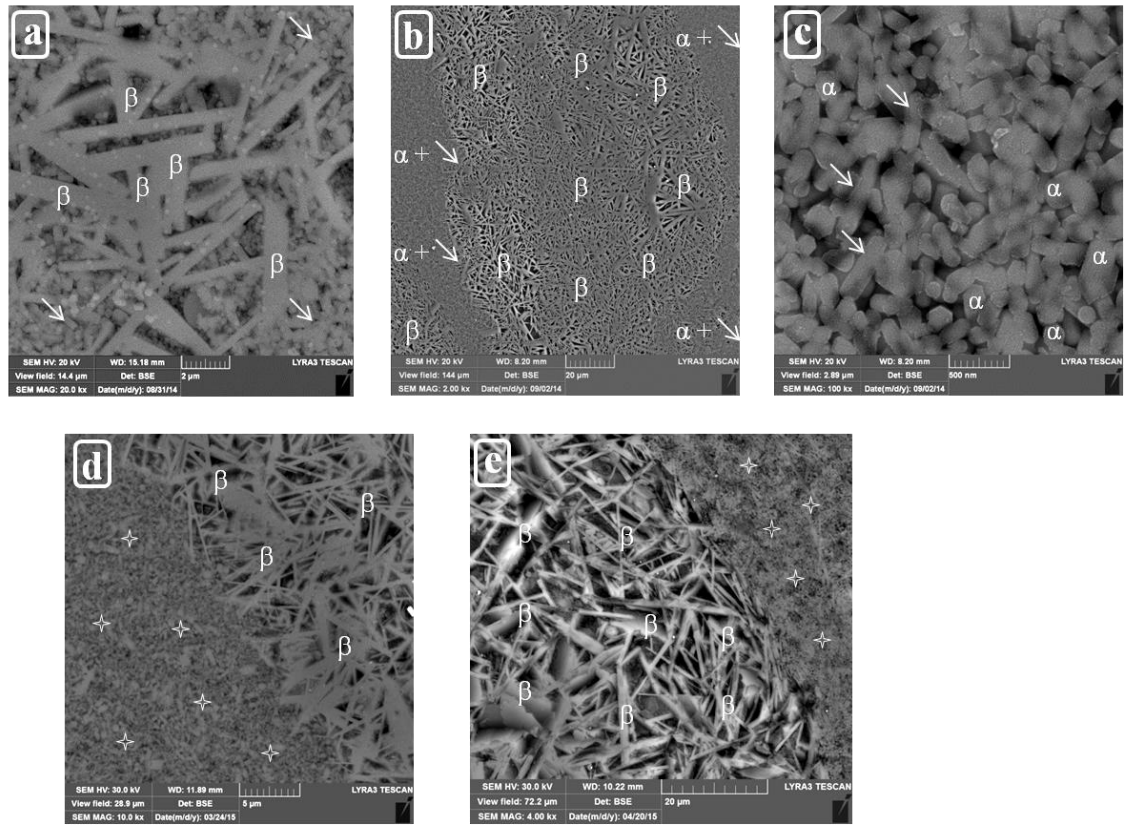

Figure 21 FESEM micrographs of samples containing amorphous-Si_3N_4 sintered at 1600°C. (a) 3-Amp, (b), (c) 3-Amp(0.1Al) , (d) 3-Amp(0.2Al) , (e) 3-Amp(0.3Al).

Label key: β-SiAlON (β), α-SiAlON (α), 15R (+), 12H (→), 21R.

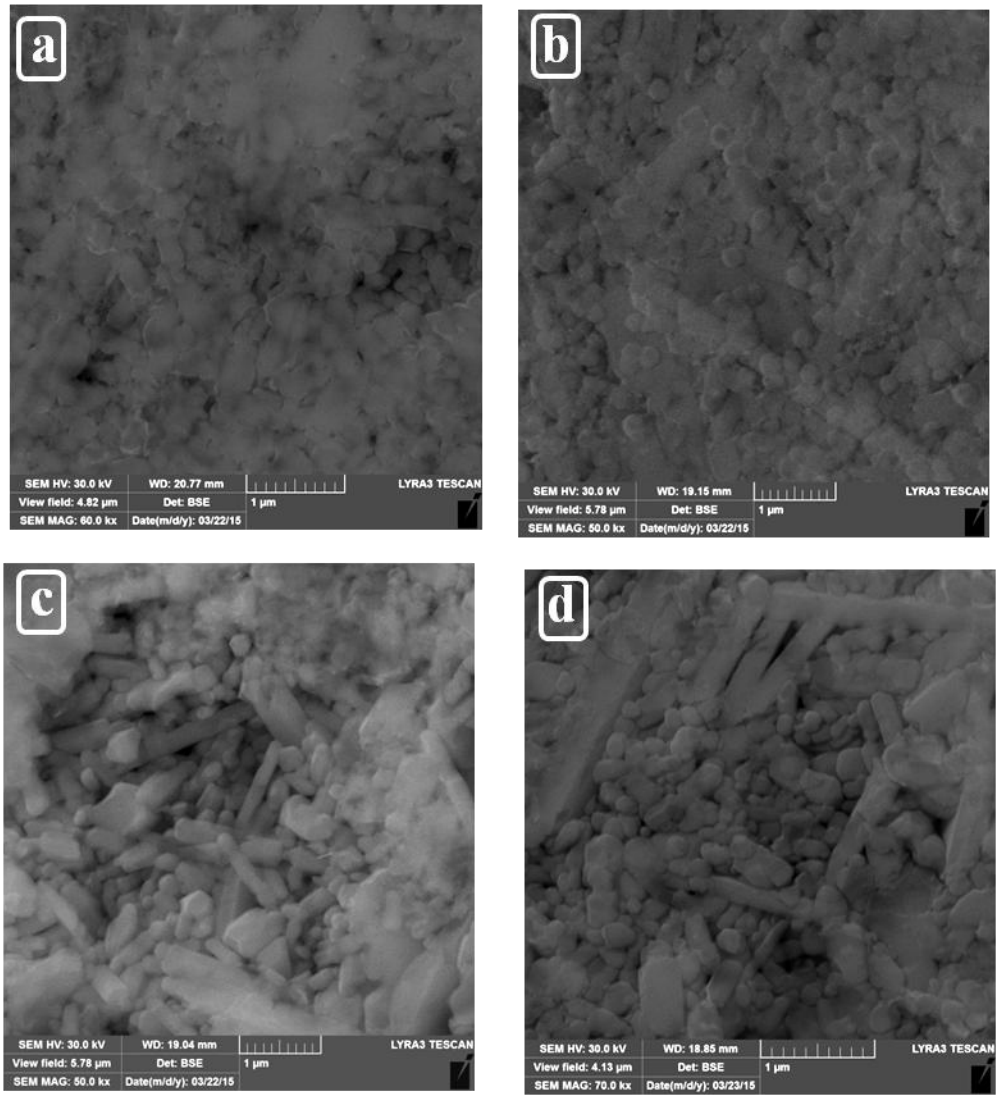

Figure 22 FESEM micrographs of samples containing α-Si_3N_4 sintered at 1450^{o}C. (a) **3-α** , (b) **3-α (0.1Al)** , (c) **3-α (0.2Al)** , (d) **3-α (0.3Al).**

4.2.5 ROLE OF Al IN PHASE FORMATION

During sintering of silicon nitride and SiAlONs, liquid phase densification occurs. In general terms, initially the precursors react with silicon nitride and silica present on the nitride particle surfaces to form a Ca-Si-Al-O-N liquid phase above the eutectic temperature which is known to be at ~1250^{o}C. This promotes densification firstly through a particle rearrangement stage and secondly by a solution-diffusion-precipitation process in which the initial α-Si_3N_4 is dissolved in the liquid and transforms to α- or β-SiAlON along with formation of the AlN polytypoids.

A pure α-SiAlON composition is nitrogen-rich and the volume of oxynitride liquid available for densification is low and of high viscosity. As α-SiAlON is precipitated, the amount of liquid gradually reduces. This means that complete reaction to form the α solid solution does not occur and some un-reacted components or residual glass are normally present after sintering. Thus, the composition needs to be tailored to make it more oxygen rich as in the case of the composition used in this work, $CaSi_6Al_6O_4N_{12}$, so that more liquid is formed, facilitating densification but inevitably resulting in residual grain boundary crystalline or vitreous phases. As the overall composition is more Al- and O-rich than for a pure α-SiAlON, this allows the formation of more liquid phase.

So for sample **3-α**, using α-Si_3N_4 as precursor, based on XRD and the microstructural observations, the overall reaction can be shown schematically as:

α-Si_3N_4 (+ surface SiO_2) + CaO + Al_2O_3 + AlN $\rightarrow$

$\rightarrow$ (1450^{o}C) α-$Ca_{0.7}Si_{10}Al_2O_{0.7}N_{15.3}$ + $SiAl_6O_2N_6$ + Ca-Si-Al-O-N liquid phase **Equation(6)**

$\rightarrow$ (1600^{o}C) β-$Si_{2.8}Al_{3.2}O_{3.2}N_{4.8}$ + $SiAl_4O_2N_4$ + Ca-Si-Al-O-N liquid phase (N-rich) **Equation(7)**

Thus it appears that following rapid heating in the SPS equipment to 1450^{o}C, a large amount of an oxygen-rich Ca-SiAlON liquid is formed from which two N-rich crystalline phases, α-$Ca_{0.7}Si_{10}Al_2O_{0.7}N_{15.3}$ and 21R ($SiAl_6O_2N_6$) are formed. At higher temperature, the oxygen rich liquid phase reacts further with the α-SiAlON to transform it to β-$Si_{2.8}Al_{3.2}O_{3.2}N_{4.8}$ leaving the liquid phase more N-rich. This has been observed previously by many researchers [53]. The liquid cools to form a grain boundary glassy phases.

For the samples containing Al in place of some of the AlN, the overall reaction at both temperatures can be shown as:

α-Si_3N_4 (+ surface SiO_2) + CaO + Al_2O_3 + AlN + Al + N_2 $\rightarrow$

$\rightarrow$ α-$Ca_{0.7}Si_{10}Al_2O_{0.7}N_{15.3}$ + $SiAl_6O_2N_6$ + Ca-Si-Al-O-N liquid phase **Equation(8)**

Al melts at 660°C and nitridation of Al occurs above ~800°C [65]. In SPS with rapid heating, the nitridation reaction would occur over a range of temperatures. Eventually, the Ca-SiAlON liquid is formed from which the two N-rich crystalline phases, α-$Ca_{0.7}Si_{10}Al_2O_{0.7}N_{15.3}$ and 21R are observed at both 1450^{o}C and 1600^{o}C. This is due to the fact that the presence of Al favors the formation of a more N-rich liquid phase at

1450^{o}C and therefore there is no further reaction and transformation at higher temperatures to form β-SiAlON.

In the case of the samples prepared using amorphous silicon nitride, for **3-Amp,** with no Al substituted for AlN, the reaction path is as follows:

Amp-Si_3N_4 (+ surface SiO_2) + CaO + Al_2O_3 + AlN →

→ β–$Si_{4.8}Al_{1.2}O_{1.2}N_{6.8}$ + $SiAl_5O_2N_5$ + Ca-Si-Al-O-N liquid phase **Equation(9)**

So in this sample, β-SiAlON with z = 1.2 is formed at the expense of α-SiAlON even at 1600^{o}C. Thus it would appear that, following rapid heating in the SPS equipment, a large amount of an oxygen-rich Ca-SiAlON liquid is formed from which β-$Si_{4.8}Al_{1.2}O_{1.2}N_{6.8}$ is precipitated along with 12H. As the amorphous Si_3N_4 is an extremely fine powder (20nm), then the amount of silica on its surface will be much higher than in the case of the α-Si_3N_4 (150nm) and therefore the overall composition will be more oxygen rich leading to precipitation of β-SiAlON.

As Al is substituted for AlN in these samples, β-SiAlON with much higher z value is still the major phase with 15R polytypoid as a minor phase according to the following reaction:

Amp-Si_3N_4 (+ surface SiO_2) + CaO + Al_2O_3 + AlN + Al + N_2 →

→ β-$Si_{2.6}Al_{3.4}O_{3.4}N_{4.6}$ + $SiAl_4O_2N_4$ + Ca-Si-Al-O-N liquid phase **Equation(10)**

It is clear that, since β-SiAlON is the major phase, the overall composition must be more oxygen rich due to the excess surface silica on this type of silicon nitride. Even in the **3-Amp(0.3Al)** composition, some crystalline SiO_2 is observed in the final phase assemblage.

From the sintering results it is clear that there is very little difference between the densities of the different groups of samples, thus indicating that in all cases a sufficient amount of liquid phase was formed which allowed full densification. However, there were obvious differences between the compositions of the liquid phases formed which affected the subsequent reactions and transformations and final phase assemblages.

4.2.6 MECHANICAL PROPERTIES

Hardness values for samples prepared using α-Si_3N_4 sintered at 1450°C were in the range 17.0 to 19.6 GPa, increasing with substitution of Al for AlN. On sintering at 1600°C, there was a significant decrease in hardness for samples **3-α** and **3-α(0.1Al).** This is clearly due to the difference in phase assemblages as these samples contain β-SiAlON in place of Ca-α-SiAlON. α-SiAlON is known to be intrinsically harder than β-SiAlON. For this reason, the low hardness values in the range 12.3 to 14.4 GPa measured for the samples using amorphous-Si_3N_4 sintered at 1600°C are due to the fact that in these samples, only β-SiAlON and AlN polytypoids and glass phase were present. In summary, hardness values can be clearly related to the particular phases

present in the microstructures and increases are observed in both sets of compositions sintered at 1450 and 1600°C as Al is substituted for AlN.

For samples prepared using α-Si_3N_4 sintered at 1450°C, fracture toughness was 4.4 MPa√m for the **3-α** and increased to values in the range 6.4 to 7.8 MPa√m when Al was substituted for AlN. After sintering at 1600°C, the fracture toughness increased for most compositions to values in the range 6.4 to 9.5 MPa√m but there was wide variations in standard deviations for samples **3-α**,**3-α(0.1Al)** and **3-α(0.2Al)**. Sample **3-α(0.3Al)** has a fracture toughness of 8.3 ± 0.7 MPa√m and this is the sample which exhibits α-SiAlON with high aspect ratio elongated grains. This, combined with a hardness of 18.5 GPa, suggests that this composition containing α-Si_3N_4 as a precursor along with 30 mol. % substitution of Al in AlN by Al metal sintered by SPS has promising mechanical properties that should be explored further.

4.2.7 CONCLUDING REMARKS

- ✓ Densification and mechanical properties of a fixed Ca-α-SiAlON composition, to allow excess liquid formation, with different precursors were investigated using SPS. Two different Si_3N_4 powders were used: (1) α-Si_3N_4 (150 nm) and (2) amorphous-Si_3N_4 (20 nm), along with other nano-sized starting powders: CaO, Al_2O_3 and AlN with substitution of 0, 10, 20, and 30 mol% of Al in AlN by Al metal.

- ✓ Following SPS processing at 1450°C and 1600°C, all densities were close to theoretical density suggesting that by using SPS with its inherent rapid heating

rate, densification can be achieved very easily even at lower peak temperatures. Densification occurs firstly through a particle rearrangement stage within a Ca-SiAlON liquid and secondly by a solution-diffusion-precipitation process in which the initial α-Si_3N_4 is dissolved in the liquid and transforms to α- or β-SiAlON along with formation of AlN polytypoids.

- ✓ For compositions using α-Si_3N_4 as precursor, following rapid heating by SPS to 1450°C, a large amount of an oxygen-rich Ca-SiAlON liquid is formed from which two N-rich crystalline phases, α-$Ca_{0.7}Si_{10}Al_2O_{0.7}N_{15.3}$ and 21R ($SiAl_6O_2N_6$) are formed. At higher temperature, the oxygen rich liquid phase reacts further with the α-SiAlON to transform it to β-$Si_{2.8}Al_{3.2}O_{3.2}N_{4.8}$ leaving the liquid phase more N-rich. When Al is substituted for AlN, α-$Ca_{0.7}Si_{10}Al_2O_{0.7}N_{15.3}$ and 21R are observed at both 1450°C and 1600°C. The presence of Al favors the formation of a more N-rich liquid phase at 1450°C and therefore, there is no further reaction and transformation at higher temperatures to form β-SiAlON.

- ✓ For compositions using amorphous nano-silicon nitride as precursor, with a high level of silica on its surface, and also when Al is partially substituted for AlN, following rapid heating during the SPS process, a large amount of an oxygen-rich Ca-SiAlON liquid is formed from which β-SiAlON is precipitated along with 12H.

- ✓ Increases in Vickers hardness are observed in both sets of compositions sintered at 1450 and 1600°C as Al is substituted for AlN but, overall, values can be related to the particular phases present in the microstructures.

- ✓ After sintering at 1600°C, fracture toughness ranges from 5 to 9 MPa√m depending on composition. The composition containing α-Si_3N_4 as a precursor along with 30 mol. % substitution of Al in AlN by Al metal sintered by SPS has a fracture toughness of 8.3 MPa√m and hardness of 18.5 GPa and with these promising mechanical properties this composition should be explored further.

TABLE 8 Mechanical properties of the samples sintered at 1600°C and 1450°C

Sample Name	1600°C Results		1450°C Results	
	HV_{10} (GPa)	**K_{IC} (MPa√m)**	**HV_{10} (GPa)**	**K_{IC} (MPa√m)**
3-α	13.4 ± 0.7	7.2 ± 2.4	17.0 ± 0.3	4.4 ± 0.8
3-α(0.1Al)	13.7 ± 0.6	6.4 ± 1.5	18.6 ± 0.4	7.8 ± 0.8
3-α(0.2Al)	16 ± 0.5	9.5 ± 1.9	19.1 ± 0.2	6.4 ± 0.4
3-α(0.3Al)	18.5 ± 0.7	8.3 ± 0.7	19.6 ± 0.3	6.5 ± 0.8
3-Amp	12.3 ± 0.8	5.2 ± 1.3	-	-
3-Amp(0.1Al)	12.2 ± 0.3	6.1 ± 1.5	-	-
3-Amp(0.2Al)	13.3 ± 0.4	5.3 ± 1.0	-	-
3-Amp(0.3Al)	14.4. ± 1.0	-	-	-

4.3 EFFECT OF Si METAL PRECURSOR ON Ca-α-SiAlON

4.3.1 INTRODUCTION

The present work intends to investigate the effect of Si metal precursor on the densification and mechanical properties of Ca-α-SiAlON ceramics using SPS. It is expected that the use of such a metal precursor will increase the amount and mobility of the liquid phase and, thus, the ceramic densification. Crystalline and amorphous Si_3N_4 starting powders were used to study the impact of its structure on the mechanical properties and densification.

Table.9 lists the investigated composition with the respective proportions of the used precursors. Similar to the Al replacement section, the chemical composition was fixed to be: $CaSi_6Al_6O_4N_{12}$ which corresponds to m = 2 and n = 4 in the general formula for α-SiAlON. For each type of silicon nitride, the α-SiAlON composition was made up using only Si_3N_4 or replacement of 10, 20, and 30 mol% of Si_3N_4 by Si metal.

TABLE 9 Starting powder chemical precursors in w.t%

Sample Name	CaO	Al_2O_3	AlN	α-Si_3N_4	Amp-Si_3N_4	Si	N*
3-α	9.31	16.92	27.21	46.56	-	-	-
3-α(0.1Si)	9.31	16.92	27.21	41.91	-	2.80	1.86
3-α(0.2Si)	9.31	16.92	27.21	37.25	-	5.59	3.72
3-α(0.3Si)	9.31	16.92	27.21	32.59	-	8.39	5.58
3-Amp	9.31	16.92	27.21	-	46.56	-	-
3-Amp(0.1Si)	9.31	16.92	27.21	-	41.91	2.80	1.86
3-Amp(0.2Si)	9.31	16.92	27.21	-	37.25	5.59	3.72
3-Amp(0.3Si)	9.31	16.92	27.21	-	32.59	8.39	5.58

*assuming stoichiometric reaction: $3Si + 2N_2 \rightarrow Si_3N_4$

4.3.2 SINTERING AND DENSIFICATION

Table.10 displays the density values of the samples sintered at 1600^{o}C with Si metal precursor. Similar to what has been said in Al replacement section, one can confirm with confidence that samples are well-densified by examining their densities based on the following two measures. Firstly, density values are comparable to the density of pure Si_3N_4, which constitute the major reactants in the system. The second measure is the similarity between these values and values obtained from literature for similar compositions, in which part of them did calculate the theoretical densities. Later in the following sections , SEM will confirm the fact of full densification of these samples.

TABLE 10 Density values of samples sintered at 1600°C

Sample Name	Density (g/ cm^3)
3-α	3.11
3-α(0.1Si)	3.14
3-α(0.2Si)	3.11
3-α(0.3Si)	3.079
3-Amp	3.11
3-Amp(0.1Si)	3.11
3-Amp(0.2Si)	3.08
3-Amp(0.3Si)	3.09

4.3.3 PHASE ASSEMBLAGE

Figure.23 presents XRD patterns of samples sintered at 1600^{o}C with Si replacement. β-SiAlON is present in all samples except in sample **3-α(0.2Si)**. The amount of β-SiAlON is the highest when Si is not involved in the reaction. Along with that, different AlN-polytypoids formed in all samples. Unexpectedly, un-reacted α-Si_3N_4 is present in sample **3-α(0.1Si)**.. When Si replacement was raised to 20 and 30% w.t , part of it remained un-dissolved/reacted with other precursors, which may reveal a threshold amount of Si metal to be dissolved/reacted in the mixture, after which agglomeration of Si metal is expected to form. α-SiAlON forms exceptionally in 20% Si replacement sample. A silicon-free phase ($Ca_3Al_2N_4$) is seen in sample **3-α(0.3Si)**, which can be explained by the consideration of un-reacted Si, that otherwise may have participated in the formation of α-SiAlON or semi- α-SiAlON phases. A fundamental question that should be asked here is related to the role of Si metal in enhancing the formation of either α-SiAlON or β-SiAlON. Extracting an answer appears difficult based on the available data, since Si replacement samples does not show any trend in any regard. A better mixing scheme for the starting powders may originate such trends, being possible after removal of agglomeration issue.

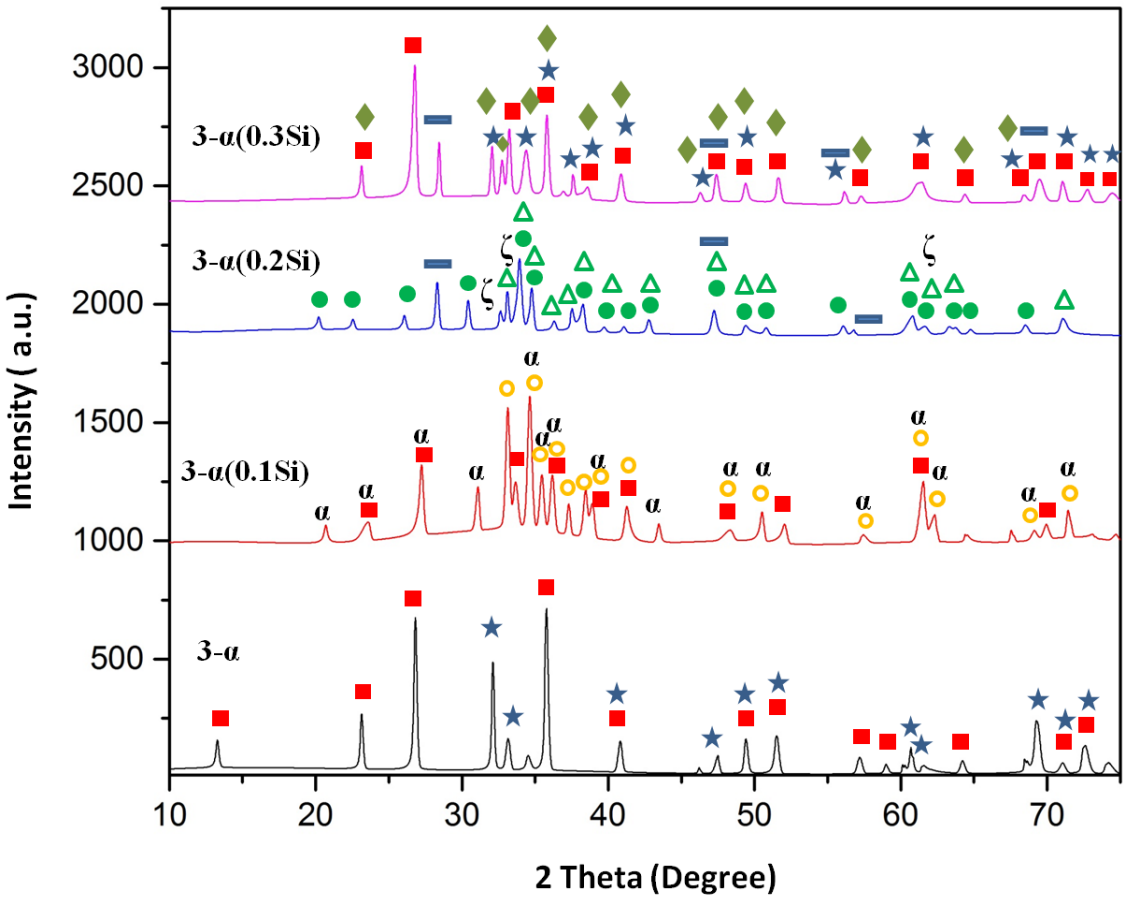

Figure 23 XRD patterns of samples **3- α , 3- α(0.1Si) , 3- α(0.2Si)** and **3-α(0.3Si)** samples, sintered at 1600°C. **Sample 3-α:** β–SiAlON z = 3 ($Si_3Al_3O_3N_5$) (■), 15R ($SiAl_4O_2N_4$) (★). **Sample 3-α(0.1Si):** β-SiAlON z=1 (Si_5AlON_7) (■), 12R ($SiAl_5O_2N_5$) (○), α–Si_3N_4 ($Ca_{0.7}Si_{10}Al_2O_{0.7}N_{15.3}$) (●) . **Sample 3-α(0.2Si):** α-SiAlON ($Ca_{0.7}Si_{10}Al_2O_{0.7}N_{15.3}$) (●), 21R ($SiAl_6O_2N_6$) (Δ), z-$Si_3Al_7O_3N_9$ (ζ), Si (▬). **Sample 3-α(0.3Si):** β–SiAlON z = 4 ($Si_4Al_2O_2N_6$) (■), 15R ($SiAl_4O_2N_4$) (★), $Ca_3Al_2N_4$ (♦),Si (▬).

The phase assemblage for samples containing Amp-Si_3N_4 is shown in **Figure.24** The level of complexity with regard to phase formation is little when compared to samples with α-Si_3N_4. It is manifest that β-SiAlON is the major phase in all samples regardless of the amount of Si replacement. This is understood, as we have discussed earlier, since amorphous Si_3N_4 tends to re-precipitate preferably into β-SiAlON phase due to its stability over other phases. Starting from 20% Si replacement sample, un-reacted Si metal appears in the final phase assemblage, indicating as in the α-Si_3N_4 samples, a critical amount that can dissolve readily in the sintered mixture, and perhaps any larger amount of Si replacement would require special mixing schemes to ensure full-reaction of Si with other reactants.

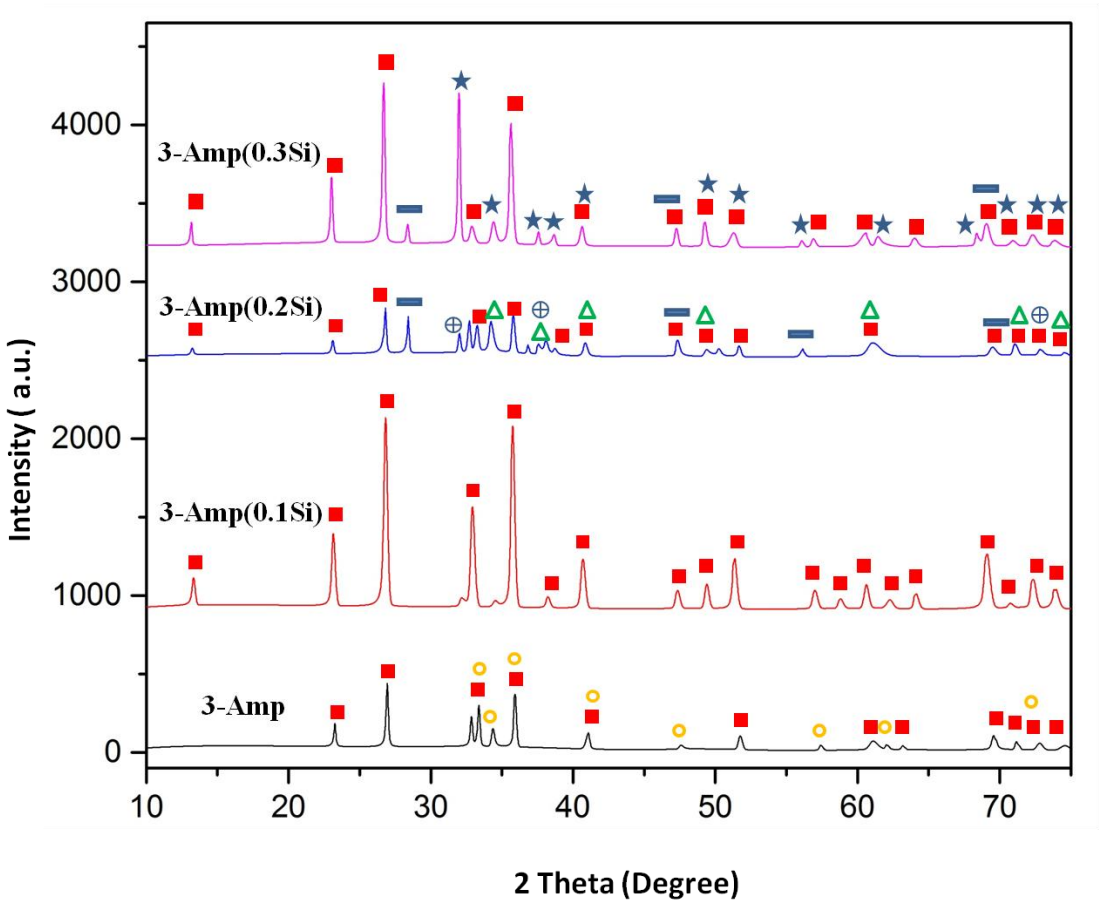

Figure 24 XRD patterns of samples **3- Amp , 3- Amp(0.1Si) , 3- Amp(0.2Si)** and **3-Amp(0.3Si)** samples, sintered at 1600°C. **Sample 3-Amp:** β–SiAlON z = 1 (Si_5AlON_7) (■), 12H ($SiAl_5O_2N_5$) (○). **Sample 3-Amp(0.1Si):** β-SiAlON z=4 ($Si_2Al_4O_4N_4$) (■). **Sample 3-Amp(0.2Si):** β–SiAlON z = 2 ($Si_4\ Al_2O_2N_6$) (■), 21R ($SiAl_6O_2N_6$) (Δ), SiO_2 (⊕) , Si (▬). **Sample 3-Amp(0.3Si):** β–SiAlON z = 3 ($Si_3Al_3O_3N_5$) (■), 15R $SiAl_4O_2N_4$ (★), Si (▬).

4.3.4 MICROSTRUCTURAL DEVELOPMENT

Figure.25 and **Figure.26** display the SEM micrographs for samples containing α-Si_3N_4. Densification appears to be good, except for some areas in which either grinding pull-out took place or the presence of high-aspect ratios phases gives an impression of porosity formation. β-SiAlON and AlN-polytypoids are good examples to illustrate the effect of aspect ratio, in which large aspect ratio grains when growing randomly, they develop empty areas which can be filled by either smaller particles or by the glassy phase. This explains the relative lower density of β-SiAlON phase when compared, for instance, with α-SiAlON phase. Mostly, AlN-polytypoids are grown in lathe-like structure, with aspect ratio larger than those of β-SiAlON. However, the O:N ratio should not be overlooked in such comparisons. XRD analysis has shown the dominance of β-SiAlON in sample **3- α**, which is also asserted here, as seen in Figure.25(a). Occasionally, and due to the growth direction, β-SiAlON grains are shown through their basal plane, as in Figure.25(b). When a comparison is made between sample **3- α** and **3- α(0.1Si)**, one would notice clearly the enhanced level of homogeneity in sample **3- α(0.1Si)**, which may open a window for a potential role of Si metal in enhancing phases dispersion, provided that it is added within the critical limit. Figure.25(c) shows the presence of α-Si_3N_4 within the grains of 12H and β-SiAlON

Figure.26 displays the SEM micrographs of samples **3- α(0.2Si)** and **3- α(0.3Si)**. Since the aspect ratio of α-SiAlON is relatively smaller, their regions look denser than β-SiAlON, as revealed from Figure.26(a). The silicon particles are distributed but not reacted, and they can be observed as circles between α-SiAlON and 21R grains (see

Figure.26(b)). As can be revealed from XRD analysis, the amount of un-reacted Si metal is higher in sample **3- α(0.2Si)** than in **3- α(0.3Si)**, in which the latter shows better phase dispersion (see Figure.26(a&c)). Thus, it can be concluded that more the amount of un-reacted Si metal, less phase dispersion/ homogeneity in the resulted microstructure. Locating $Ca_3Al_2N_4$ phase within the microstructure is pretty difficult, due to its limited presence.

Figure.27 shows the SEM micrographs of samples **3-Amp** and **3-Amp(0.1Si)**. The presence of 12H and β-SiAlON is evident in sample **3-Amp**, as shown in Figure.27(a & b). As discussed earlier, β-SiAlON may be shown through their basal or perpendicular planes. Both orientations can be viewed in sample **3-Amp(0.1Si)** (see Figure.27 (c & d)).

4.3.5 MECHANICAL PROPERTIES

Vickers hardness and indentation fracture toughness values are shown in **Table.11**. The basic observation from the collected data is the retrograded effect of Si replacement on the mechanical properties of the sintered samples. One possible explanation is the randomness in phase structuring when Si entered the reaction. For each weight percentage of silicon metal, different and un-expected phases were coming out. A second possible explanation, especially for 20-30% w.t replacement, is the accumulation of un-reacted Si metal in the sintered samples, decreasing their mechanical strength and thereafter hardness and fracture toughness.

4.3.6 CONCLUDING REMARKS

- ✓ The use of nano precursors and SPS aids the densification at low temperature.
- ✓ In contrary to Al, there is a threshold limit, beyond which Si will not dissolve in the mixture to participate in phases formation. This limit is temperature-dependent.
- ✓ There is a possible role of Si in enhancing the homogeneity of the sintered microstructure, however, this needs further investigation.

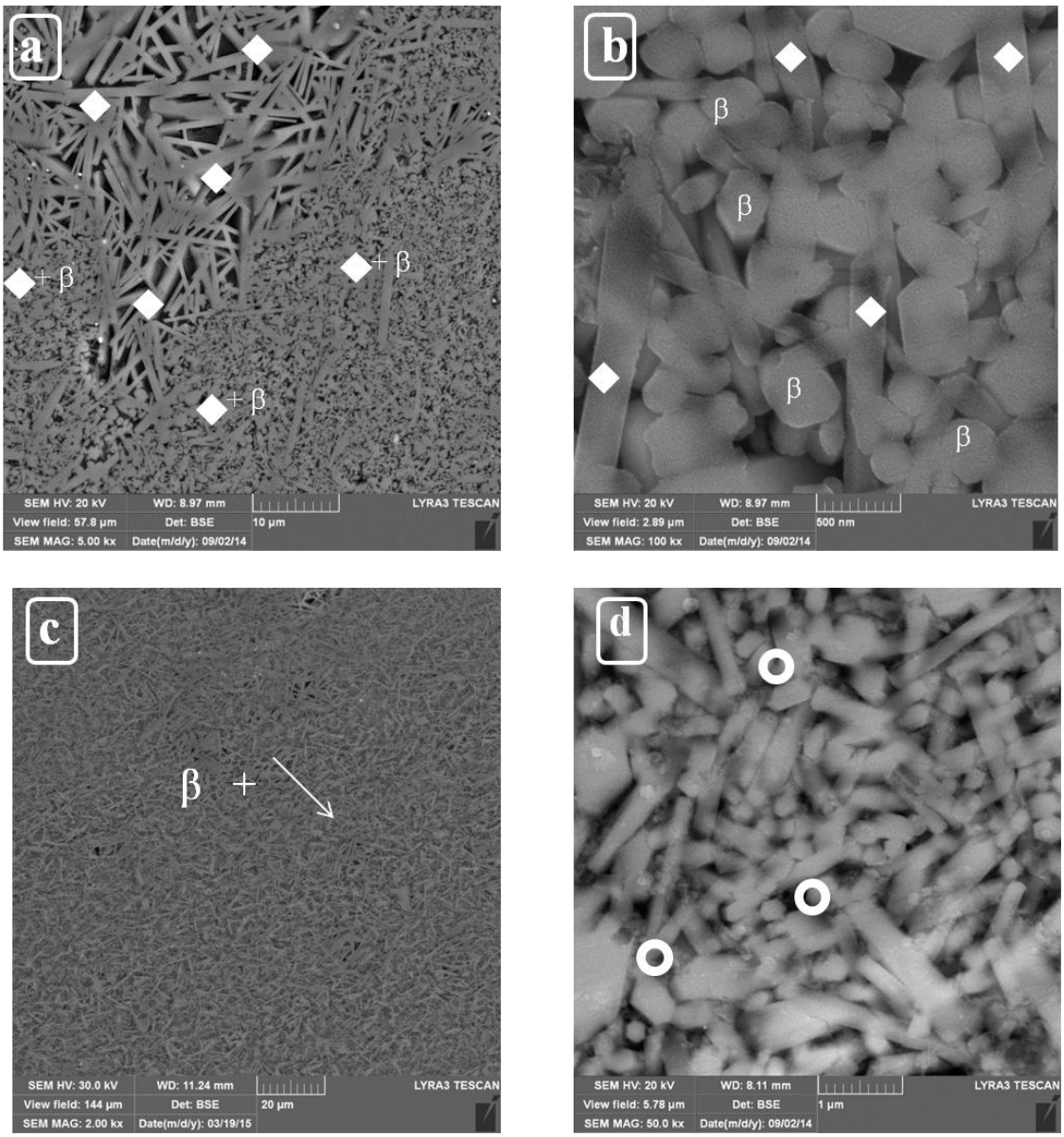

Figure 25 FESEM micrographs of samples containing α-Si_3N_4 sintered at 1600°C. (a), (b) **3-α,** (c)(d) **3-α (0.1Si)**. **Label key**: β-SiAlON (**β**), α-SiAlON (**α**), α-Si_3N_4 (**o**), 12H (→),15R(♦)

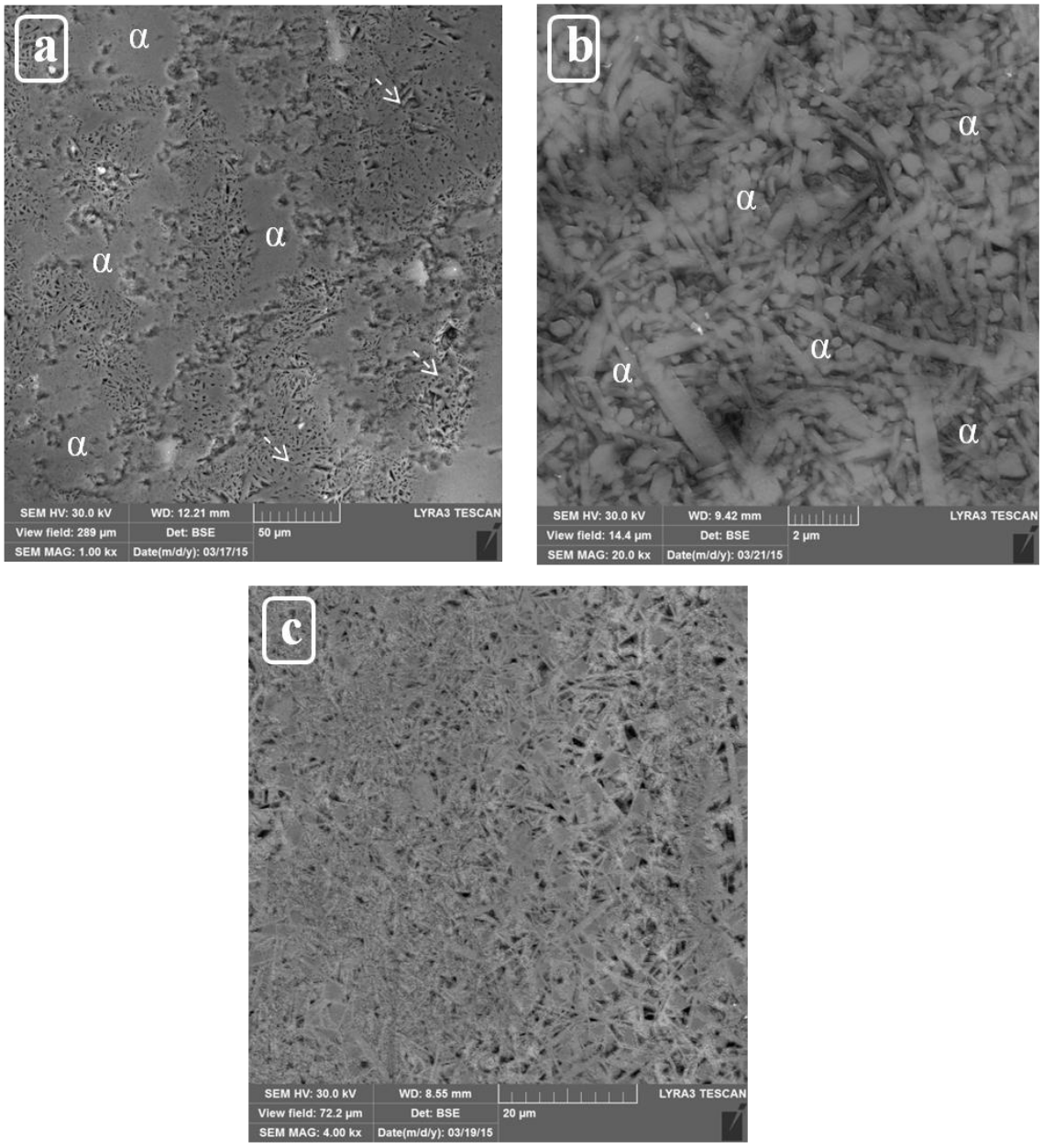

Figure 26 FESEM micrographs of samples containing α-Si_3N_4 sintered at 1600°C. (a), (b) **3-α(0.2Si),** (c) **3-α (0.3Si)**. **Label key**: α-SiAlON (**α**), 21R (--►)

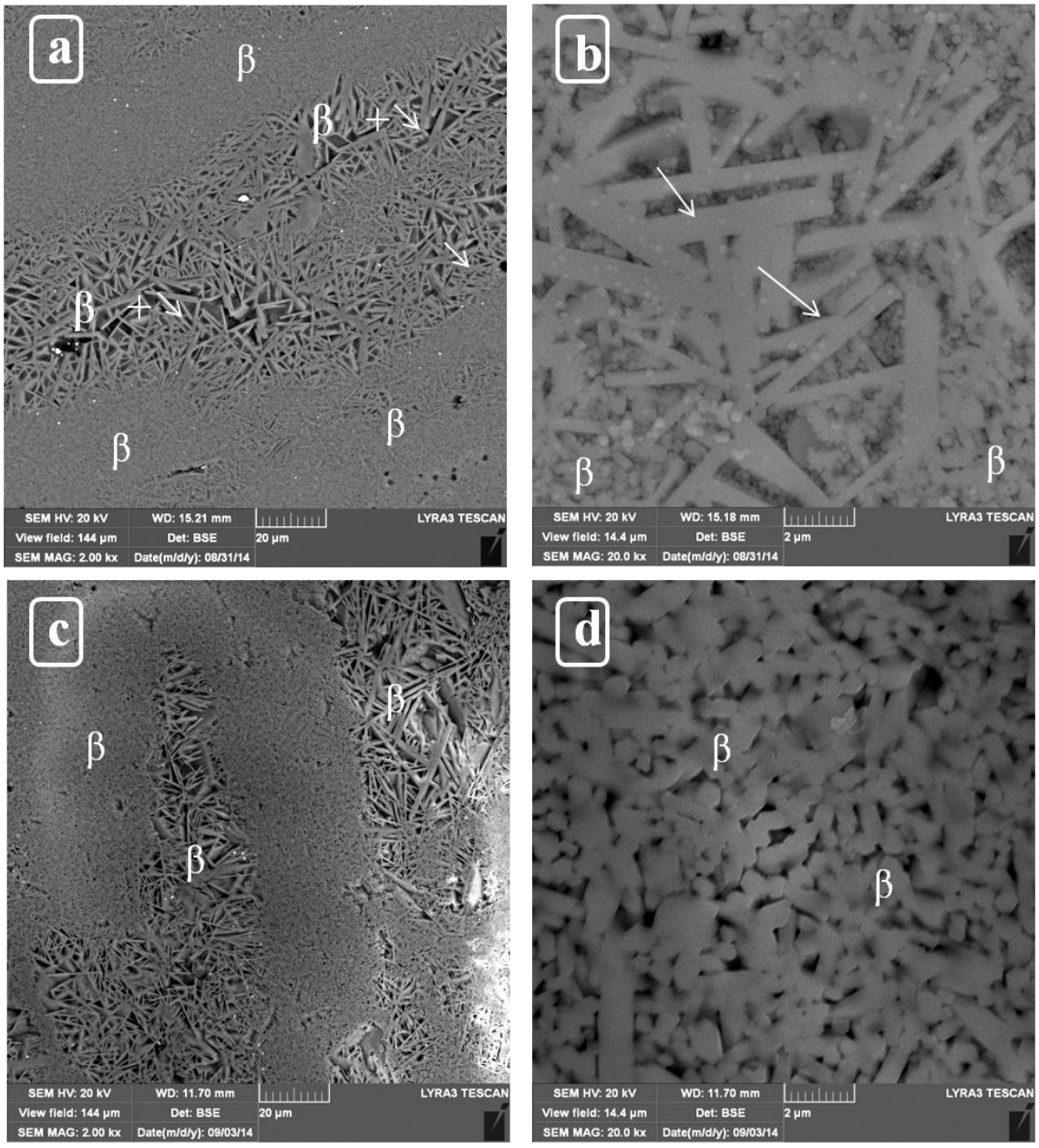

Figure 27 FESEM micrographs of samples containing Amp-Si_3N_4 sintered at 1600°C.

(a)(b) **3-Amp,** (c)(d) **3-Amp(0.1Si)**. **Label key**: β-SiAlON (**β**), 12H (→)

TABLE 11 The mechanical properties of the samples sintered at 1600^{o}C

Sample Name	H_{V10} (GPa)	K_{IC} (MPa√m)
3-α	13.4 ± 0.7	7.2 ± 2.4
3-α(0.1Si)	11.4 ± 0.5	7.8 ± 0.7
3-α(0.2Si)	13.2 ± 0.3	4.2 ± 0.8
3-α(0.3Si)	12.9 ± 0.5	4.2 ± 0.5
3-Amp	12.3 ± 0.8	5.2 ± 1.3
3-Amp(0.1Si)	13.6 ± 0.3	-
3-Amp(0.2Si)	12.5 ± 0.4	3.7
3-Amp(0.3Si)	11.8 ± 0.5	-

4.4 EFFECT OF CRYSTAL STRUCTURE OF Si_3N_4 ON Ba-α-SIALON

4.4.1 INTRODUCTION

The objective of this section is to examine the effect of altering the structure of the starting Si_3N_4 powder on the mechanical properties**. Table.12** lists the examined compositions with the corresponding chemical precursors in w.t%. Mainly, we are focusing here on three compositions, but with different precursors. The three compositions include $BaSi_4Al_2O_6N_4$, $BaSi_6Al_6O_4N_{12}$ and $BaSi_5AlO_2N_7$, in which the latter forms Ba-S-SiAlON [66]. Al metal replaced either Al_2O_3, as in 1b and ac, or AlN, as in 2b, 2c, 3b and 3c. Samples were sintered in spark plasma sintering at 1400^{o}C for 30 minutes at a pressure of 50 MPa. Sample 1c is an exception, in which it was sintered at 1150^{o}C because it melted at 1200^{o}C.

4.4.2 PHASE ASSEMBLAGE

X-ray diffraction patterns for the first composition are shown in **Figure.28**. The major phase in sample 1a is β-$BaSi_2Al_2O_8$, along with β-SiAlON and $Ba_2Si_{10}Al_2O_4N_{14}$ in less quantity. The replacement by Al in 1b reduces the amount of oxygen rich phase β-$BaSi_2Al_2O_8$. Similarly, and as it can be revealed from our discussion in the previous sections, β-SiAlON amount is lowered down in 1b when compared to 1a. Starting by β-Si_3N_4 is a well-known way to end up with β-SiAlON as a major phase. This is pretty clear in sample 1c when compared to sample 1b, in which the former

incorporates β-Si_3N_4 as a starting material. The nitrogen-rich phase $Ba_2Si_{10}Al_2O_4N_{14}$ seems to be unaffected by Al replacement or the structure of Si_3N_4.

TABLE 12 Starting chemical precursors in powder form in w.t%

Sample ID	Starting Composition	BaO	Amp-Si_3N_4	β-Si_3N_4	Amp-SiO_2	Al_2O_3	AlN	Al
1a	$BaSi_4Al_2O_6N_4$	34	31	---	13	22	---	
1b	$BaSi_4Al_2O_6N_4$	34	31	---	13	21	---	1
1c	$BaSi_4Al_2O_6N_4$	34	---	31	13	21	---	1
2a	$BaSi_6Al_6O_4N_{12}$	22	40	---	---	15	23	
2b	$BaSi_6Al_6O_4N_{12}$	22	40	---	---	15	21	2
2c	$BaSi_6Al_6O_4N_{12}$	22	---	40	---	15	21	2
3a	$BaSi_5AlO_2N_7$	33	48	---	7	---	10	
3b	$BaSi_5AlO_2N_7$	33	48	---	7	---	9	1
3c	$BaSi_5AlO_2N_7$	33	---	48	7	---	9	1

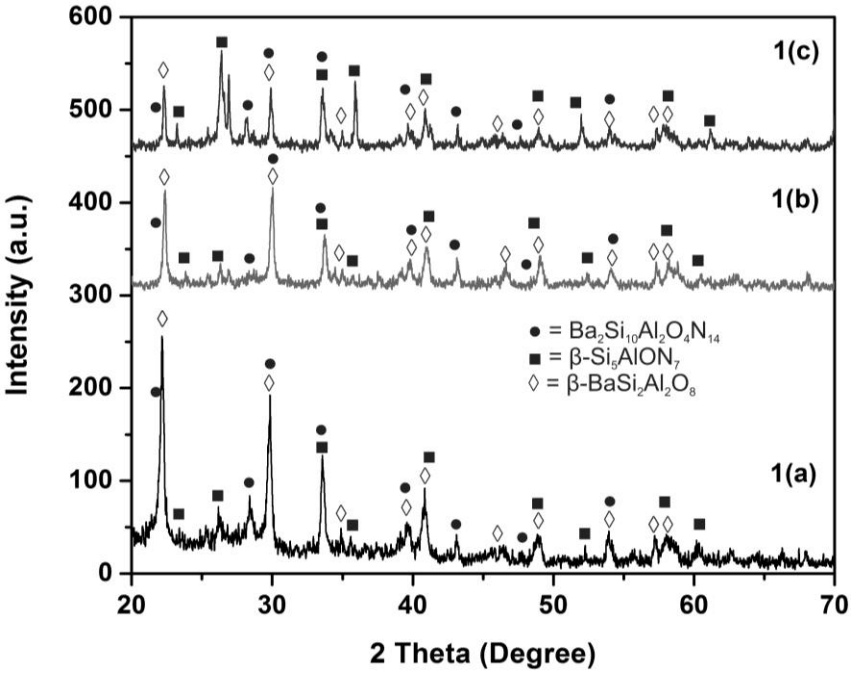

Figure 28 XRD patterns of samples 1a,1b and 1c

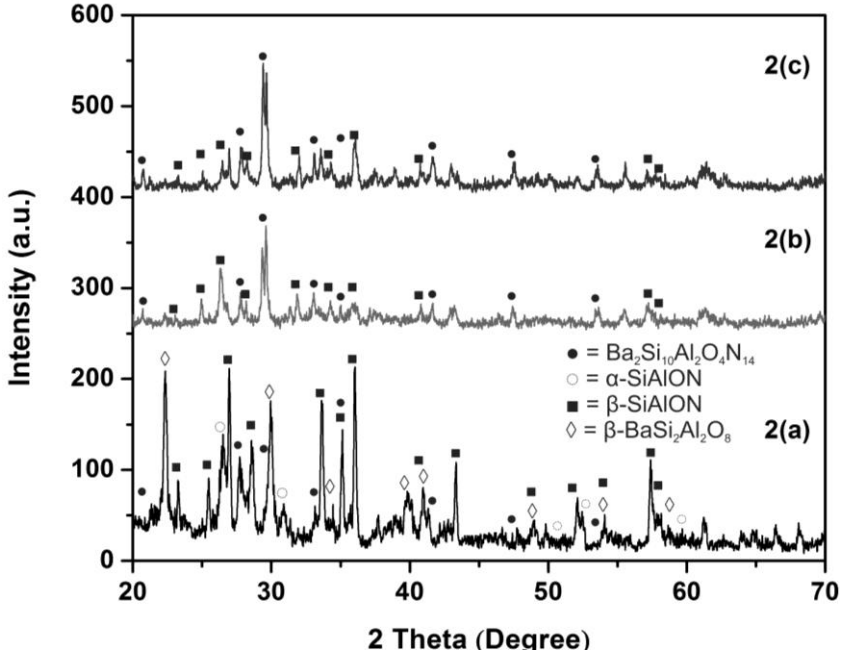

Figure 29 XRD patterns of samples 2a, 2b and 2c

The designed composition for these three samples does not show up in the resultant phases.

Figure.29 presents the XRD patterns for the second composition $BaSi_6Al_6O_4N_{12}$. α-SiAlON formed exceptionally in sample 2a, in which AlN was used as a starting material. The formation of β-SiAlON is known to be enhanced by either starting up with β-Si_3N_4 or by Amp- Si_3N_4, since the latter would crystallize into the most stable phase of SiAlON; the beta phase. However, once Al enters the equation, β-SiAlON amount diminishes, as in samples 2b and 2c. There is no much difference between samples 2b and 2c, eliminating, roughly for this composition, the role of the structure of Si_3N_4 on phase assemblage. Again, the designed composition does not appear in any of the examined samples.

Figure.30 displays the XRD patterns for the third composition $BaSi_5AlO_2N_7$. β-SiAlON and SiO_2 are present as major phases in all samples. The amount of β-SiAlON is reduced in 3b because of the incorporation of Al metal. Although peaks present in the patterns fit well the SiO_2 phase, it is possible that an unknown phase in silicon, oxygen and nitrogen, with similar diffraction pattern to SiO_2, has formed during the sintering process, as it is unlikely to preserve SiO_2 at 1400^oC, since diffusion into other species starts before the melting temperature, which is normally 1700^oC in the case of SiO_2 . Lastly, the amount of SiO_2 decreases when β-Si_3N_4 was used, favoring the formation of β-SiAlON (compare sample 3c and to 3b).

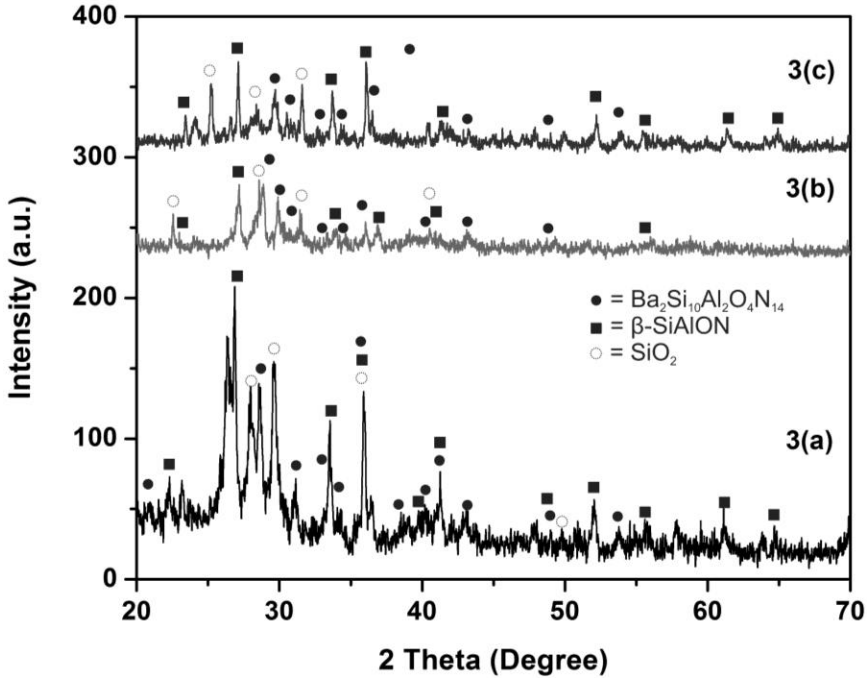

Figure 30 XRD patterns of samples 3a,3b and 3c

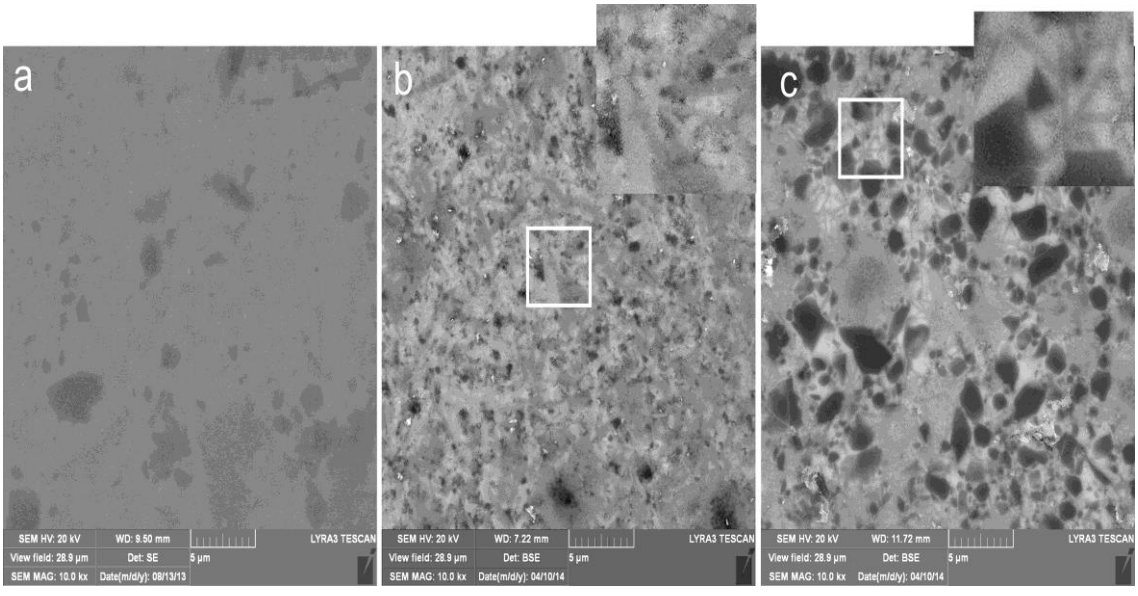

Figure 31 SEM micrographs of samples 1a, 1b and 1c (from left to right)

4.4.3 MICROSTRUCTRAL DEVELOPMENT

Figure.31 displays the FESEM micrographs of samples 1a, 1b and 1c, respectively. Sample 1a shows SEM image with fine structured equi-axed grains which, according to the X-ray peaks observed, correspond to β-$BaSi_2Al_2O_8$ and $Ba_2Si_{10}Al_2O_4N_{14}$ as the major phases. A small amount of an elongated structure can be observed. However, more of these fine elongated whisker-like grains are observed between the equiaxed grains in samples 1b and 1c, as shown in Figure.31 (b & c) as inset enlargement, corresponding to β-Si_5AlON_7 phase.

Generally, this whisker formation and change in the morphology is considered to be a slow reaction in nitrides because of low driving force and comparatively slow reaction kinetics during synthesis. As a result, very little structural transformation takes place at relatively low synthesis temperature. However, in the case of nanopowder precursors, SPS allows the possibility of faster reactions and grain growth enhanced by dynamic ripening mechanisms [64,67]. Another possibility for the formation of elongated grains would be the presence of liquid phase at 1400^oC and the addition of aluminum is thought to enhance the formation of liquid phase in the matrix [68]. Subsequently, this low temperature of liquid phase formation facilitates the growth of elongated grains with less pinning by the surrounding equiaxed grains in the matrix [69]. Nonetheless, the formation of these microstructures has a significant impact on the mechanical properties, as eplained later.

Figure.32 shows the FESEM micrographs for samples 2a, 2b and 2c, which consist of mixed morphologies of micron and submicron dark gray grains. According to XRD and EDX observations, sample 2a contains β-Si_5AlON_7 and β-$BaSi_2Al_2O_8$ as major phases and $Ba_2Si_{10}Al_2O_4N_{14}$ in less quantity. Samples 2b and 2c exhibit different microstructure/morphology with needle-like structures of β-Si_5AlON_7, with lengths of 4-8 µm and diameters of 0.2-0.4 µm (2b) and 0.4-0.6 µm (2c) within the fine equiaxed $Ba_2Si_{10}Al_2O_4N_{14}$ matrix.

Figure.33 exhibits the FESEM micrographs for samples 3a, 3b and 3c, which are very comparable to those observed in samples of composition 1 (Figure.31). There is no evidence of formation of fine whiskers in the equiaxed matrix. However, dark grey grains and light grey grains originate from β-Si_5AlON_7 and $Ba_2Si_{10}Al_2O_4N_{14}$, respectively.

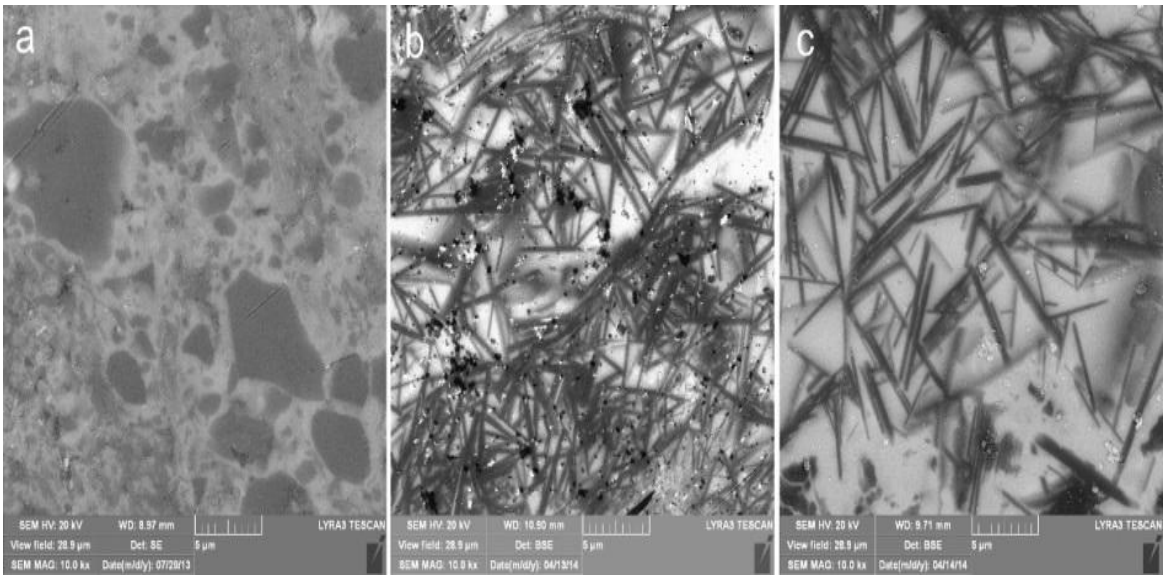

Figure 32 SEM micrographs of samples 2a, 2b and 2c (from left to right)

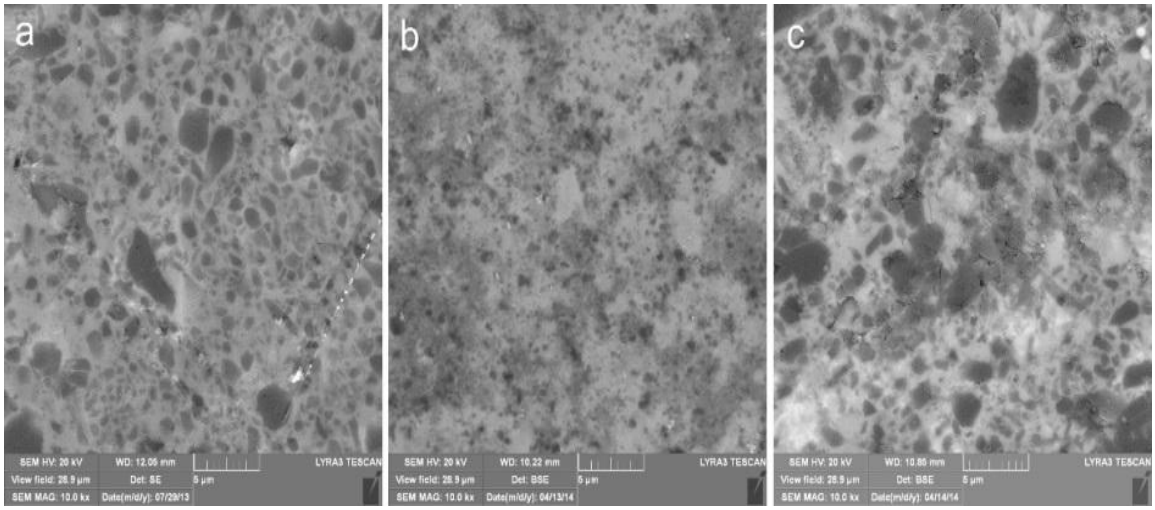

Figure 33 SEM micrographs of samples 3a, 3b and 3c (from left to right)

4.4.4 MECHANICAL PROPERTIES

Table.13 lists the density and hardness values of the sintered samples. The presence of nitrogen-free phase (β-$BaSi_2Al_2O_8$) in large quantity in the first set of samples is responsible for the low hardness values, even thought densification seems to be perfect. Despite the fact that the amount of β-$BaSi_2Al_2O_8$ is almost fixed in samples 1b and 1c, the hardness of sample 1c is relatively higher due to the increase in the β-SiAlON phase which results in higher nitrogen amount in the sample as a whole.

The presence of α-SiAlON in sample 2a is seen to be limited, as revealed from SEM analysis, which is also confirmed by the hardness value. β-SiAlON and $BaSi_6Al_6O_4N_{12}$ phases are thought to be responsible of the relative increase in hardness in the second set of samples due to their nitrogen content. Further, sample 2c shows higher hardness due to the increase in the amount $BaSi_6Al_6O_4N_{12}$ relative to β-SiAlON phase.

SiO_2 is known to have a hardness value of ≈ 9 GPa. Hence, it is predictable to see the drop in the hardness values of the third set of samples, even though β-SiAlON and $Ba_2Si_{10}Al_2O_2N_{14}$ are present. However, once the relative amount of the latter phases increases at the expense of SiO_2, the hardness jumps from 10 to 12 GPa. Another effect of the SiO_2 presence is the low density value of sample 3b which exhibits the highest relative amount of silicon dioxide.

TABLE 13 Hardness and density values of the sintered samples

Sample ID	ρ (g/cm^3)	H_{v10} (GPa)
1a	3.39	8
1b	3.29	7
1c	3.39	8
2a	3.43	11
2b	3.49	11
2c	3.41	13
3a	3.35	10
3b	3.07	10
3c	3.04	12

4.4.5 CONCLUDING REMARKS

- ✓ Ba-SiAlONs samples can be densified full by using this sintering route at 1400°C.
- ✓ According to the X-ray diffraction and SEM analyses, the synthesized Ba-SiAlONs shows mainly β-Si_5AlON_7 and $Ba_2Si_{10}Al_2O_4N_{14}$ phases but exhibit various morphologies, e.g. equiaxed, elongated, and whisker-like grains.
- ✓ An increase in the amount of β-phase occurs when β-Si_3N_4 was introduced into the starting mixtures in place of amorphous Si_3N_4, and this also results in higher hardness in the sintered ceramic.

4.5 THE ROLE OF POST-SINTERING HEAT TREATMENT ON THE FRACTURE TOUGHNESS OF Ca-α-SIALON CERAMICS

4.5.1 INTRODUCTION

This part of the work intends to investigate the effect of post-sintering heat treatment on the fracture toughness of Ca-α-SiAlON ceramic through the crystallization of grain boundary glass. The chemical composition was fixed in all samples as $CaSi_6Al_6O_4N_{12}$, which quantifies m=2 and n=4 in the general formula of α-SiAlON. Spark plasma sintering was carried out at 1500^{o}C under a pressure of 50 MPa for 30 minutes holding time in 20 mm graphite dies. Sintering was performed in either vacuum environment or in nitrogen atmosphere as per the reaction requirement (see **Table.14)**. A heating rate of 100^{o}C/min was adopted to avoid secondary-phase formation, beside a fast cooling rate to freeze the formed microstructure at the sintering temperature.

Samples were, then, heat treated in tube furnace for 12 hours in flowing Ar to keep the reaction environment protected. Heat treatment was carried out at 1500^{o}C, which is relatively higher than any reported temperature in the literature.

TABLE 14 Starting powder chemical precursors in w.t%

Sample Name	CaO	Al_2O_3	α -Si_3N_4	AlN	Al	Si	N
3-α / 3-α-HT	9.31	16.92	46.56	27.21	-	-	-
3-α(0.1Al) / 3-α(0.1Al) - HT	9.31	16.92	46.56	24.49	1.79	-	0.93
3-α(0.1Si) / 3-α(0.1Si) - HT	9.31	16.92	41.91	27.21	-	2.8	1.86
3-α(0.1Al+0.1Si) / 3-α(0.1Al+0.1Si) - HT	9.31	16.92	41.91	24.49	1.79	2.8	2.79

4.5.2 SINTERING AND DENSIFICATION

Table.15 lists down the density values of the sintered samples in g/cm^3. Samples are seen to be fully-dense when compared to the density of the major component in the powder mixture; namely Si_3N_4 (≈3.2 g/cm^3). The evaluation of the theoretical density is perhaps difficult due to the unavailability of the densities of the individual resultant phases in the sintered samples. A trend is seen in almost all samples in which heat treatment process reduces the density, a result of alpha to beta phase transformation that took place in most samples.

TABLE 15 Density values of the sintered/heat-treated samples

Sample Name	**ρ (g/cm^3)**
3-α	3.15
3-α-HT	3.15
3-α(0.1Al)	3.18
3-α(0.1Al)-HT	3.15
3-α(0.1Si)	3.16
3-α(0.1Si)-HT	3.15
3-α(0.1Al+0.1Si)	3.16
3-α(0.1Al+0.1Si)-HT	3.12

4.5.3 PHASE ASSEMBLAGE

Figure.34 displays the XRD patterns of samples **3-α, 3-α-HT, 3-α(0.1Al)** and **3-α(0.1Al)-HT** sintered at 1500^{o}C. Sample **3-α** is composed of α-SiAlON and 12H. After heat-treatment, α-SiAlON transformed entirely to β-SiAlON and the form of the AlN-polytypoid changed from 12H to 15R. $CaAl_2Si_2O_8$ crystallized from the grain boundary glass, leaving larger amount of nitrogen, compared to the un-treated sample.

XRD pattern of sample **3-α(0.1Al)** shows the presence of α-SiAlON and 12H. We have shown in section-2 in the results chapter the novel role of Al metal precursor on enhancing the stability of α-SiAlON and hindering the alpha to beta transformation. Another reflection of this stability in seen here, in which α-SiAlON has been kept as the major phase after the extensive heat treatment.

Figure.35 presents the XRD patterns of samples **3-α(0.1Si)**, **3-α(0.1Si)-HT**, **3-α(0.1Al+0.1Si)** and **3-α(0.1Al+0.1Si)-HT**. α-SiAlON and 21R constitute sample **3-α(0.1Si)**, with small amount of un-reacted Si metal. It should be noted that when Si metal is considered in the reaction, complex array of phases would form after heat treatment, as in sample **3-α(0.1Si)-HT**, in which α-SiAlON transformed to β-SiAlON and 21R changed form to 15R, i.e. lower N:O ratio. Free-nitrogen phases did form as well, namely $Ca_2Al_4Si_8O_{24}$ and $CaSiO_3$, yielding perhaps a nitrogen-rich grain boundary phase.

For sample **3-α(0.1Al+0.1Si)**, α-SiAlON and ζ-SiAlON are the only continuant phases. After heat-treatment, part of α-SiAlON transformed to β-SiAlON, leaving the other part un-touched as a result of the presence of Al metal precursor. $CaAl_2O_4$ and

Ca_2SiO_4 appeared, as well, after heat treatment with a distinctive mark of having no nitrogen in both phases.

4.5.4 MICROSTRUCTURAL DEVELOPMENT

Figure.36 displays SEM micrographs of samples **3-α**, **3-α-HT, 3-α(0.1Al)** and **3-α(0.1Al)-HT**, sintered at 1500^{o}C. The presence of α–SiAlON and 12H in sample **3-α** is evident as in micrograph (a). The microstructure is seen to be homogenous both before and after the heat treatment. Sample **3-α(0.1Al)** and **3-α(0.1Al)-HT** microstructures are seen to be similar as they both hold the same phases, with SiO_2 exceptionally present in sample **3- α (0.1Al)-HT**.

Figure.37 shows the SEM micrographs of samples **3-α(0._1Si)**, **3-α(0.1Si)-HT**, **3-α-(0.1Al+0.1Si) and 3-α(0.1Al+0.1Si)-HT**, sintered at 1500^{o}C. α–SiAlON and 21R phases appear in sample **3-α(0.1Si)**, as indicated as well by the XRD analysis. The heat treatment process of sample **3-α(0.1Si)** enhanced the homogeneity of the microstructure, as seen in micrograph(b). The oxygen-free phases shown by XRD results to be present in sample **3-α(0.1Al+0.1Si)-HT** could not be resolved by SEM here and TEM imaging should be performed.

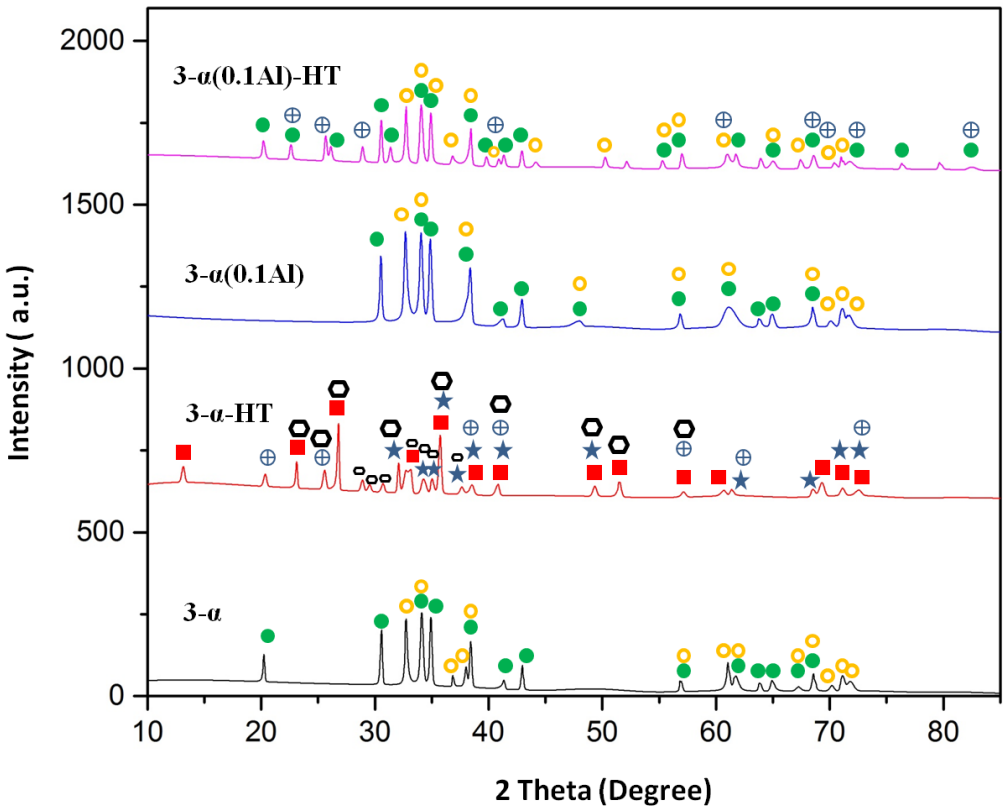

Figure 34 XRD patterns of samples **3-α**, **3-α-HT**, **3-α(0.1Al)** and **3-α(0.1Al)-HT** sintered at 1500°C. **Sample 3-α:** α–SiAlON ($Ca_{0.68}Si_{9.96}Al_{2.04}O_{0.68}N_{15.32}$) (●), 12H ($SiAl_5O_2N_5$) (○). **Sample 3-α-HT**: β-SiAlON z=2 ($Si_4\ Al_2O_2N_6$) (■),15R ($SiAl_4O_2N_4$) (★), SiO_2 (⊕), $CaAl_2Si_2O_8$ (⬡). **Sample 3-α(0.1Al)**: α–SiAlON ($Ca_{0.68}Si_{9.96}Al_{2.04}O_{0.68}N_{15.32}$) (●), 12H ($SiAl_5O_2N_5$) (○). **Sample 3-α(0.1Al)-HT**: α–SiAlON ($Ca_{0.8}Si_{9.2}Al_{2.8}O_{1.2}N_{14.8}$) (●), 12H ($SiAl_5O_2N_5$) (○), SiO_2 (⊕).

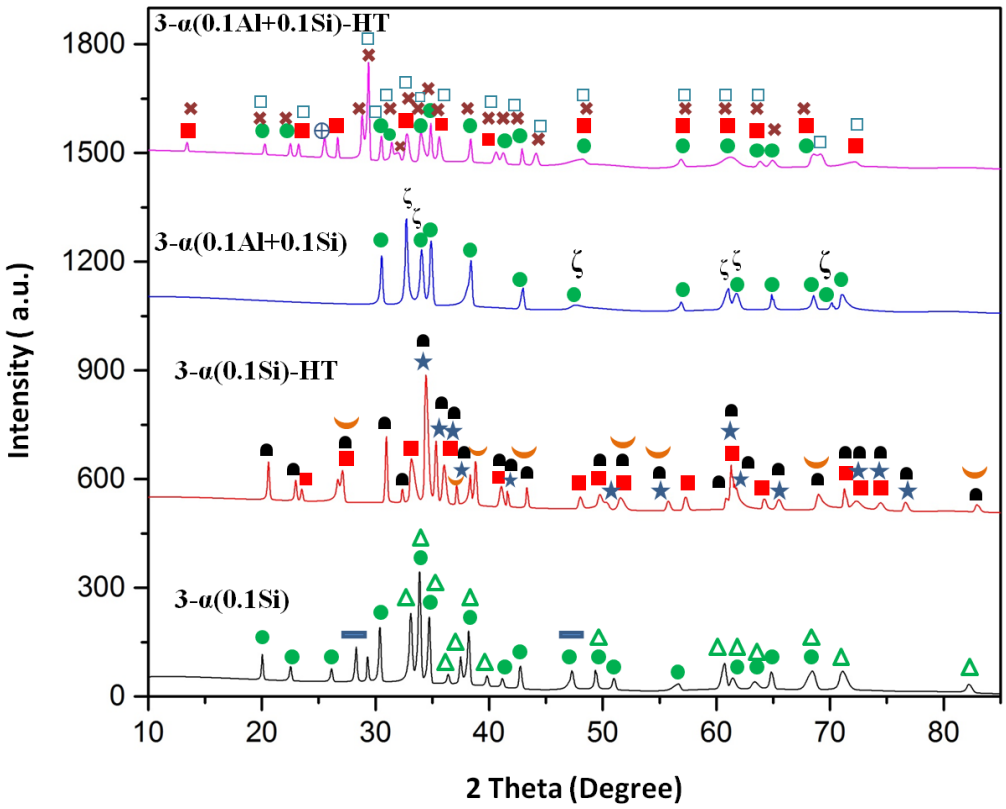

Figure 35 XRD patterns of samples **3-α(0.1Si)**, **3-α(0.1Si)-HT**, **3-α(0.1Al+0.1Si)** and **3-α(0.1Al+0.1Si)-HT** sintered at 1500°C. **Sample -α(0.1Si):** α–SiAlON ($Ca_{0.68}Si_{9.96}Al_{2.04}O_{0.68}N_{15.32}$) (●),21R ($SiAl_6O_2N_6$) (Δ), Si (▬). **Sample 3-α(0.1Si)-HT:** β-SiAlON z=1 (Si_5AlON_7), 15R ($SiAl_4O_2N_4$) (★),$Ca_2Al_4Si_8O_{24}$ **(◗),** $CaSiO_3$ **(◡).** **Sample 3-α(0.1Al+0.1Si)**: α–SiAlON ($Ca_{0.8}Si_{9.2}Al_{2.8}O_{1.2}N_{14.8}$) (●), zeta-$Si_3Al_7O_3N_9$ (ζ). **Sample 3-α(0.1Al+0.1Si)-HT:** α–SiAlON ($Ca_{0.68}Si_{9.96}Al_{2.04}O_{0.68}N_{15.32}$) (●), β-SiAlON z=4 ($Si_2Al_4O_4N_4$), $CaAl_2O_4$ **(✖),** Ca_2SiO_4 **(□),** SiO_2 (⊕).

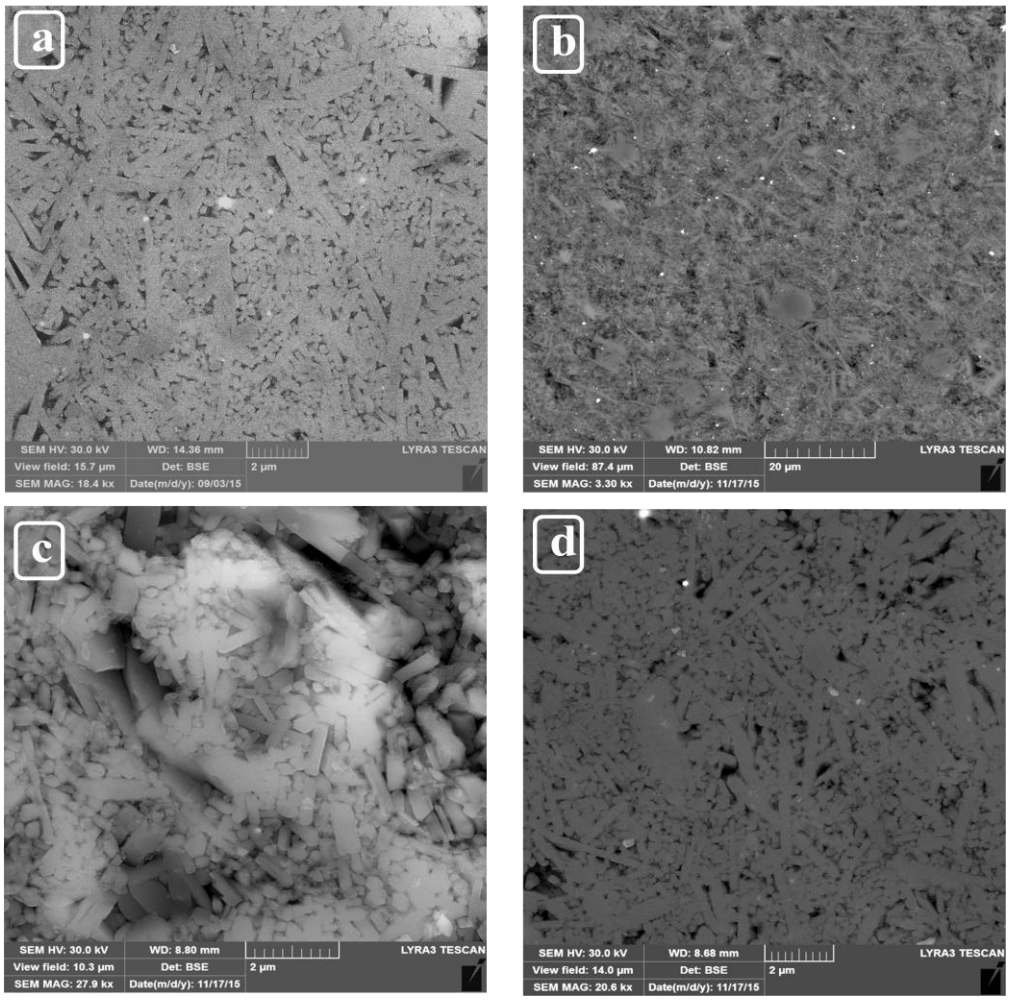

Figure 36 SEM micrographs of samples (a) **3-α** (b) **3-α-HT** (c) **3-α(0.1Al)** (d) **3-α(0.1Al)-HT**, sintered at 1500^{o}C.

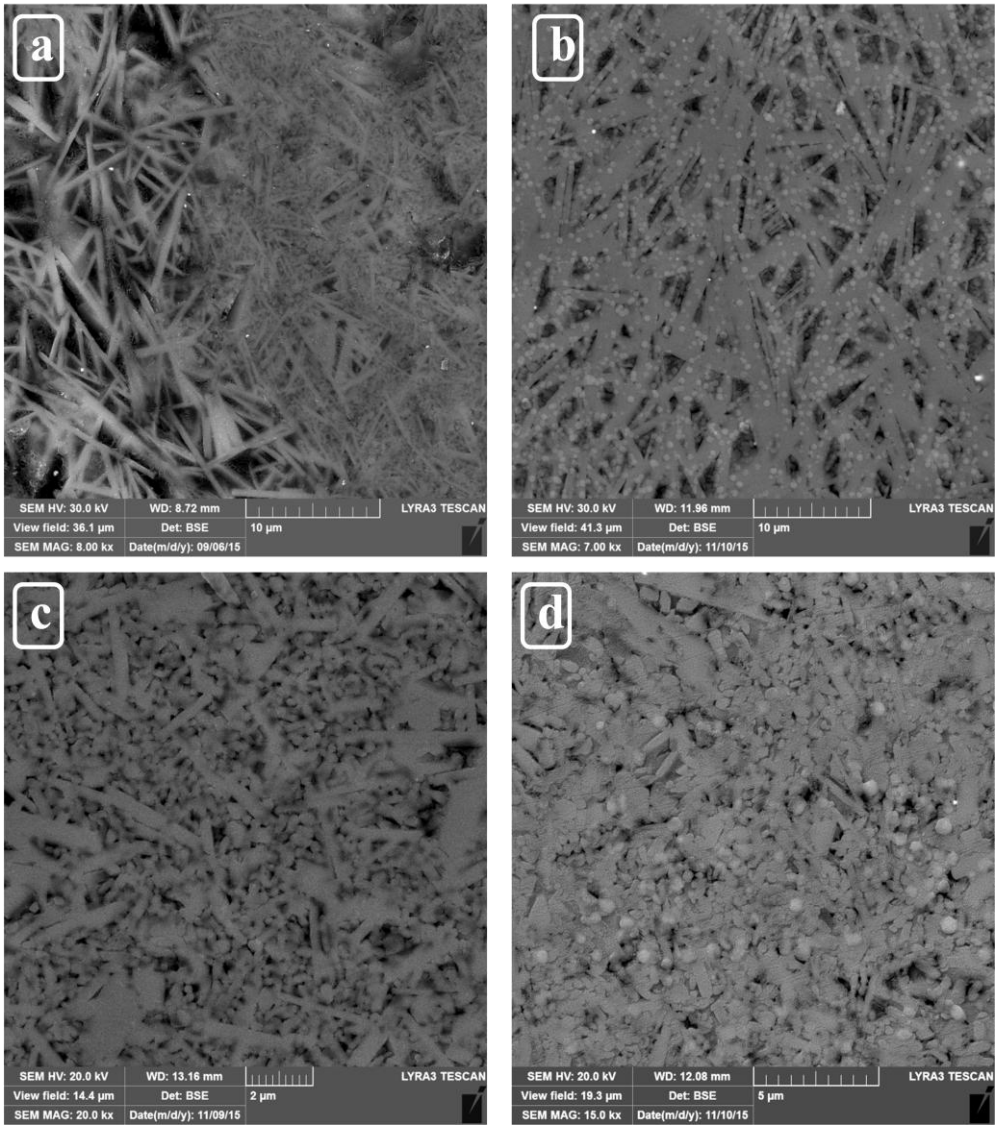

Figure 37 SEM micrographs of (a) **3-α(0.1Si) (b) 3-α(0.1Si)-HT (c) 3-α-(0.1Al+0.1Si)** (d**) 3-α(0.1Al+0.1Si)-HT,** sintered at 1500^{o}C.

EDS analysis is helpful in such studies to reveal the grain boundary composition before and after the heat-treatment. One notable change in the grain boundary of all samples, as seen in **Figure.38**, is the reduction in the amount of Ca, which is consumed partially to form the calcium aluminum silicate phases, as in samples **3-α-HT**, **3-α(0.1Si)-HT** and **3- α(0.1Al+0.1Si)-HT**, or to form another phase of α-SiAlON, as in sample **3-α(0.1Al)-HT**. The nitrogen to oxygen ratio of the grain boundary of sample **3-α** did increase, while it was reduced a little in samples **3-α(0.1Al)** and **3-α(0.1Al+0.1Si)**. However, the Al amount was increased in sample **3-α(0.1Al+0.1Si)**. The composition of the grain boundary in all samples indicates incomplete crystallization since none of the observed phases after the heat treatment matches the composition of the grain boundary. Complete crystallization is mostly unattainable for different reasons [40]. The increase in the viscosity of grain boundary during the heat treatment is one possible cause, since diffusion of cations and other species is difficult. The increase in N:O ratio and the reduction in the amount of Ca are typical causes for viscosity increase.

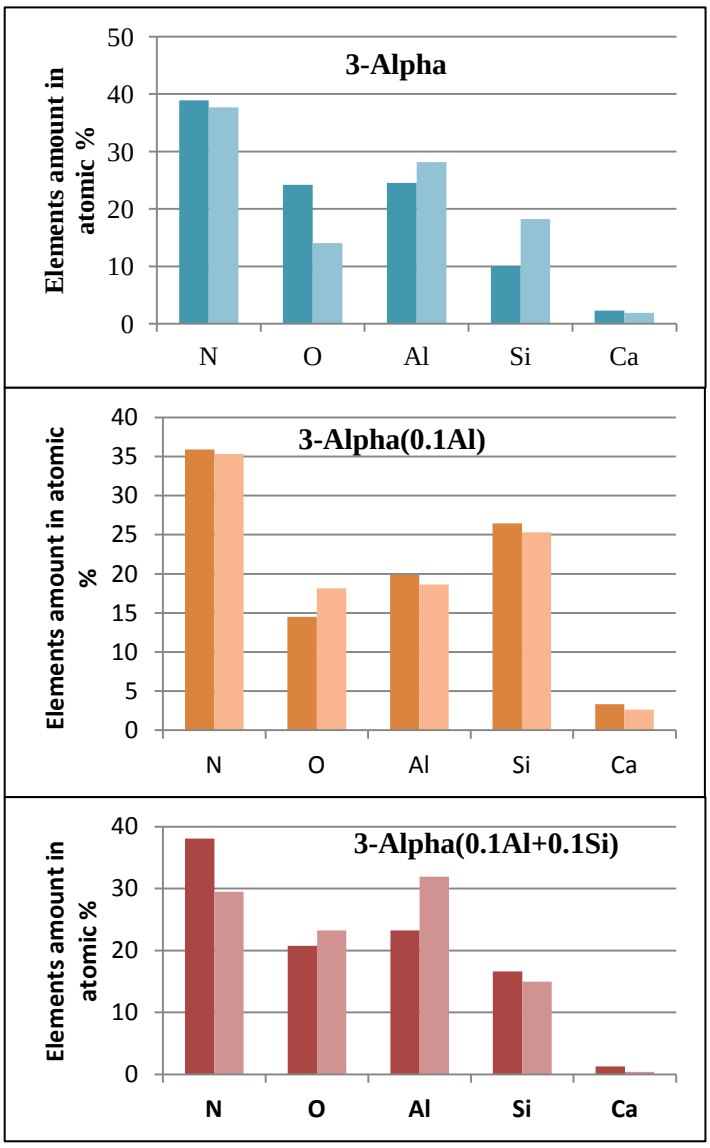

Figure 38 EDS analysis of grain boundary in samples **3-α, 3-α-HT, 3-α(0.1Al), 3-α(0.1Al)-HT,) 3- α(0.1Al+0.1Si)** and **3-α(0.1Al+0.1Si)-HT**. The untreated samples are represented by the left bars and the heat –treated ones by the right bars

4.5.5 MECHANICAL PROPERTIES

Mechanical properties of the as-sintered samples and the corresponding heat-treated samples are shown in **Table.16.** As a general trend, the fracture toughness increases in all samples after heat treatment, reaching a maximum in sample **3-α(0.1Al+0.1Si)-HT**. Vickers hardness decreases in all samples except for sample **3-α(0.1Al)-HT**, due to the role played by Al in stabilizing α-SiAlON phase.

The improvement in the fracture toughness after the heat treatment is not uniquely caused by the devitrification of the grain boundary phase, but rather phase transformation and structural change play an important role . For instance, in addition to the increase in the N:O ratio in the grain boundary aiding the intergranular crack propagation , the alpha to beta transformation and the change in the structure of AlN-polytypoid from 12H to 15R in sample **3-α-HT** are thought to be the origin of the crack-deflection mechanism. Hampshire *et al*. has shown similar behavior of Y-SiAlON ceramic when it undergoes heat treatment, in which the process is not simple devitrification of the grain boundary, but several phase transformation take place [70,71].

Figure.39 shows clearly that crack growth through the grain boundary is dominant, although in certain places, transgranular crack propagation mode is also present. This explains the fracture toughness enhancement via the well-known crack deflection toughening mechanism. Moreover, as shown by micrographs b and d, crack bridging is also observed.

4.5.6 CONCLUDING REMARKS

- ✓ The devitrification of the of the grain boundary contribute towards enhancement of the fracture toughness of SiAlON ceramics.

- ✓ The heat-treatment process induces devitrification of the grain boundary, as well as a complex array of phase transformations, which should be considered to optimally design the resultant microstructure.

- ✓ Al metal precursor is capable of stabilizing α-SiAlON, even after extensive heating at 1500^{o}C for 12 hours, which is reflected in enhanced fracture toughness along with retained hardness.

- ✓ The mixed crack propagation mode, i.e. intergranular and transgranular, is apparent in such ceramics due to the irregular binding strength between the grains and the grain boundary phases.

TABLE 16 Mechanical properties of as-sintered samples and the corresponding heat-treated samples

Sample Name	Hardness (HV_{10}) (GPa)	Fracture Toughness (MPa√m)
3-α	15.8 ± 0.35	5.9 ± 0.35
3-α-HT	13.8 ± 0.20	7.1 ± 0.60
3-α(0.1Al)	17.7 ± 0.18	8.3 ± 0.44
3-α(0.1Al)-HT	17.7 ± 0.58	9.0 ± 0.24
3-α(0.1Si)	14.6 ± 0.38	7.6 ± 0.36
3-α(0.1Si)-HT	14 ± 0.36	8.4 ± 0.66
3-α(0.1Al+0.1Si)	14.9 ± 0.26	6.8 ± 0.61
3-α(0.1Al+0.1Si)-HT	13.8 ± 0.13	9.5 ± 0.56

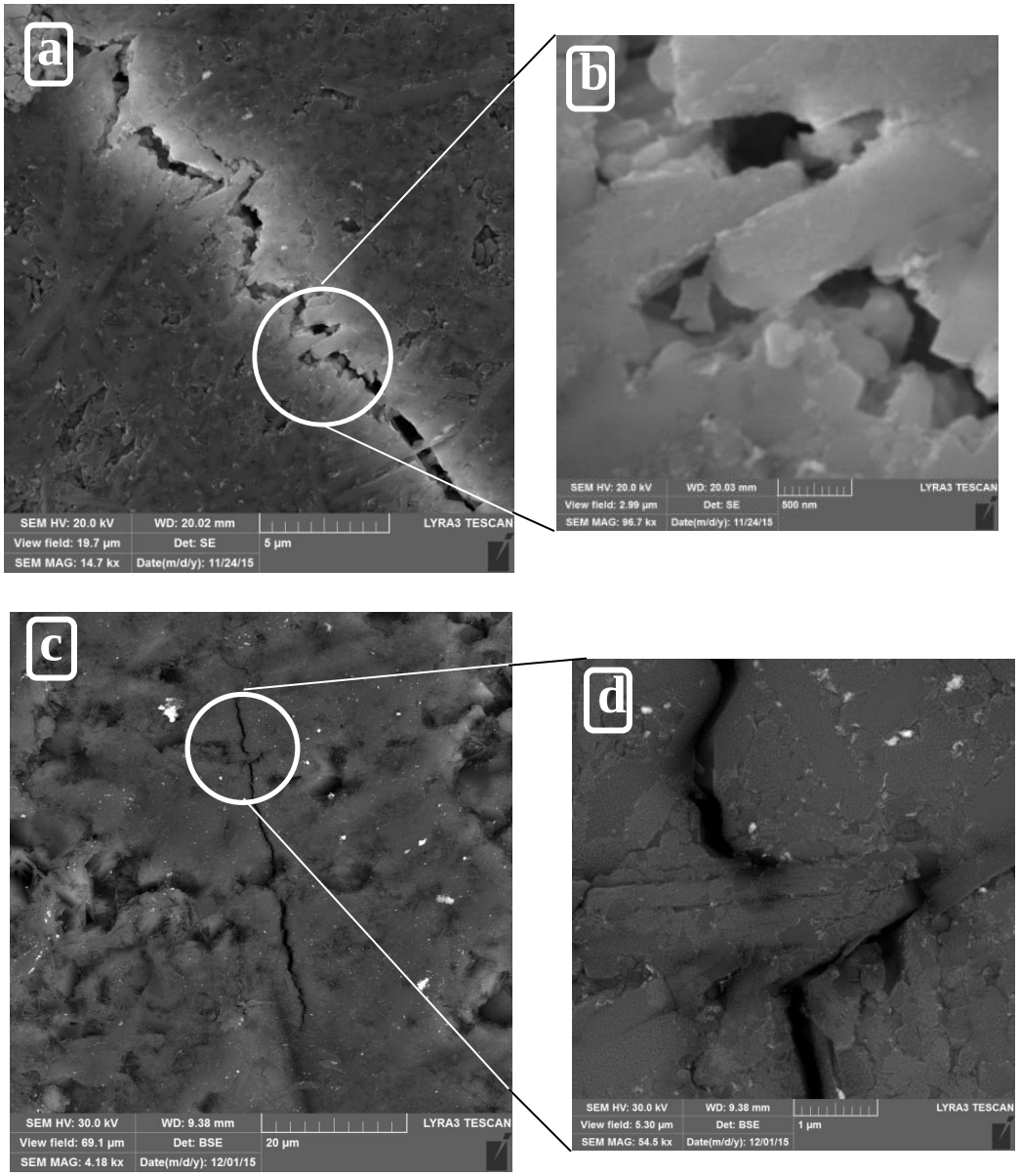

Figure 39 SEM micrographs showing the crack propagation mode and the associated toughening mechanisms for samples after heat treatment. (a) (b) sample **3- α-HT**. (c) (d) sample **3- α(0.1Al)-HT**

CONCLUSIONS

1. The use of nano precursors aids the densification and sinterability at relatively low temperature and shorter holding time.

2. Utilization of SPS has proven its novelty in reducing the sintering temperature and dwell time.

3. Among competitors, Ca is one of the best candidates in forming stable structure of α-SiAlON and, further, in densifying α-SiAlON ceramics at relatively low temperature **(1450^{o}C-1600^{o}C).**

4. Al metal precursor has shown its novelty in retaining α-SiAlON at high temperature **(1600^{o}C)** and yielding good mechanical properties **(HV_{10}=18.5 , K_{IC}=8.3 MPa$\sqrt{m}$)** at low sintering temperature **(1450^{o}C)**, for α-Si_3N_4 based SiAlONs.

5. Si metal precursor does not show the same tendency as that of Al, which is understood in terms of the melting point of Si and its chemical reactivity.

6. Amorphous Si_3N_4 tends to crystallize into β-SiAlON, due to the stability of the latter phase and the extra oxygen content on the surface of the powder.

7. Crystallization of the grain boundary phase through post-heat treatment is a suitable route to improve the fracture toughness of the sintered samples, however, proper design of the heat treatment is required to control the associated phase transformation.

FUTURE WORK

- ✓ Plotting a tentative ternary phase diagram, focusing on α-SiAlON region, for samples prepared by SPS at low temperatures
- ✓ Studying the effect of reducing further the initial powder size on the sinterability and mechanical properties
- ✓ Testing the wear behavior of the sintered SiAlON samples, both at ambient and elevated temperatures, to simulate their application as cutting tools.

LIST OF PUBLICATIONS AND PATENTS

1. Hakeem, Abbas Saeed, Raja Muhammad Awais Khan, Moath Mohammad Al-Malki, Faheemuddin Patel, Akolade Idris Bakare, Sadaqat Ali, Stuart Hampshire, and Tahar Laoui. "**Development and processing of SiAlON nano-ceramics by Spark Plasma Sintering.**" *Advances in Science and Technology*. Vol. 89. 2014.

2. Moath Mohammad Al Malki, Raja Muhammad Awais Khan, Abbas Saeed Hakeem, Stuart Hampshire, Tahar Laoui. "**Effect of metallic Al precursors on the sinterability and the mechanical properties of SiAlON nano-ceramic prepared by spark plasma sintering**". *Journal of the European Ceramic Society* (Ready For Submission)

3. Moath Mohammad Al Malki, Raja Muhammad Awais Khan, Muhammad Ali Ehsan, Abbas Saeed Hakeem, Stuart Hampshire, Tahar Laoui,. "**The Role of Post-Sintering Heat Treatment on The Fracture Toughness of Ca-α-SiAlON Ceramics** ". *Journal of the American Ceramic Society* (Ready For Submission)

4. Raja Muhammad Awais Khan, **Moath Al Malki**, Abbas Hakeem, Stuart Hampshire, and Tahar Laoui. " **Synthesis of single phase Ca-α-SiAlON using nano sized precursors in spark plasma sintering"**. (Ready For Submission)

5. Raja Muhammad Awais Khan, **Moath Al Malki**, Abbas Hakeem, Stuart Hampshire, and Tahar Laoui. "**Effect of SiC and WC reinforcement on the wear and**

mechanical properties of Ca-α-SiAlON ceramics ." *Journal of the European Ceramic Society*. (under preparation)

Patents Contribution

- Abbas Saeed Hakeem, Tahar Laoui, **Moath Mohammad Al Malki**, RAJA MUHAMMAD AWAIS KHAN, and Faheem Petal. **SiAlON Ceramics, Preparation by Adding Metallic Aluminum and Nano-Precursors**. (Filed)

REFERENCES

[1] Jack, KH. "Sialons and Related Nitrogen Ceramics." *Journal of materials science* 11.6 (1976): 1135-58.

[2] Deeley, GG, JM Herbert, and NC Moore. "Dense Silicon Nitride*." *Powder metallurgy* 4.8 (1961): 145-51.

[3] Katz, R. N. "U.S. National Programs for Energy Conversion."Progress in Nitrogen Ceramics, NATO ASI Series E: Applied Sciences: 727–35.

[4] Riley, Frank L. "Silicon Nitride and Related Materials." *Journal of the American Ceramic Society* 83.2 (2000): 245-65.

[5] Bando, YOSHIO. "Weak Asymmetry in-Si3n4 as Revealed by Convergent-Beam Electron Diffraction." *Acta Crystallographica Section B: Structural Science* 39.2 (1983): 185-89.

[6] R. Marchand, Y. Laurent, and J. Lang. "Structure of A-Silicon Nitride." *Acta. Crystallogr., Sect. B: Struct. Crystallogr. Cryst. Chem* 25: 2157–60.

[7] Jack, KH. "The Characterization of A'-Sialons and the A-B Relationships in Sialons and Silicon Nitrides." *Progress in Nitrogen Ceramics*. Springer, 1983. 45-60.

[8] Grieveson, P, KH Jack, and S Wild. "The Crystal Structures of Alpha- and Beta-Silicon and Germanium Nitrides." (1968).

[9] Priest, HF, FC Burns, GL Priest, and EC Skaar. "Oxygen Content of Alpha Silicon Nitride." *Journal of the American Ceramic Society* 56.7 (1973): 395-95.

[10] Thompson, DS, and PL Pratt. "The Structure of Silicon Nitride." *Science of Ceramics* 3 (1967): 33-51.

[11] Messier, Donald R, FL Riley, and RJ Brook. "The A/B Silicon Nitride Phase Transformation." *Journal of Materials Science* 13.6 (1978): 1199-205.

[12] Cao, GZ, and Ruud Metselaar. ". Alpha.'-Sialon Ceramics: A Review." *Chemistry of Materials* 3.2 (1991): 242-52.

[13] Ye, Feng, Chun-Feng Liu, and Li-Meng Liu. "Microstructure and Mechanical Properties of Multi-Cation Containing A-Sialons." *Ceramics International* 35.2 (2009): 725-31.

[14] Peng, Hong, Zhijian Shen, and Mats Nygren. "Formation of in Situ Reinforced Microstructures in a-Sialon Ceramics: Part Ii. In the Presence of a Liquid Phase." *Journal of materials research* 17.5 (2002): 1136-42.

[15] Wang, PL, C Zhang, WY Sun, and DS Yan. "Characteristics of Ca-A-Sialon—Phase Formation, Microstructure and Mechanical Properties." *Journal of the European Ceramic Society* 19.5 (1999): 553-60.

[16] Drew, P, and MH Lewis. "The Microstructures of Silicon Nitride/Alumina Ceramics." *Journal of Materials Science* 9.11 (1974): 1833-38.

[17] Wood, CA, and Y-B Cheng. "Phase Relationships and Microstructures of Ca and Al-Rich A-Sialon Ceramics." *Journal of the European Ceramic Society* 20.3 (2000): 357-66.

[18] German, Randall M. "Sintering Theory and Practice." *Sintering Theory and Practice, by Randall M. German, pp. 568. ISBN 0-471-05786-X. Wiley-VCH, January 1996.* 1 (1996).

[19] De Jonghe, LUTGARD C and MOHAMED N. Rahaman. "Sintering of Ceramics." *Handbook of Advanced Ceramics* 2003. 187-264.

[20] Tokita, M. "Mechanism of spark plasma sintering." *Proceeding of NEDO International Symposium on Functionally Graded Materials*. Vol. 22. Japan, 1999.

[21] Nishimura, TBANIFRIIM, MBANIFRIIM Mitomo, HBADKK Hirotsuru, and MBASCM Kawahara. "Fabrication of Silicon Nitride Nano-Ceramics by Spark Plasma Sintering." *Journal of materials science letters* 14.15 (1995): 1046-47.

[22] Belmonte, M, J González-Julián, P Miranzo, and MI Osendi. "Spark Plasma Sintering: A Powerful Tool to Develop New Silicon Nitride-Based Materials." *Journal of the European Ceramic Society* 30.14 (2010): 2937-46.

[23] Liu, Limeng, Feng Ye, Yu Zhou, Zhiguo Zhang, and Qinglong Hou. "Fast Bonding A-Sialon Ceramics by Spark Plasma Sintering." *Journal of the European Ceramic Society* 30.12 (2010): 2683-89.

[24] Salamon, David, Zhijian Shen, and Pavol Šajgalík. "Rapid Formation of A-Sialon During Spark Plasma Sintering: Its Origin and Implications." *Journal of the European Ceramic Society* 27.6 (2007): 2541-47.

[25] Nishimura, Toshiyuki, Xin Xu, Koji Kimoto, Naoto Hirosaki, and Hidehiko Tanaka. "Fabrication of Silicon Nitride Nanoceramics—Powder Preparation and Sintering: A Review." *Science and Technology of Advanced Materials* 8.7 (2007): 635-43.

[26] Liu, Guanghua, Kexin Chen, Heping Zhou, Junming Guo, C Pereira, and JMF Ferreira. "Low-Temperature Preparation of in Situ Toughened Yb A-Sialon Ceramics by Spark Plasma Sintering (Sps) with Addition of Combustion Synthesized Seed Crystals." *Materials Science and Engineering: A* 402.1 (2005): 242-49.

[27] Smirnov, KL. "Spark Plasma Sintering of Sialon Ceramics." *International Journal of Self-Propagating High-Temperature Synthesis* 18.2 (2009): 92-96.

[28] Izhevskiy, VA, LA Genova, JC Bressiani, and F Aldinger. "Progress in Sialon Ceramics." *Journal of the European Ceramic Society* 20.13 (2000): 2275-95.

[29] Söderlund, E, and T Ekström. "Pressureless Sintering of Y2o3-Ceo2-Doped Sialons." *Journal of Materials Science* 25.11 (1990): 4815-21.

[30] Mandal, Hasan. "New Developments in A-Sialon Ceramics." *Journal of the European Ceramic Society* 19.13 (1999): 2349-57.

[31] Camuşcu, Necip, Derek P Thompson, and Hasan Mandal. "Effect of Starting Composition, Type of Rare Earth Sintering Additive and Amount of Liquid Phase on Aa⇆ B Sialon Transformation." *Journal of the European Ceramic Society* 17.4 (1997): 599-613.

[32] Cao, GZ, Ruud Metselaar, and G Ziegler. "Relations between Composition and Microstructure of Sialons." *Journal of the European Ceramic Society* 11.2 (1993): 115-22.

[33] Van Rutten, JWT, HT Hintzen, and Ruud Metselaar. "Densification Behaviour of Ca-A-Sialons." *Ceramics international* 27.4 (2001): 461-66.

[34] Li, Ya-Wen, Pei-Ling Wang, Wei-Wu Chen, Yi-Bing Cheng, and Dong-Sheng Yan. "Effect of Additives on Microstructure of Ca A-Sialon." *Materials Letters* 47.4 (2001): 281-85.

[35] Wang, PL, YW Li, and DS Yan. "Effect of Dual Elements (Ca, Mg) and (Ca, La) on Cell Dimensions of Multi-Cation A-Sialons." *Journal of the European Ceramic Society* 20.9 (2000): 1333-37.

[36] Li, Ya-Wen, Pei-Ling Wang, Wei-Wu Chen, Yi-Bing Cheng, and Dong-Sheng Yan. "Phase Formation and Microstructural Evolution of Ca A-Sialon Using Different Si 3 N 4 Starting Powders." *Journal of the European Ceramic Society* 20.11 (2000): 1803-08.

[37] Zhang, C, E Narimatsu, K Komeya, J Tatami, and T Meguro. "Control of Grain Morphology in Ca-A Sialon Ceramics by Changing the Heating Rate." *Materials Letters* 43.5 (2000): 315-19.

[38] Sun, Ellen Y, Paul F Becher, Kevin P Plucknett, Chun-Hway Hsueh, Kathleen B Alexander, Shirley B Waters, Kiyoshi Hirao, and Manuel E Brito. "Microstructural Design of Silicon Nitride with Improved Fracture Toughness: Ii, Effects of Yttria and Alumina Additives." *Journal of the American Ceramic Society* 81.11 (1998): 2831-40.

[39] Ramesh, R, E Nestor, MJ Pomeroy, and S Hampshire. "Formation of Ln□ Si□ Al□ O□ N Glasses and Their Properties." *Journal of the European Ceramic Society* 17.15 (1997): 1933-39.

[40] Hampshire, S, E Nestor, R Flynn, J-L Besson, T Rouxel, H Lemercier, P Goursat, M Sebai, DP Thompson, and K Liddell. "Yttrium Oxynitride Glasses: Properties and Potential for

Crystallisation to Glass-Ceramics." *Journal of the European Ceramic Society* 14.3 (1994): 261-73.

[41] Lange, F. F., B. I. Davis, and D. R. Clarke. "Compressive Creep of Si3n4/Mgo Alloys." *Journal of Materials Science* 15.3 (1980): 616-18.

[42] Iskoe, JL, FF Lange, and ES Diaz. "Effect of Selected Impurities on the High Temperature Mechanical Properties of Hot-Pressed Silicon Nitride." *Journal of Materials Science* 11.5 (1976): 908-12.

[43] Rae, AWJM, DP Thompson, NJ Pipkin, and KH Jack. "The Structure of Yttrium Silicon Oxynitride and Its Role in the Hot-Pressing of Silicon Nitride with Yttria Additions." *Special ceramics 6* (1975): 358-60.

[44] Hirosaki, Naoto, Akira Okada, and Mamoru Mitomo. "Effect of Oxide Addition on the Sintering and High-Temperature Strength of Si3n4 Containing Y2o3." *Journal of materials science* 25.3 (1990): 1872-76.

[45] Clarke, David R. "On the Equilibrium Thickness of Intergranular Glass Phases in Ceramic Materials." *Journal of the American Ceramic Society* 70.1 (1987): 15-22.

[46] Kessler, H, H-J Kleebe, RW Cannon, and W Pompe. "Influence of Internal Stresses on Crystallization of Intergranular Phases in Ceramics." *Acta metallurgica et materialia* 40.9 (1992): 2233-45.

[47] Zhang, Yongsheng, and Y-B Cheng. "Grain Boundary Devitrification of Ca A-Sialon Ceramics and Its Relation with the Fracture Toughness." *Journal of materials science* 38.6 (2003): 1359-64.

[48] Kleebe, Hans-Joachim, Giuseppe Pezzotti, and Günter Ziegler. "Microstructure and Fracture Toughness of Si3n4 Ceramics: Combined Roles of Grain Morphology and Secondary Phase Chemistry." *Journal of the American Ceramic Society* 82 (1999).

[49] Mandal, H., et al. "Mechanical property control of rare earth oxide densified a-b." *5 th International Symposium on Ceramic materials and Components for Engines, ed. DS Yan, YR Fu and SY Shi*. World Scientific Publishers. Singapore. 1995.

[50] Mandal, H., and D. P. Thompson. "Vacuum Heat Treatment of Sialon Ceramics." *Br. Ceram. Proc.*. No. 55. 1995.

[51] Mandal, H, and DP Thompson. "New Heat Treatment Methods for Glass Removal from Silicon Nitride and Sialon Ceramics." *Journal of materials science* 35.24 (2000): 6285-92.

[52] Camuscu, N., H. Mandal, and D. P. Thompson. "Optimised high-temperature sialon ceramics containing melilite as the grain boundary phase." *Br. Ceram. Proc.*. No. 55. 1995.

[53] Cheng, Yi-Bing, and Derek P Thompson. "Aluminum-Containing Nilrogen Melilite Phases." *Journal of the American Ceramic Society* 77.1 (1994): 143-48.

[54] Ramesh, Raghavendra, Elizabeth Nestor, Michael J Pomeroy, and Stuart Hampshire. "Classical and Differential Thermal Analysis Studies of the Glass-Ceramic Transformation in a Ysialon Glass." *Journal of the American Ceramic Society* 81.5 (1998): 1285-97.

[55] Torres, Y, D Casellas, M Anglada, and L Llanes. "Fracture Toughness Evaluation of Hardmetals: Influence of Testing Procedure." *International Journal of Refractory Metals and Hard Materials* 19.1 (2001): 27-34.

[56] Minyoung Lee, Milivoj K. Brun and Tseng-Ying Tien. "The High Temperature Fracture Toughness of Sialon". *7th Annual Conference on Composites and Advanced Ceramic Materials: Ceramic Engineering and Science Proceedings*, Volume 4. 2009.

[57] Zenotchkine, Misha, Roman Shuba, and I-Wei Chen. "Effect of Heating Schedule on the Microstructure and Fracture Toughness of A-Sialon—Cause and Solution." *Journal of the American Ceramic Society* 85.7 (2002): 1882-84.

[58] Evans, Aw G, and E Arn Charles. "Fracture Toughness Determinations by Indentation." *Journal of the American Ceramic society* 59.7-8 (1976): 371-72.

[59] Van Rutten, JWT, HT Hintzen, and Ruud Metselaar. "Phase Formation of Ca-A-Sialon by Reaction Sintering." *Journal of the European Ceramic Society* 16.9 (1996): 995-99.

[60] Wild, S, P Grieveson, and KH Jack. "The Crystal Structure of Alpha and Beta Silicon and Germanium Nitrides." *Special Ceramics* 5 (1972): 385-95.

[61] Zhao, Rupeng, Steven P Swenser, and Yi-Bing Cheng. "Formation of Aln-Polytypoid Phases During A-Sialon Decomposition." *Journal of the American Ceramic Society* 80.9 (1997): 2459-63.

[62] Hakeem, Abbas S, Rachel Daucé, Ekaterina Leonova, Mattias Edén, Zhijian Shen, Jekabs Grins, and Saeid Esmaeilzadeh. "Silicate Glasses with Unprecedented High Nitrogen and Electropositive Metal Contents Obtained by Using Metals as Precursors." *Advanced Materials* 17.18 (2005): 2214-16.

[63] Kurama, S, M Herrmann, and H Mandal. "The Effect of Processing Conditions, Amount of Additives and Composition on the Microstructures and Mechanical Properties of A-Sialon Ceramics." *Journal of the European Ceramic Society* 22.1 (2002): 109-19.

[64] Shen, Zhijian, and Mats Nygren. "Kinetic Aspects of Superfast Consolidation of Silicon Nitride Based Ceramics by Spark Plasma Sintering." *Journal of Materials Chemistry* 11.1 (2001): 204-07.

[65] Visuttipitukul, Patama, Tatsuhiko Aizawa, and Hideyuki Kuwahara. "Advanced Plasma Nitriding for Aluminum and Aluminum Alloys." *Materials Transactions* 44.12 (2003): 2695-700.

[66] Lewis, MH, B Basu, ME Smith, M Bunyard, and T Kemp. "S-Phase Sialon Ceramics; Microstructure and Properties." *Silicates industriels*.7-8 (2004): 225-31.

[67] Shen, Zhijian, Zhe Zhao, Hong Peng, and Mats Nygren. "Formation of Tough Interlocking Microstructures in Silicon Nitride Ceramics by Dynamic Ripening." *Nature* 417.6886 (2002): 266-69.

[68] Wu, Yuanwen, Hanrui Zhuang, Fengying Wu, David Dollimore, Baolin Zhang, Shen Chen, and Wenlan Li. "Mechanism of the Formation of B–Sialon by Self-Propagating High-Temperature Synthesis." *Journal of materials research* 13.01 (1998): 166-72.

[69] Yi, Xuemei, Kotaro Watanabe, and Tomohiro Akiyama. "Fabrication of Dense B-Sialon by a Combination of Combustion Synthesis (Cs) and Spark Plasma Sintering (Sps)." *Intermetallics* 18.4 (2010): 536-41.

[70] Pomeroy, Michael J, and Stuart Hampshire. "Controlled Crystallisation of a Y-Si-Al-on Glass Typical of Grain Boundary Glasses Formed in Silicon Nitride-Based Ceramics." *Journal of the Ceramic Society of Japan* 116.1354 (2008): 722-26.

[71] Hampshire, Stuart, and Michael J Pomeroy. "Grain Boundary Glasses in Silicon Nitride: A Review of Chemistry, Properties and Crystallisation." *Journal of the European Ceramic Society* 32.9 (2012): 1925-32.

NOMENCLATURE

α	Alpha
β	Beta
Si_3N_4	Silicon nitride
AlN	Aluminum nitride
Al_2O_3	Aluminum oxide
CaO	Calcium oxide
BaO	Barium oxide
BeO	Beryllium oxide
Ar	Argon
Ln	Lanthanides elements
SPS	Spark plasma sintering
HIP	Hot isostatic pressing
HP	Hot pressing
PLS	Pressureless sintering
PAS	Pressure assisted sintering
CIP	Cold isostatic pressing
SEM	Scanning electron microscope
BSE	Backscattered electron
SE	Secondary electron
EDS	Energy dispersive spectroscopy
XRD	X-ray diffraction
DSC	Differential scanning calorimetry
HV	Vickers hardness
SENB	Single-edge notched beam
SEVNB	Single-edge V-notched beam
IM	Indentation method
hr	Hour
min	Minute
MPa	Mega Pascal
GPa	Giga Pascal
wt. %	Weight percentage
pm	Pico meter
nm	Nano meter
μm	Micro meter

VITA

Moath Mohammad Fahd Al Malki
Graduate assistant in the mechanical engineering department
King Fahd University for Petroleum and Minerals
Dhahran – Eastern Province – Saudi Arabia
Email : moath6666@gmail.com
mmalki@kfupm.edu.sa

Education BS : Aerospace Engineering from KFUPM (2012)

MS : Material Science and Engineering from KFUPM (2015)

Research Interests Developing nano ceramic composites – Hard Materials – Wear resistance materials

Conference Papers

- Hakeem, Abbas Saeed, Raja Muhammad Awais Khan, Moath Mohammad Al-Malki, Faheemuddin Patel, Akolade Idris Bakare, Sadaqat Ali, Stuart Hampshire, and Tahar Laoui. "**Development and processing of SiAlON nano-ceramics by Spark Plasma Sintering.**" *Advances in Science and Technology*. Vol. 89. 2014

Journal Papers

1. **Moath Mohammad Al Malki**, Raja Muhammad Awais Khan, Abbas Saeed Hakeem, Stuart Hampshire, Tahar Laoui. "**Effect of different precursors on the phase formation and mechanical properties of SiAlON nano-ceramics prepared by spark plasma sintering**". *Journal of the European Ceramic Society* (Submitted)

2. **Moath Mohammad Al Malki**, Raja Muhammad Awais Khan, Muhammad Ali Ehsan, Abbas Saeed Hakeem, Stuart Hampshire, Tahar Laoui,. "**The Role of Post-Sintering Heat Treatment on The Fracture Toughness of Ca-α-SiAlON Ceramics** ". *Journal of the American Ceramic Society* (Ready For Submission)

3. Raja Muhammad Awais Khan, **Moath Al Malki**, Abbas Hakeem, Stuart Hampshire, and Tahar Laoui. " **Synthesis of single phase Ca-α-SiAlON using nano sized precursors in spark plasma sintering"**. (Ready For Submission)

4. Raja Muhammad Awais Khan, **Moath Al Malki**, Abbas Hakeem, Stuart Hampshire, and Tahar Laoui. "**Effect of SiC and WC reinforcement on the wear and mechanical properties of Ca-α-SiAlON ceramics ."** *Journal of the European Ceramic Society*. (under preparation)

Patents

- Abbas Saeed Hakeem, Tahar Laoui, **Moath Mohammad Al Malki**, RAJA MUHAMMAD AWAIS KHAN, and Faheem Petal. **SiAlON Ceramics, Preparation by Adding Metallic Aluminum and Nano-Precursors**. (Filed)